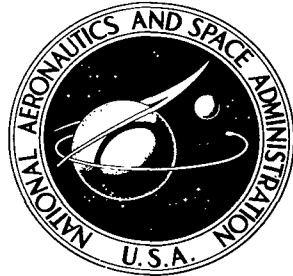


NASA TN D-5936

**NASA TECHNICAL NOTE**



**NASA TN D-5936**

C. I

LOAN COPY: RETURN  
AFWL (WLOL)  
KIRTLAND AFB, N M



**LOW-SPEED WIND-TUNNEL  
INVESTIGATION OF A SERIES  
OF TWIN-KEEL ALL-FLEXIBLE PARAWINGS**

*by Rodger L. Naeseth*

*Langley Research Center  
Hampton, Va. 23365*

**NATIONAL AERONAUTICS AND SPACE ADMINISTRATION • WASHINGTON, D. C. • OCTOBER 1970**



0132703

1. Report No. NASA TN D-5936	2. Government Accession No.	3. Recipient's Catalog No.	
4. Title and Subtitle <b>LOW-SPEED WIND-TUNNEL INVESTIGATION OF A SERIES OF TWIN-KEEL ALL-FLEXIBLE PARAWINGS</b>	5. Report Date October 1970	6. Performing Organization Code	
7. Author(s) By Rodger L. Naeseth	8. Performing Organization Report No. L-7096	10. Work Unit No. 126-13-10-03	
9. Performing Organization Name and Address NASA Langley Research Center Hampton, Va. 23365	11. Contract or Grant No.	13. Type of Report and Period Covered Technical Note	
12. Sponsoring Agency Name and Address National Aeronautics and Space Administration Washington, D.C. 20546	14. Sponsoring Agency Code		
15. Supplementary Notes			
16. Abstract  Low-speed wind-tunnel studies were made to obtain the static aerodynamic characteristics of a series of 10 twin-keel all-flexible parawings. The parawings, in flat planform, had a leading-edge sweep angle of 45° and generally a 20-percent keel length cut off of the apex of the basically triangular shape. The nose of each parawing model was contoured in such a manner that the airfoil sections in the center panel of the model had rounded leading edges.  Twin-keel parawings were found to have improved performance characteristics as compared with single-keel parawings. The maximum lift-drag ratios of the models ranged from 2.6 to 3.2. Results of a limited flight-test program indicated that the twin-keel parawings would glide when the rigging, except for control-line length, was set as determined in the small-scale wind-tunnel tests.			
17. Key Words (Suggested by Author(s)) Twin-keel all-flexible parawings Aerodynamic characteristics	18. Distribution Statement Unclassified - Unlimited		
19. Security Classif. (of this report) Unclassified	20. Security Classif. (of this page) Unclassified	21. No. of Pages 102	22. Price* \$3.00

LOW-SPEED WIND-TUNNEL INVESTIGATION OF A SERIES OF  
TWIN-KEEL ALL-FLEXIBLE PARAWINGS

By Rodger L. Naeseth  
Langley Research Center

SUMMARY

Low-speed wind-tunnel studies were made to obtain the static aerodynamic characteristics of a series of twin-keel all-flexible parawings. The parawings, in flat planform, had a leading-edge sweep angle of 45° and generally a 20-percent keel length cut off the apex of the basically triangular shape. Suspension lines were attached to the inner part of each parawing in two rows or keels to form three lobes when the parawing was inflated. The arrangement of the keels was varied to form a series of 10 parawing models. The nose of each model was contoured in such a manner that the airfoil sections in the center panel of the model had rounded leading edges.

The maximum observed lift-drag ratios of the models ranged from 2.6 to 3.2. The model with the center panel which tapered from 40-percent keel length at the nose to 80-percent keel length at the trailing edge had the highest lift-drag ratio. The resultant-force coefficient for this model was about 0.75 at the maximum lift-drag ratio. Maximum resultant-force coefficient was increased and maximum lift-drag ratio was decreased by shortening the aft keel lines. The maximum value of resultant-force coefficient shown for the series of models was 1.28 (at a lift-drag ratio of 2.0); this value was obtained for the model with the center panel which tapered from 40-percent keel length at the leading edge to 20-percent keel length at the trailing edge. The model with parallel keels and a center-panel width of 40-percent length reached a lift-drag ratio of 2.95 at a resultant-force coefficient of 0.95.

Line-load measurements indicated a high loading at the front of the keels and a decrease in loading toward the trailing edge of the parawing. This keel loading differs significantly from previously reported measurements on a single-keel model. The leading-edge line loads were similar for the twin- and single-keel parawings.

Results of a limited flight-test program indicated that the twin-keel parawing would glide when the rigging, except for control-line length, was set as determined in the small-scale wind-tunnel tests.

## INTRODUCTION

The National Aeronautics and Space Administration has been investigating all-flexible fabric wings to define and evaluate their performance, stability, control, and deployment characteristics. Wind-tunnel test results for a variety of single-keel configurations are presented in reference 1, and test results for a single-keel parawing applied to a lifting-body model are presented in reference 2. The present investigation was undertaken as part of a research effort to provide advanced wing configurations having improved aerodynamic characteristics over the single-keel design of references 1 and 2. Systematic variations in the planforms of a family of twin-keel parawings were of primary interest.

Some of the twin-keel configurations had relatively large center-panel widths, and it was recognized that the design details used on the nose of the center panel could have a significant effect on the wing performance characteristics. An investigation of nose design details was therefore undertaken to provide a satisfactory center-panel leading edge for the planform investigation. Various leading-edge treatments have been used in the past and some are shown in references 3 and 4. A contoured nose shape was developed in the present study and was used throughout the planform investigation.

Preliminary test results for one of the parawings of the present twin-keel planform study are presented in reference 5 and show that a maximum lift-drag ratio of 3.0 was achieved. This twin-keel wing, along with a single-keel wing, was selected for development of deployment technology and controlled flight at a larger scale. The results of this wing-technology work are given in references 6 and 7, and wind-tunnel test results obtained on a twin-keel parawing in this program are presented in reference 8.

The present investigation included determination of the rigging and aerodynamic characteristics for a family of twin-keel, all-flexible parawings. The flat planform was held nearly constant for the main series of parawings, the nose cutoff being about 20-percent keel length. In a subseries of parawings the center-panel width and hence the nose cutoff was varied. The primary variable in the family of 10 parawings was the arrangement of the twin keels. The limits of variation of the keel flat-planform arrangement were from a Y-shaped arrangement in which the twin keels were merged in the rear part of the parawing to a tapered center-panel arrangement for which the aft ends of the keels were more widely spaced than the front ends of the keels. A practical contoured nose fairing was evaluated on an intermediate model and applied to all the models.

Most of the present work was done in the wind tunnel by the tether-test method. Elevated-platform and helicopter drop tests were also made of two of the parawings to demonstrate stable gliding flight.

The tests of the parawings in the wind tunnel were made at two dynamic pressures. The confluence of lines was held by a clamp. The angle of the sting to which the clamp was attached was varied during the tests. The investigation was made in the 17-foot (5.18-meter) test section of the Langley 300-MPH 7- by 10-foot tunnel. Drop tests were made at the NASA Wallops Station and at the Langley Research Center.

## SYMBOLS

The data presented in this report are referred to the axis system shown in figure 1. The reference area and the reference length used in computing the coefficients are presented in table I.

$c$	reference length, $l_k$ minus nose cutoff
$C_D$	drag coefficient, $\frac{\text{Drag}}{qS}$
$C_L$	lift coefficient, $\frac{\text{Lift}}{qS}$
$C_m$	pitching-moment coefficient, $\frac{\text{Pitching moment}}{qSc}$
$C_R$	resultant-force coefficient, $\sqrt{C_L^2 + C_D^2}$
$C_T$	tension coefficient, $\frac{\text{Line tension}}{qS}$
$L/D$	lift-drag ratio, $\frac{C_L}{C_D}$
$l_k$	keel length of theoretical parawing-canopy flat planform, measured from theoretical apex to trailing edge at plane of symmetry, ft (m)
$l/l_k$	nondimensional length of keel and leading-edge suspension lines, measured from parawing to top of clamp, $\frac{\text{Line length}}{l_k}$
$\Delta l / l_k$	incremental nondimensional length of a line
$q$	free-stream dynamic pressure, lb/ft <sup>2</sup> (N/m <sup>2</sup> )
$S$	area of parawing-canopy flat planform, ft <sup>2</sup> (m <sup>2</sup> )

$x_k, x_{le}$	parawing keel and leading-edge linear dimensions, respectively, ft (m)
$x/l_k$	line attachment point along parawing keel or leading edge, $x_k/l_k$ or $x_{le}/l_k$
$\alpha$	angle of support sting measured from direction of windstream to sting center line, deg
$\alpha_w$	angle of keel line number 8 measured from normal to windstream when viewed from side, positive for rearward displacement of line, deg (for the model with the solid nose fairings, keel line number 9 was used)
$\Lambda_0$	angle of sweepback of leading edge of parawing-canopy flat planform, deg

#### DESCRIPTION OF MODELS

##### Wind-Tunnel Models

Flat-planform drawings of the 10 models tested are shown in figure 2. A more detailed drawing of each model is presented just prior to presentation of the associated aerodynamic data, and the line lengths used in the tests are plotted with the aerodynamic data. Pertinent model geometric characteristics are given in table I. The models were all of sewed construction. The canopy material was 1.1-oz/yd<sup>2</sup> (37.3-g/m<sup>2</sup>) acrylic-coated rip-stop nylon and had zero permeability. All wind-tunnel models were rigged with 135-lb (600-N) test dacron line which was used because it had low-stretch characteristics.

The models (fig. 2) all had 45° sweepback of the leading edges of the flat planforms, but differed, mainly, in the arrangement of the twin keels and in the amount of nose cutoff. (See table I.) All models, except model 10, can be arranged in two series of wings. Models 1, 2, 3, 5, 6, 8, and 9 form the main series, with constant nose cutoff ( $0.20l_k$ ) and various keel-cant angles; models 4, 5, 6, and 7 form a subseries of parawings varying in center-panel width and hence nose cutoff but all having parallel keels. The center-panel widths for the subseries were as follows:  $0.333 l_k$ , model 4;  $0.400 l_k$ , models 5 and 6; and  $0.462 l_k$ , model 7. The design of model 10 was based on early test results; model 10 had keel-cant angles about the same as those of model 8 and, as discussed subsequently, a modified nose shape.

A change in the sweep of the trailing edge and in the length of the unswept part of the trailing edge resulted from the variation of the twin-keel arrangement. Two keel-line-attachment spacings were used. Models 4, 5, and 7 had the keel lines evenly spaced,

and the other models used an unequal spacing previously used on many single-keel parawings.

The model support fixture is shown in figure 3. Most of the lines were held by the clamp; however, the two aft keel lines passed through the eyebolt and the two wing-tip lines were attached outboard on the crosspiece.

Model 5 was tested with three solid nose fairings in work which led to the air-supported contoured nose fairing, which was incorporated into the design of all the models. Photographs of the solid fairings are shown in figure 4(a), and drawings of these three fairings are given subsequently with the aerodynamic data. Photographs of the contoured nose fairing for model 5 are given in figures 4(b) and 4(c). Photographs of the other models with this fairing are given in figures 5 to 7. (A photograph of model 6 is not shown; however, its appearance is very much the same as model 5 (see fig. 4(b)) since the models differed only in line spacing along the keel.) The details of the darts and ties used to shape the nose fairings of models 1 to 9 are shown in figure 8(a). These details are given for model 10 in figure 8(b). Model 10 had more darts in the center panel than the other parawings and had no darts in the outer panels. Planform drawings are shown with the data for each parawing, but the nose-shape details are not repeated.

#### Flight-Test Models

Wind-tunnel models of parawings 5 and 9 were tested in free flight. Line lengths used in these flight tests are given in table II. In addition, a larger model of parawing 5 planform was constructed and tested in free flight; this larger model had a keel length of 22.76 ft (6.937 m). The canopy for the larger model was made of 2.9-oz/yd<sup>2</sup> (98.3-g/m<sup>2</sup>) nylon cloth, and the lines were nylon of 1000-lb (4448-N) rated strength. The nylon cloth had a permeability of  $10.9 \frac{\text{ft}^3/\text{min}}{\text{ft}^2} \left( 3.32 \frac{\text{m}^3/\text{min}}{\text{m}^2} \right)$  at a pressure of 0.5 in. (1.27 cm) of water.

Weights were used as payloads for the flight tests of models 5 and 9 for which  $l_k = 75$  in. (190.50 cm). The lines were attached to the payload either by an eyebolt or by a frame scaled down from the dimensions in figure 9 to simulate the attachment points of an Apollo spacecraft deck.

A model of the Apollo spacecraft (see fig. 9) was used as a payload for the larger model of parawing 5 planform, for which  $l_k = 22.76$  ft (6.937 m). The lines of this model were attached by connectors to 28-in. (0.71-m) straps which in turn snapped into the eyebolts shown in figure 9(b). The straps were made of nylon webbing of 5500-lb (24 464-N) rated strength. The lines were grouped on the connectors as shown in figure 9(a).

## EXPERIMENTAL PROCEDURE

### Test Conditions

Static wind-tunnel tests were conducted in the 17-foot (5.18-meter) test section of the Langley 300-MPH 7- by 10-foot tunnel. Tests were made at dynamic pressures of  $1.0 \text{ lb}/\text{ft}^2$  ( $47.9 \text{ N}/\text{m}^2$ ) and  $2.0 \text{ lb}/\text{ft}^2$  ( $95.8 \text{ N}/\text{m}^2$ ).

Free-flight tests were made at the Langley Research Center and at Wallops Station from an elevated platform and from a helicopter. Drop tests from the elevated platform were made from a height of 90 ft (27.4 m) with a wing loading of  $0.25 \text{ lb}/\text{ft}^2$  ( $11.97 \text{ N}/\text{m}^2$ ). Drop tests from the helicopter were made from heights of 300 and 500 ft (91.4 and 152.4 m) with a wing loading of  $0.55 \text{ lb}/\text{ft}^2$  ( $26.33 \text{ N}/\text{m}^2$ ).

### Tether-Test Method

Sketches of line attachments to the balance for wind-tunnel tests are shown in figure 3. The line-attachment fixture was mounted to the model support sting, which was varied through the sting-angle range during the tests. Because the model attitude relative to the sting is not fixed, but varies somewhat as the sting is moved, the angle of attack of one of the parawing keel lines  $\alpha_w$  was measured in addition to the sting angle  $\alpha$ . Tests made in this manner are referred to as tether tests and are discussed in reference 1. Tests were made through a range of  $\alpha_w$  limited at the low end of the range (highest lift-drag ratio) by the angle at which the nose started to tuck under and at the high end of the range by model instability. The aft keel lines and/or wing-tip lines were used to adjust the model attitude relative to the sting system. Longitudinal and lateral oscillations at the high angles of attack limited the test range to the values shown in the data figures. Data were obtained by means of a six-component strain-gage balance.

### Free-Flight Tests

The wind-tunnel model of parawing 5 planform was dropped from the elevated platform either with the lines in a confluence-point configuration (attached to a single eye-bolt) or with the lines separated to simulate the deck attachment configuration of the Apollo spacecraft.

A larger model of parawing 5 planform was dropped from a helicopter, with a model of the Apollo spacecraft (fig. 9) used as a payload. In these tests, the parawing was packed in a cylindrical bag which was placed in a receptacle provided in the Apollo model (fig. 9(b)). A bomb shackle attached to the helicopter was used to hold the spacecraft and release it in flight (fig. 10). A static line was used to break the pack out of

the spacecraft and deploy the parawing. The details of the drop equipment and procedures are reported in reference 9, and test conditions are given in table III.

### Line-Tension Measurements

Line-tension measurements were made with a hand-held tensiometer developed and described in reference 1. The tensiometer had a wide range of sensitivity. The measurements were made at dynamic pressures of 1.0 and 2.0 lb/ft<sup>2</sup> (47.9 and 95.8 N/m<sup>2</sup>).

### Corrections

Jet-boundary corrections to angle of attack and drag coefficient and blocking corrections to dynamic pressure have been applied to the wind-tunnel results. The jet-boundary corrections were determined from reference 10, and the blocking corrections were determined from reference 11.

## PRESENTATION OF DATA

The present results were obtained in an investigation of a number of similar models. In order to avoid possible confusion in matching results with configurations, the data for each model are preceded by a detailed drawing of the model. The data consist of longitudinal aerodynamic characteristics over a sting-angle range, angle-of-attack variation of one of the parawing keel lines, and line lengths and rigging variations. Line-tension coefficients are presented for models 5 and 9. The results are summarized in a plot of lift-drag ratio of the models as a function of resultant-force coefficient.

The data and model drawings are presented in the following figures:

	Figure
Solid nose fairings:	
Sketch of model 5 with solid nose fairings . . . . .	11
Effect of nose fairings . . . . .	12
Model 1:	
Sketch of model . . . . .	13
Effect of dynamic pressure . . . . .	14
Effect of aft-keel-line shortening . . . . .	15
Effect of tip-line and aft-keel-line shortening . . . . .	16
Model 2:	
Sketch of model . . . . .	17
Effect of dynamic pressure . . . . .	18

	Figure
Effect of aft-keel-line shortening . . . . .	19
Effect of tip-line and aft-keel-line shortening . . . . .	20
<b>Model 3:</b>	
Sketch of model . . . . .	21
Effect of dynamic pressure . . . . .	22
Effect of aft-keel-line shortening . . . . .	23
Effect of tip-line and aft-keel-line shortening . . . . .	24
<b>Model 4:</b>	
Sketch of model . . . . .	25
Effect of dynamic pressure . . . . .	26
<b>Model 5:</b>	
Sketch of model . . . . .	27
Effect of dynamic pressure . . . . .	28
Effect of dynamic pressure (check tests) . . . . .	29
Effect of tip-line and aft-keel-line shortening ( $C_T$ included) . . . . .	30
<b>Model 6:</b>	
Sketch of model . . . . .	31
Effect of dynamic pressure . . . . .	32
Effect of aft-keel-line shortening . . . . .	33
Effect of tip-line and aft-keel-line shortening . . . . .	34
Effect of dynamic pressure (rerigged model) . . . . .	35
<b>Model 7:</b>	
Sketch of model . . . . .	36
Effect of dynamic pressure	
Six-line leading-edge configuration . . . . .	37
Five-line leading-edge configuration . . . . .	38
<b>Model 8:</b>	
Sketch of model . . . . .	39
Effect of dynamic pressure . . . . .	40
<b>Model 9:</b>	
Sketch of model . . . . .	41
Effect of dynamic pressure ( $C_T$ included) . . . . .	42
<b>Model 10:</b>	
Sketch of model . . . . .	43
Effect of dynamic pressure . . . . .	44

	Figure
Effect of aft-keel-line shortening . . . . .	45
Effect of tip-line and aft-keel-line shortening . . . . .	46
Lift-drag ratio as a function of resultant-force coefficient:	
Effect of control-line shortening . . . . .	47
Effect of center-panel width . . . . .	48
Effect of keel-cant angle . . . . .	49
Comparison of line-tension coefficients for single- and twin-keel parawings . . . . .	50

## DISCUSSION

### Application of Nose Fairing

As shown in figure 11, several solid fairings were used at the leading edge of the center panel of model 5. Photographs of model 5 with solid nose fairings, taken during tunnel tests, are shown in figure 4(a). The results of the tests are shown in figure 12. Increases in lift-drag ratio and angle-of-attack range are indicated as the fairing diameter is increased.

Because any solid material would add to the packing volume of the parawing, a cloth fairing held by string ties and supported by local air pressure was applied to all the parawings. The flap used to form the solid fairings and the front keel lines were removed. As sketched in figure 8, darts were taken in the nose area to shape or contour this area, and ties were added to stabilize the edge of the cloth. Photographs of the contoured nose fairing on model 5 are shown in figures 4(b) and 4(c). All the models were made with fairings similar to this one.

### Effect of Dynamic Pressure

The basic longitudinal aerodynamic characteristics of the 10 models investigated along with the rigging determined in the tether tests are presented in figures 13 to 46. Each wing was tested at dynamic pressures of 1.0 and 2.0 lb/ft<sup>2</sup> (47.9 and 95.8 N/m<sup>2</sup>). Typically, the results show a shift of the data to a lower  $\alpha_w$  at the higher dynamic pressure (see, for example, fig. 14). This effect was probably the result of stretch of the lines and canopy fabric under the stress of the increased loading and a lessening of the effects of the weight of the fabric in the nose area as the wing weight became a smaller part of the total forces on the wing. The maximum lift-drag ratio and resultant-force coefficient at the higher dynamic pressure were equal to or greater than the values shown for the lower dynamic pressure in most cases. Therefore, the discussion of various control-line settings is generally given throughout this paper for only the higher dynamic pressure.

## Performance

Comparison of models with various keel-cant angles.- The results obtained from models with various keel-cant angles (models 1, 2, 3, 5, 8, 9, and 10) are presented in figure 49. In general, the lowest values of lift-drag ratio were obtained with model 1, which had the aft ends of the keels canted inward to form a Y-shaped arrangement. Model 1 had a maximum lift-drag ratio of about 2.6. As the aft ends of the keels were swung outward from this position (models 2, 3, and 5), lift-drag ratio and resultant-force coefficient increased. Increasing the cant angle beyond a parallel-keel arrangement (models 8, 9, and 10) increased lift-drag ratio slightly, but reduced the resultant-force coefficient appreciably. Model 9 had the highest lift-drag ratio (3.2 at  $C_R \approx 0.75$ ); however, model 5 had lift-drag ratios nearly as high and they were indicated over a higher range of  $C_R$ . Model 10, which had a modified nose shape and a keel-cant angle about the same as that of model 8, did not show an improvement in characteristics over those of model 8.

The values of lift-drag ratio and resultant-force coefficient obtained for the better twin-keel parawings, show considerable improvement over values for small-scale single-keel parawings, for which  $L/D \approx 2.4$  at  $C_R = 0.92$  is typical (ref. 12).

Flight testing.- Models 5 and 9 were dropped from an elevated platform about 90 ft (27.43 m) high. The resulting flights indicated good lift-drag ratio and stability. The line lengths for flight were the same as for tether tests in the tunnel except that the control lines had to be lengthened. This has been the general experience in flight testing models for which the rigging was determined in tunnel tests. By comparing the line lengths for model 5 in table II with those in figure 28, it is found that an increase in the aft-keel-line length of about  $0.04 l_k$  and an increase in tip-line length of about  $0.07 l_k$  was necessary to rig for free flight.

In helicopter drop tests the small-scale rigging determined in the elevated-platform drop tests was used for the model of parawing 5 planform having the 22.76-ft (6.937-m) keel length. This parawing model was attached to an approximately 1/4-scale Apollo spacecraft. This configuration was not provided with controls, but was tested at Wallops Station with the use of equipment and techniques described in reference 9. A record of the tests is given in table III. As shown, the parawing with no turn (flight 1) and with moderate turn (flight 3) had vertical velocities of 12.74 and 10.13 ft/sec (3.88 and 3.09 m/sec); however, the wing with a high rate of turn (flight 2) had a vertical velocity of 21.05 ft/sec (6.42 m/sec). These results confirm other observations of parawings in turns, for which a high rate of descent in sharp turns has been noted.

Results of extensive free-flight tests of both a single-keel parawing and twin-keel parawings were reported in references 6 and 7. The stable free-flight characteristics of the twin-keel parawings indicated in the very limited free-flight results of the present

paper were confirmed in these references, and the twin-keel parawing was judged relatively easy to fly (as compared with the single-keel parawing) and capable of holding a heading for long periods of time without control inputs.

Comparison of parallel-keel parawings with various center-panel widths.- The results for models 4, 5, 6, and 7 are plotted in figure 48 for two dynamic pressures. The widths of the center panels for these models were as follows:  $0.333 l_k$ , model 4;  $0.400 l_k$ , models 5 and 6; and  $0.462 l_k$ , model 7. Models 5 and 6 differed only in keel-line location. A lift-drag ratio of 3.17 is shown for model 4 at a resultant-force coefficient of 0.81 for the lower dynamic pressure (fig. 48(a)). Test results in figure 48(b) show that at the higher dynamic pressure, model 5 had a maximum value of lift-drag ratio of 2.95, which was nearly as high as the maximum value of 3.00 shown for the model 4, and that this value for model 5 occurred at a much higher resultant-force coefficient ( $C_R \approx 0.95$ ) than did the maximum value for model 4.

Effect of control-line changes.- Tests were conducted for some of the models with different lengths of keel control lines (aft keel lines) or with different lengths of all four rear lines (tip lines and aft keel lines). The values of lift-drag ratio for these tests are plotted as functions of resultant-force coefficient in figure 47. As shown in the figure, shortening only the aft keel lines decreased the maximum lift-drag ratio somewhat and increased the values of maximum resultant-force coefficient. The maximum value of  $C_R$  obtained in the present study was 1.28 (at  $L/D = 2.0$ ) for model 3. Pulling in all the control lines should essentially shift the range of sting angle of attack in which the parawing operates and, therefore, result in a series of coinciding curves for  $L/D$  as a function of  $C_R$ . The curves in figure 47 for all control lines shortened do not exactly coincide, but generally support the expected result, as shown, for example, in figure 47(c).

#### Comparison With Results of Previous Large-Scale Tests

Parawings with the model 5 planform have been tested previously, and the results are reported in references 6, 7, and 8. Tests of a parawing with a 15-ft (4.572-m) keel length are reported in references 6 and 8; tests of a parawing with a 22.7-ft (6.919-m) keel length are also reported in reference 6; and tests of a parawing with a 72.0-ft (21.946-m) keel length are reported in reference 7. The rigging determined in these tests was essentially the same as that determined in the present tests; however, a higher value of lift-drag ratio (3.4) was reported in reference 6 and a slightly lower value (2.8) was obtained in the tests of reference 7. When flight tests were made for the parawing with a 22.7-ft (6.937-m) keel length (ref. 6), it was found that the tip lines could be best set at  $0.617 l_k$  and the aft keel lines at  $0.916 l_k$ . This result indicates that the tip-line setting during the previously discussed elevated-platform tests of model 5 may have been nearly  $0.08 l_k$  too long. The small-scale wind-tunnel tests and elevated-platform flight tests were found adequate to determine the basic rigging for the large-scale tests.

### Comparison With Line-Tension Coefficients of a Single-Keel Model

Line-tension coefficients were measured for parawings 5 and 9, and the results are included in figures 30 and 42. Results from reference 1 for a single-keel parawing and values obtained for twin-keel model 5 are compared in figure 50. Note that although the test points in these figures are connected by lines for clarity they represent discrete line loads. The measurements indicated that there was a high loading (high line-tension coefficient) near the front of the keels of the twin-keel parawing and that this loading decreased toward the trailing edge of the parawing. The character of this loading differs considerably from the loading on the keel of the single-keel parawing (see fig. 50). Similar characteristics of loading are shown for the leading-edge lines of the single-keel and twin-keel models.

The differences shown in the general level of the values of  $C_T$  for the two parawing planforms may be explained by the differences in the number of lines and in the distribution of loads for a single-keel and a twin-keel parawing of the same area at the same dynamic pressure. The area of the triangular panels of the twin-keel parawing is 60 percent of the area of the similar panels of the single-keel parawing. Therefore, if the distribution of loads in the lines attached to the triangular panels of a single-keel parawing and of a twin-keel parawing is about the same, then the line-tension coefficient for the leading-edge lines on the twin-keel parawing would be about 60 percent of that for the corresponding lines on the single-keel parawing. The loads from the center panel of the twin-keel parawing and from the triangular panels acting on the keel lines should also be about 60 percent of the line loads of the single-keel parawing if calculated on a constant-load-per-unit-area basis. This reduced loading and the more even distribution of the loads on the lines account for the apparently low values of line-tension coefficients shown for the twin-keel parawing.

### CONCLUDING REMARKS

An investigation has been made in the 17-foot (5.18-meter) test section of the Langley 300-MPH 7- by 10-foot tunnel and in free flight to obtain the rigging and aerodynamic characteristics of a series of twin-keel parawings designed to have increased lift-drag ratio and usable lift-coefficient range as compared with a single-keel parawing.

The maximum observed lift-drag ratios of the models ranged from 2.6 to 3.2. The model with the center panel which tapered from 40-percent keel length at the nose to 80-percent keel length at the trailing edge had the highest lift-drag ratio. The resultant-force coefficient for this model was about 0.75 at the maximum lift-drag ratio. Maximum resultant-force coefficient was increased and maximum lift-drag ratio was decreased by shortening the aft keel lines. The maximum value of resultant-force coefficient shown for the series of models was 1.28 (at a lift-drag ratio of 2.0); this value was obtained for the model with the center panel which tapered from 40-percent keel length at the leading

edge to 20-percent keel length at the trailing edge. The model with parallel keels and a center-panel width of 40-percent keel length reached a lift-drag ratio of 2.95 at a resultant-force coefficient of 0.95.

Line-load measurements indicated a high loading at the front of the keels and a decrease in loading toward the trailing edge of the parawing. This keel loading differs significantly from previously reported measurements on a single-keel model. The leading-edge line loads were similar for the twin- and single-keel parawings.

Results of a limited flight-test program indicated that the twin-keel parawing would glide when the rigging, except for control-line length, was set as determined in the small-scale wind-tunnel tests.

Langley Research Center,  
National Aeronautics and Space Administration,  
Hampton, Va., June 5, 1970.

## REFERENCES

1. Naeseth, Rodger L.; and Fournier, Paul G.: Low-Speed Wind-Tunnel Investigation of Tension-Structure Parawings. NASA TN D-3940, 1967.
2. Bugg, Frank M.; and Sleeman, William C., Jr.: Low-Speed Tests of an All-Flexible Parawing for Landing a Lifting-Body Spacecraft. NASA TN D-4010, 1967.
3. Heinrich, H. G.; Neitz, Thomas; and Lippa, Harvey: Aerodynamic Characteristics of the Parafoil Glider and Other Gliding Parachutes. RTD-TDR-63-4022, U.S. Air Force, Apr. 1964. (Available from DDC as AD-600861.)
4. Weiberg, James A.; and Mort, Kenneth W.: Wind-Tunnel Tests of a Series of Parachutes Designed for Controllable Gliding Flight. NASA TN D-3960, 1967.
5. Rogallo, Francis M.: NASA Research on Flexible Wings. Paper presented at International Congress of Subsonic Aeronautics (New York), Apr. 1967.
6. Linhart, E. M.; and Buhler, W. C.: Wind-Tunnel and Free Flight Investigation of All-Flexible Parawings at Small Scale. NASA CR-66879, 1969.
7. Moeller, J. H.; Linhart, E. M.; Gran, W. M.; and Parson, L. T.: Free Flight Investigation of Large All-Flexible Parawings and Performance Comparison With Small Parawings - Final Report. NASA CR-66918, 1970.
8. Ware, George M.: Wind-Tunnel Investigation of the Aerodynamic Characteristics of a Twin-Keel Parawing. NASA TN D-5199, 1969.
9. Naeseth, Rodger L.: Model Wind-Tunnel and Flight Investigation of a Parawing-Lifting-Body Landing System. NASA TN D-5893, 1970.
10. Gillis, Clarence L.; Polhamus, Edward C.; and Gray, Joseph L., Jr.: Charts for Determining Jet-Boundary Corrections for Complete Models in 7- by 10-Foot Closed Rectangular Wind Tunnels. NACA WR L-123, 1945. (Formerly NACA ARR L5G31.)
11. Herriot, John G.: Blockage Corrections for Three-Dimensional-Flow Closed-Throat Wind Tunnels, With Consideration of the Effect of Compressibility. NACA Rep. 995, 1950. (Supersedes NACA RM A7B28.)
12. Fournier, Paul G.; and Sleeman, William C., Jr.: Wind-Tunnel Studies of Effects of Construction Methods, Design Details, and Canopy Slots on the Aerodynamic Characteristics of Small-Scale All-Flexible Parawings. NASA TN D-5974, 1970.

TABLE I.- GEOMETRIC CHARACTERISTICS OF TWIN-KEEL MODELS

Model number	$l_k$ , in. (cm)	c, in. (cm)	Flat span, in. (cm)	$S, ft^2 (m^2)$
1	75.0 (190.50)	60.0 (152.40)	114.9 (291.85)	28.35 (2.634)
2	75.0 (190.50)	60.0 (152.40)	114.9 (291.85)	28.35 (2.634)
3	75.0 (190.50)	60.0 (152.40)	114.9 (291.85)	29.26 (2.718)
4	72.0 (182.88)	60.0 (152.40)	108.9 (276.60)	27.86 (2.588)
5	75.0 (190.50)	60.0 (152.40)	114.9 (291.85)	30.18 (2.804)
6	75.0 (190.50)	60.0 (152.40)	114.9 (291.85)	30.18 (2.804)
7	78.0 (198.12)	60.0 (152.40)	120.9 (307.09)	32.69 (3.037)
8	75.0 (190.50)	60.0 (152.40)	114.9 (291.85)	31.09 (2.888)
9	75.0 (190.50)	60.0 (152.40)	114.9 (291.85)	32.01 (2.974)
10	70.6 (179.32)	60.0 (152.40)	105.9 (268.99)	27.36 (2.542)

TABLE II.- LINE LENGTHS USED IN FLIGHT TESTS

Line	Model 5		Model 9	
	Leading-edge $l/l_k$	Keel $l/l_k$	Leading-edge $l/l_k$	Keel $l/l_k$
Elevated-platform drop tests				
1	0.9275	0.9688	0.9354	0.9948
2	.9062	.9825	.9213	.9921
3	.8879	.9775	.8745	.9790
4	.8413	.9696	.8189	.9743
5	.7767	.9746	.7528	.9638
6	.6971	.9721	.6614	.9517
7		.9788		.9475
8		.9733		.9396
9		.9646		.9286
10		.9571		.9202
11		.9312		.8950
12		.9071		.8719
Helicopter drop tests				
(All lines the same as in elevated-platform tests except aft keel lines and tip lines)				
6	0.6847			
12		0.8897		

TABLE III.- RECORD OF HELICOPTER DROP TESTS AT WALLOPS STATION

[22.76-ft (6.937-m) parawing model 5 and an  
 approximately 1/4-scale Apollo spacecraft]

Measurement	Flight 1	Flight 2	Flight 3
Altitude, ft (m) . . . . .	300.0 (91.4)	300.0 (91.4)	500.0 (152.4)
Flight time, sec . . . . .	18.2	12.0	42.0
Control, $\Delta l/l_k$ . . . . .	0	0.0439 right	0.0330 right
Mass, lb (kg) . . . . .	221.8 (100.6)	221.8 (100.6)	221.8 (100.6)
Vertical velocity, <sup>a</sup> ft/sec (m/sec) . .	12.74 (3.88)	21.05 (6.42)	10.13 (3.09)

<sup>a</sup>Vertical velocity calculated with 100 ft (30.5 m) allowed for deployment of the parawing.

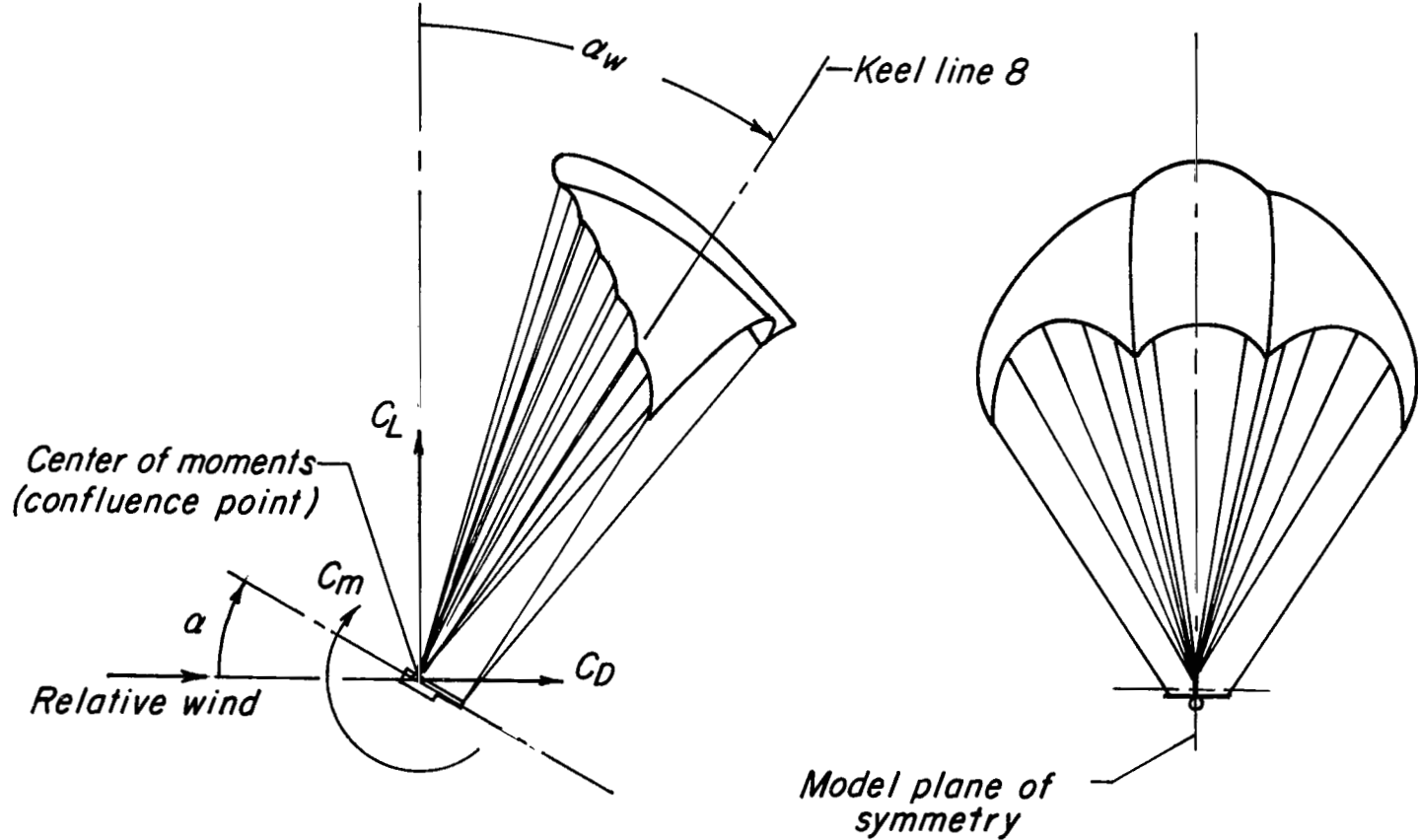
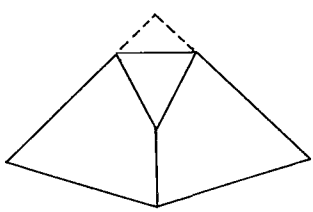
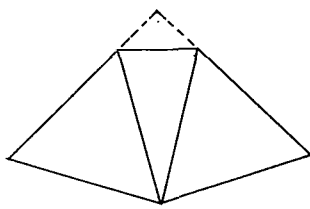


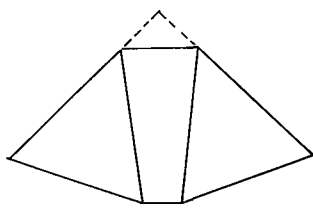
Figure 1.- Sketch showing positive direction of forces, moments, and angles used in presentation of data.



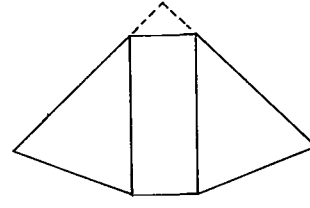
*Model 1*



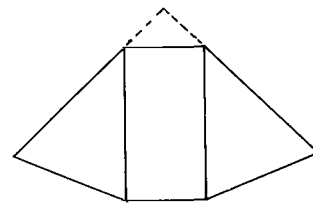
*Model 2*



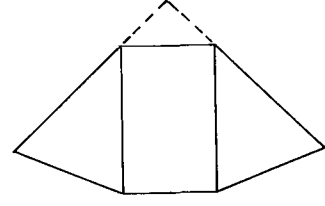
*Model 3*



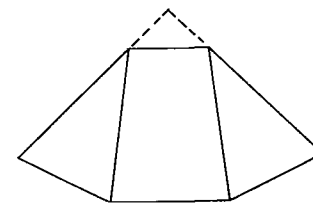
*Model 4*



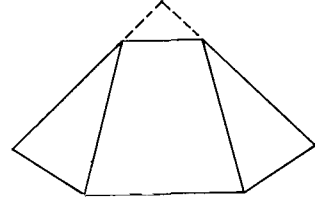
*Models 5 and 6*



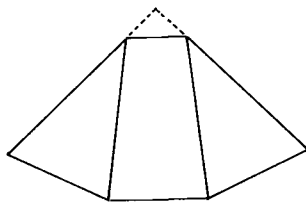
*Model 7*



*Model 8*



*Model 9*



*Model 10*

Figure 2.- Planforms of models tested.

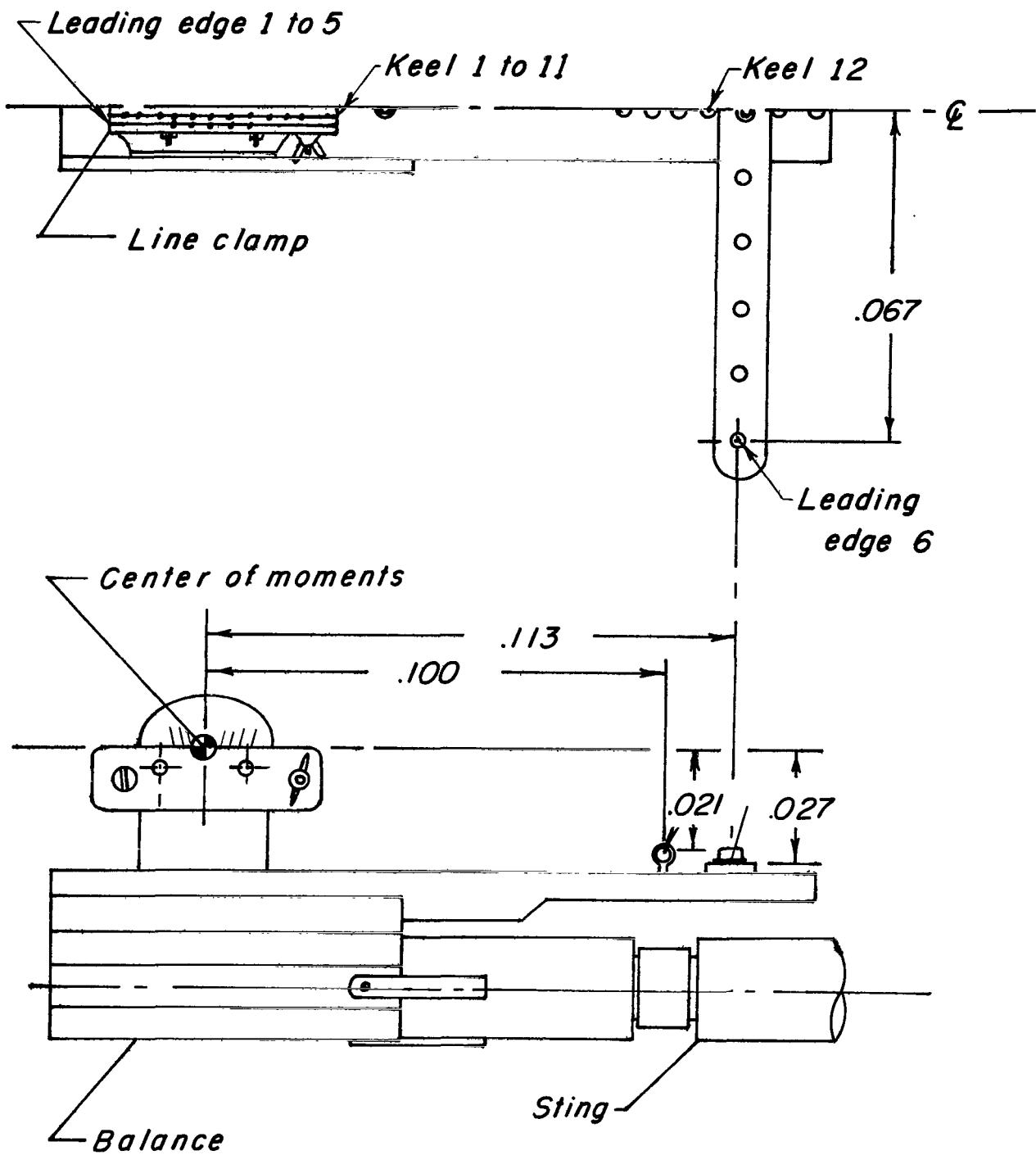
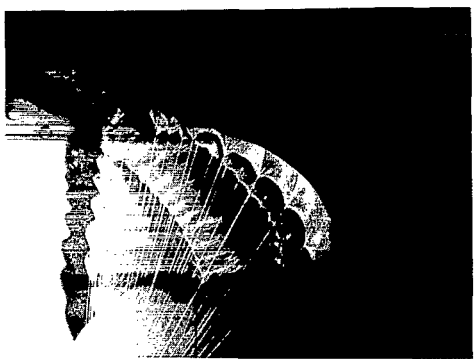
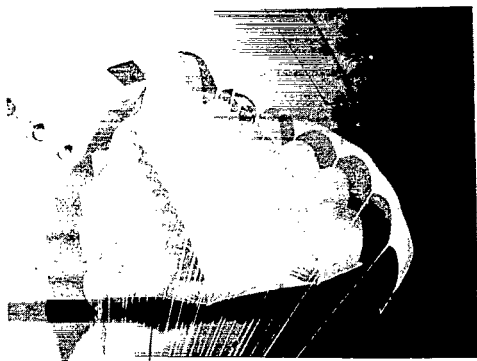
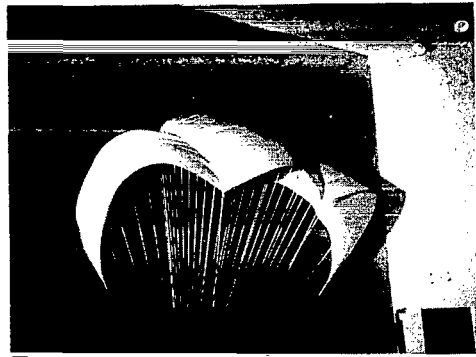
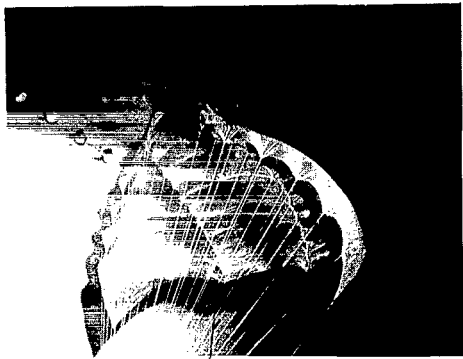


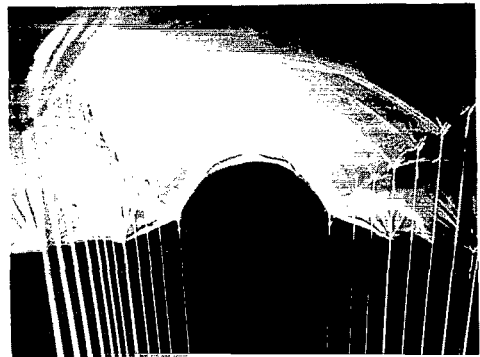
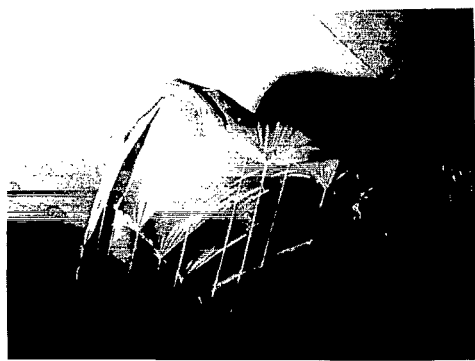
Figure 3.- Parawing line attachments to balance for tunnel tests. (Dimensions are fractions of the twin-keel length for the main series of parawings,  $l_k = 75$  in. (190.50 cm).)



(a) Solid nose fairings.



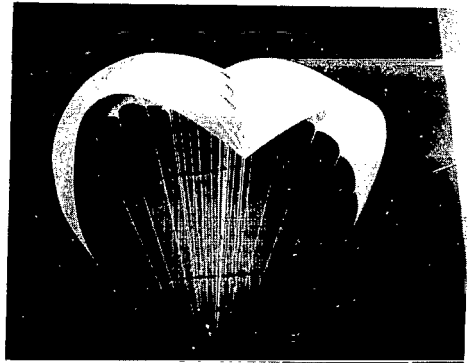
(b) Contoured nose fairing.



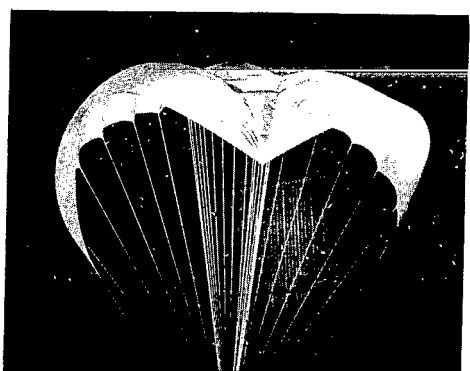
(c) Front and rear enlarged views of contoured nose fairing.

Figure 4.- Photographs of fairings tested on twin-keel model 5.

L-70-1666



(a) Model 1.



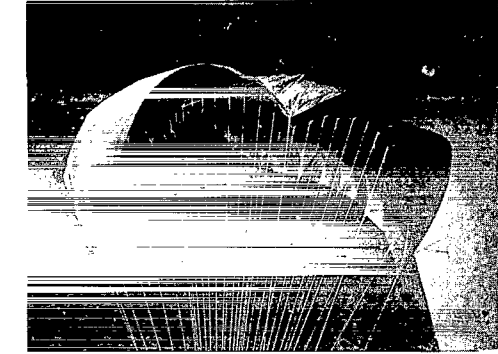
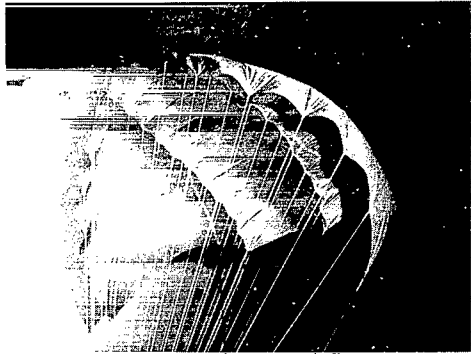
(b) Model 2.



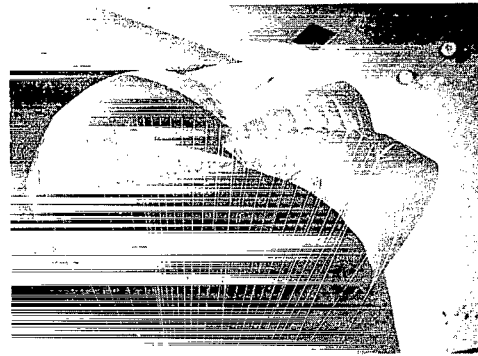
(c) Model 3.

Figure 5.- Photographs of twin-keel models 1, 2, and 3.

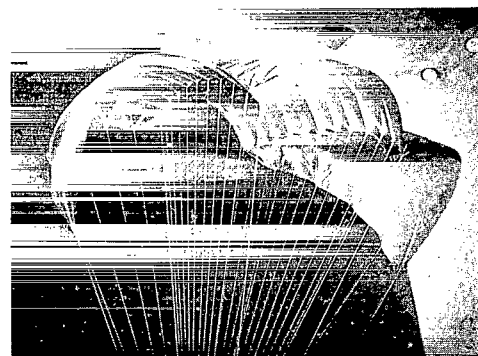
L-70-1667



(a) Model 4.



(b) Model 7 with six leading-edge lines.



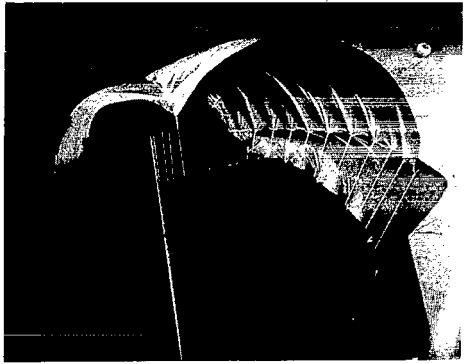
(c) Model 7 with five leading-edge lines.

Figure 6.- Photographs of twin-keel models 4 and 7.

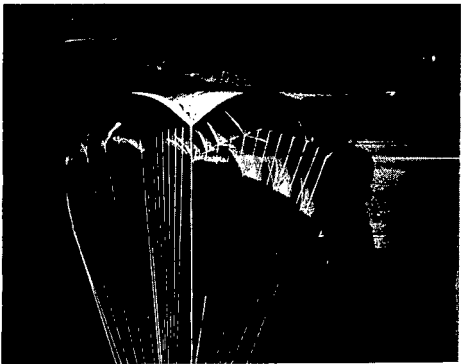
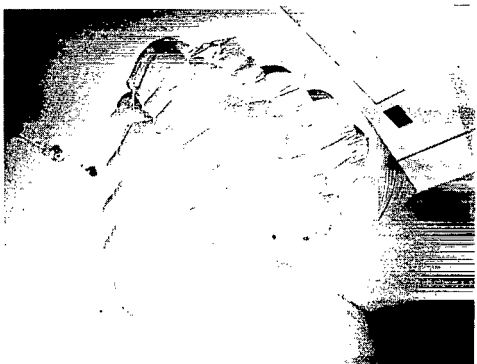
L-70-1668



(a) Model 8.



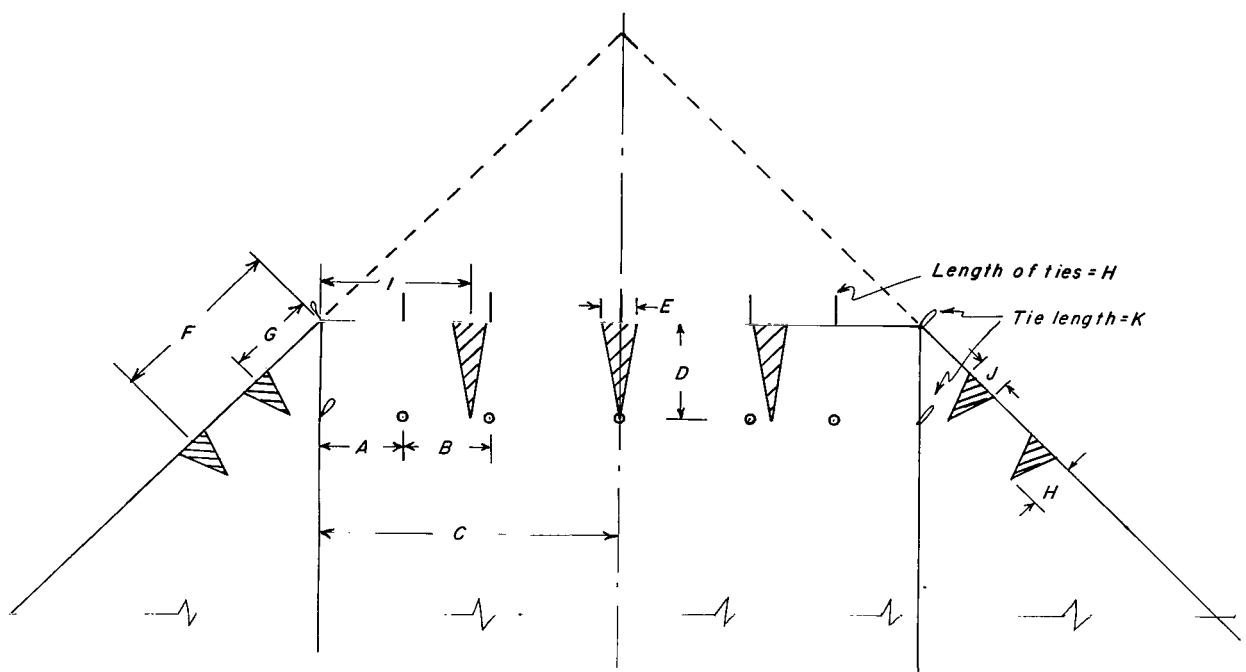
(b) Model 9.



(c) Model 10.

Figure 7.- Photographs of twin-keel models 8, 9, and 10.

L-70-1669

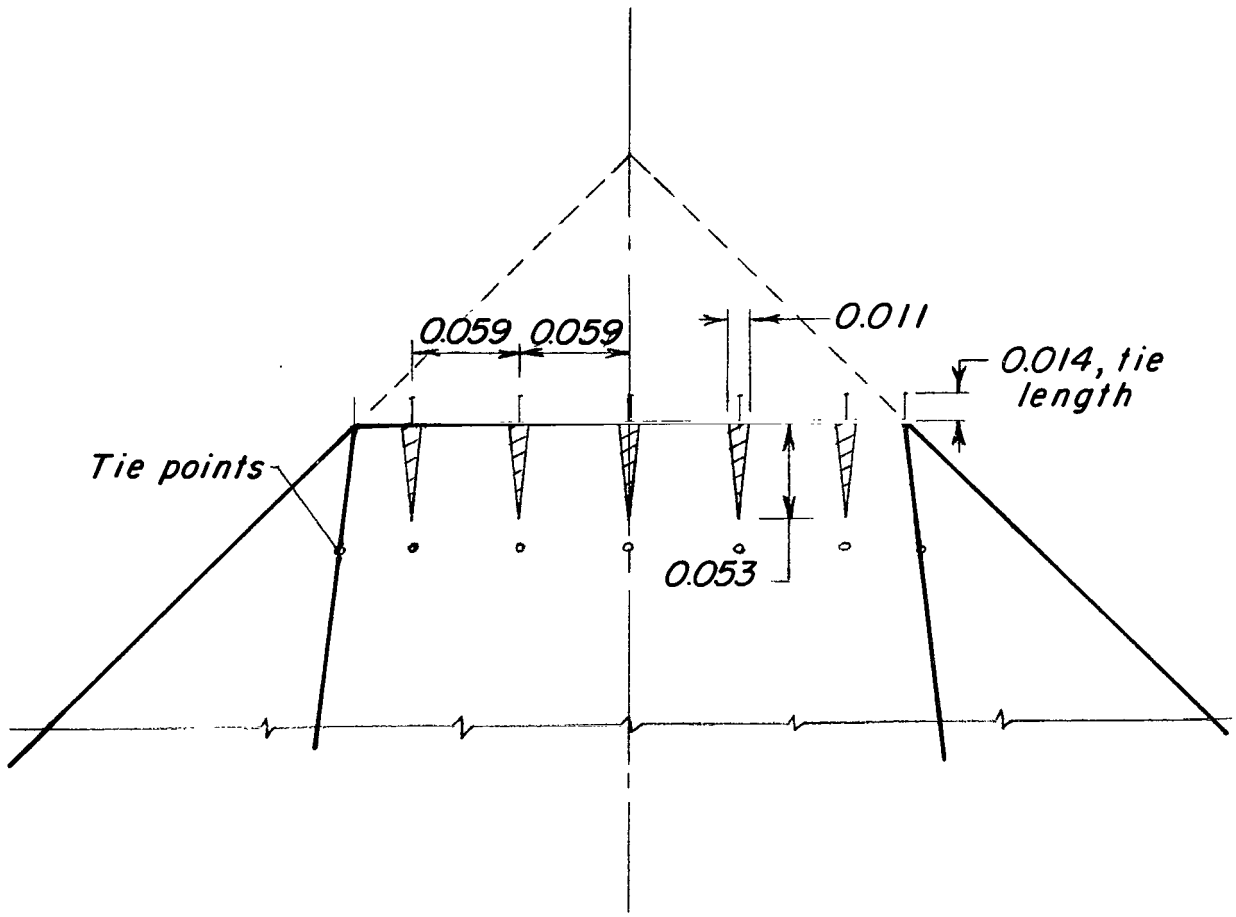


Dimensions in fraction of  $l_k$

Letter dimension	Models 1,2,3,5,6,8,9 $l_k=75\text{ in.}(190.50\text{cm})$	Model 4 $l_k=72\text{ in.}(182.88\text{cm})$	Model 7 $l_k=78\text{ in.}(198.12\text{cm})$
A	0.054	0.045	0.062
B	.063	.052	.073
C	.200	.167	.231
D	.066	.069	.064
E	.017	.014	.019
F	.080	.083	.077
G	.040	.042	.038
H	.026	.028	.025
I	.096	.079	.111
J	.020	.021	.019
K	.022	.023	.021

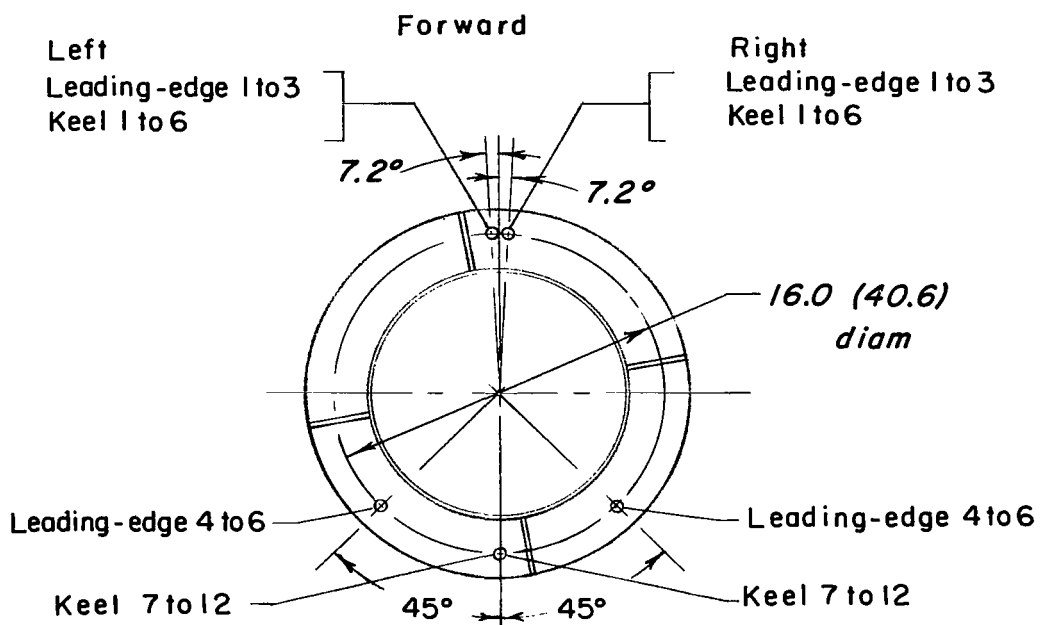
(a) Models 1 to 9.

Figure 8.- Dimensions of darts and ties used in contouring the nose. (All dimensions are in percent keel length; hatched areas indicate darts made to shape the nose.)

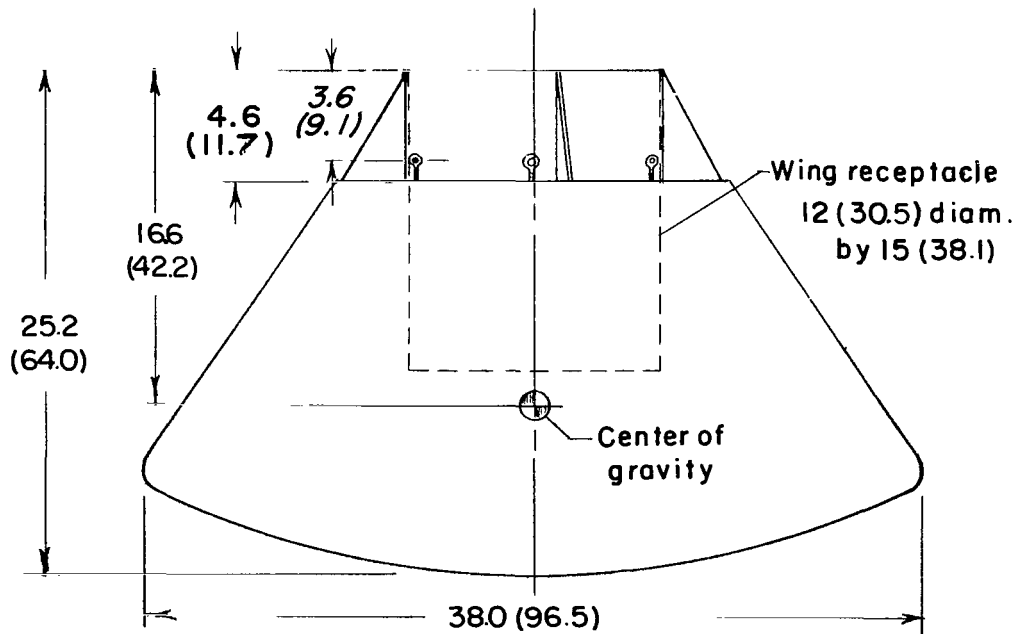


(b) Model 10.

Figure 8.- Concluded.



(a) Details of line attachments.



(b) Side view of Apollo spacecraft model.

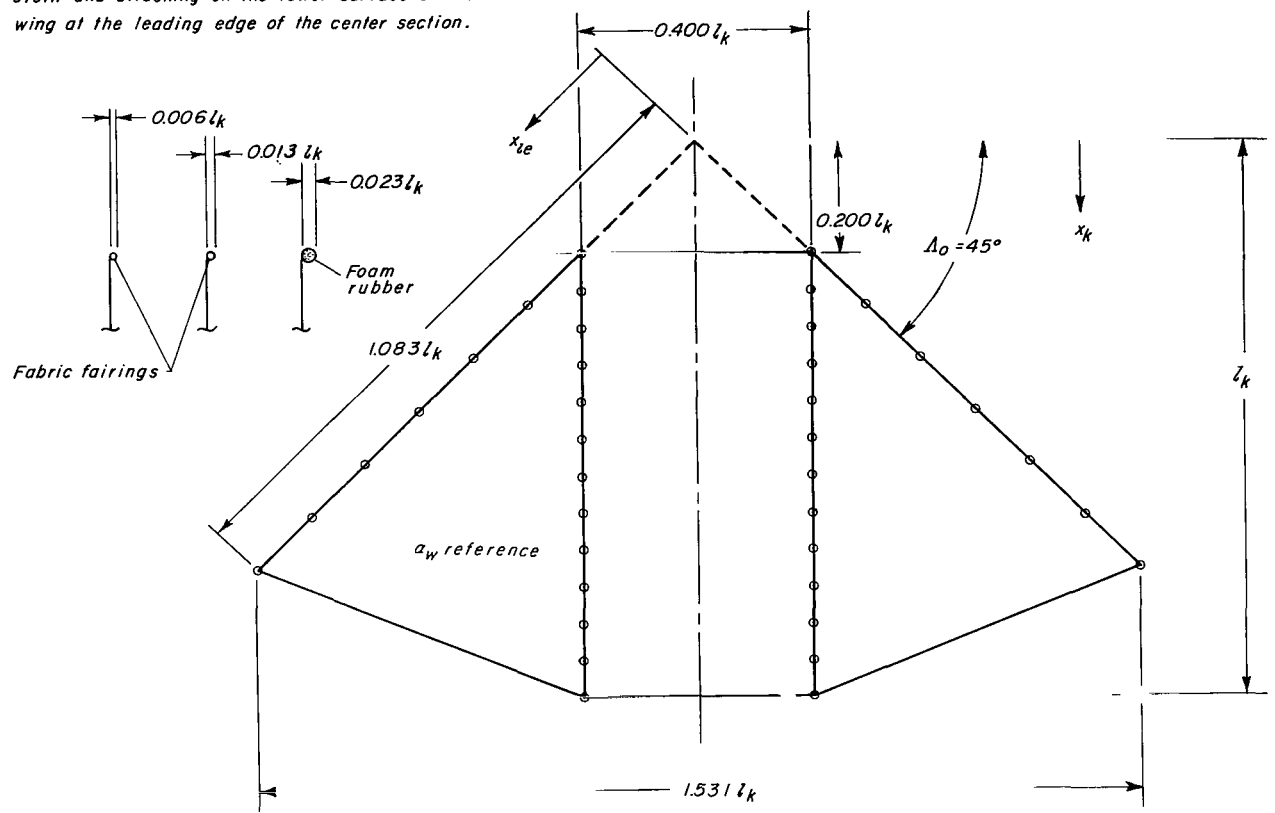
Figure 9.- Line attachments for the larger model of twin-keel parawing 5 used with Apollo spacecraft model as payload. (Dimensions are given in inches and parenthetically in centimeters.)



Figure 10.- Model of Apollo spacecraft mounted on the helicopter.

L-70-1670

Cross sections of nose fairings made by rolling up a  $0.400 l_k$ -span by  $0.106 l_k$ -chord piece of cloth and attaching on the lower surface of the wing at the leading edge of the center section.



Line attachment locations

$x/z_k$

Keel	Leading edge
.200	.416
.267	.549
.333	.683
.400	.816
.466	.949
.533	1.083
.600	
.666	
.733	
.799	
.866	
.933	
1.000	

Figure 11.- Solid nose fairings used on model 5.

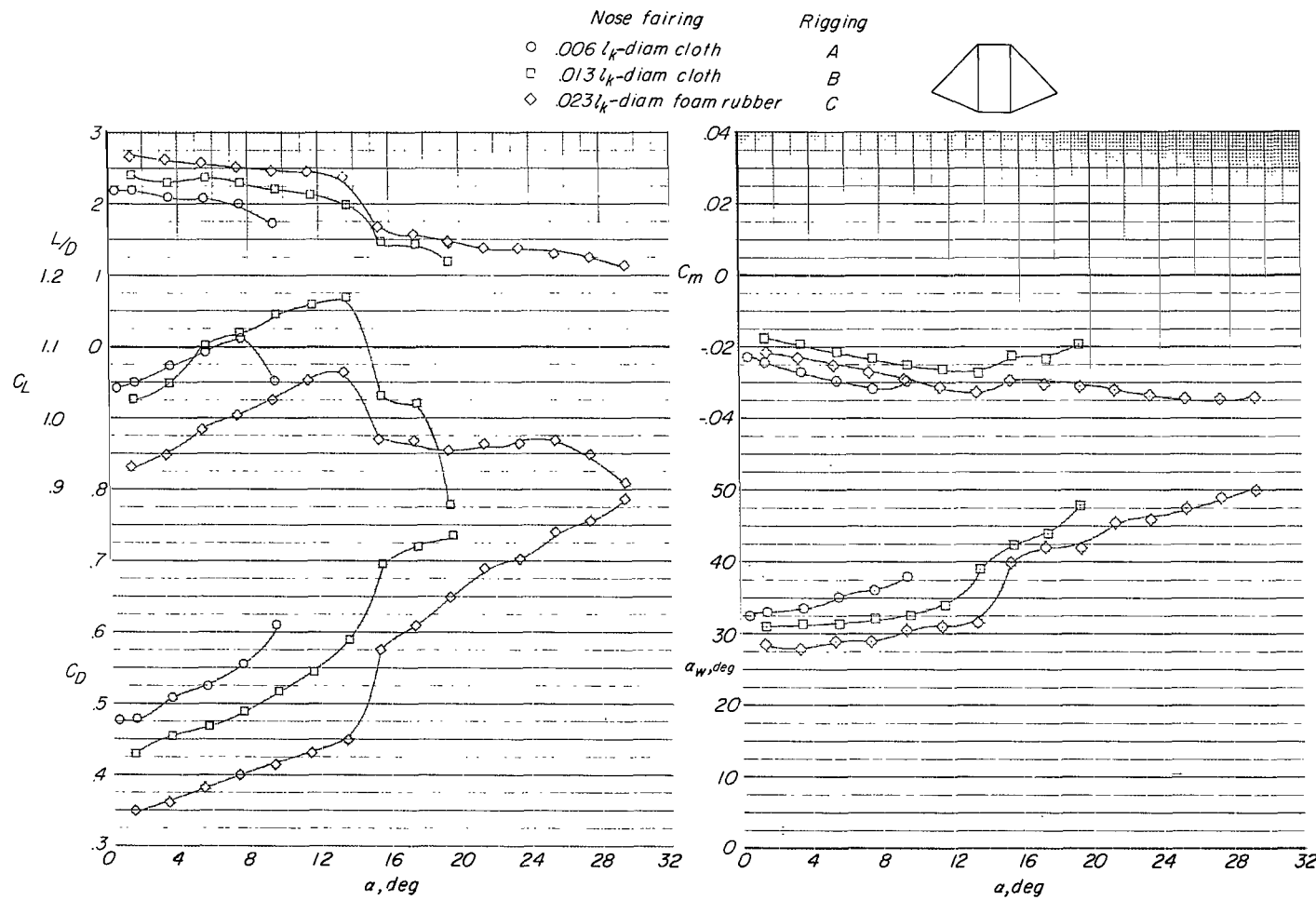


Figure 12.- Aerodynamic characteristics for twin-keel parawing model 5, with each of three solid nose fairings.  $q = 2.0 \text{ lb/ft}^2$  ( $95.8 \text{ N/m}^2$ ).

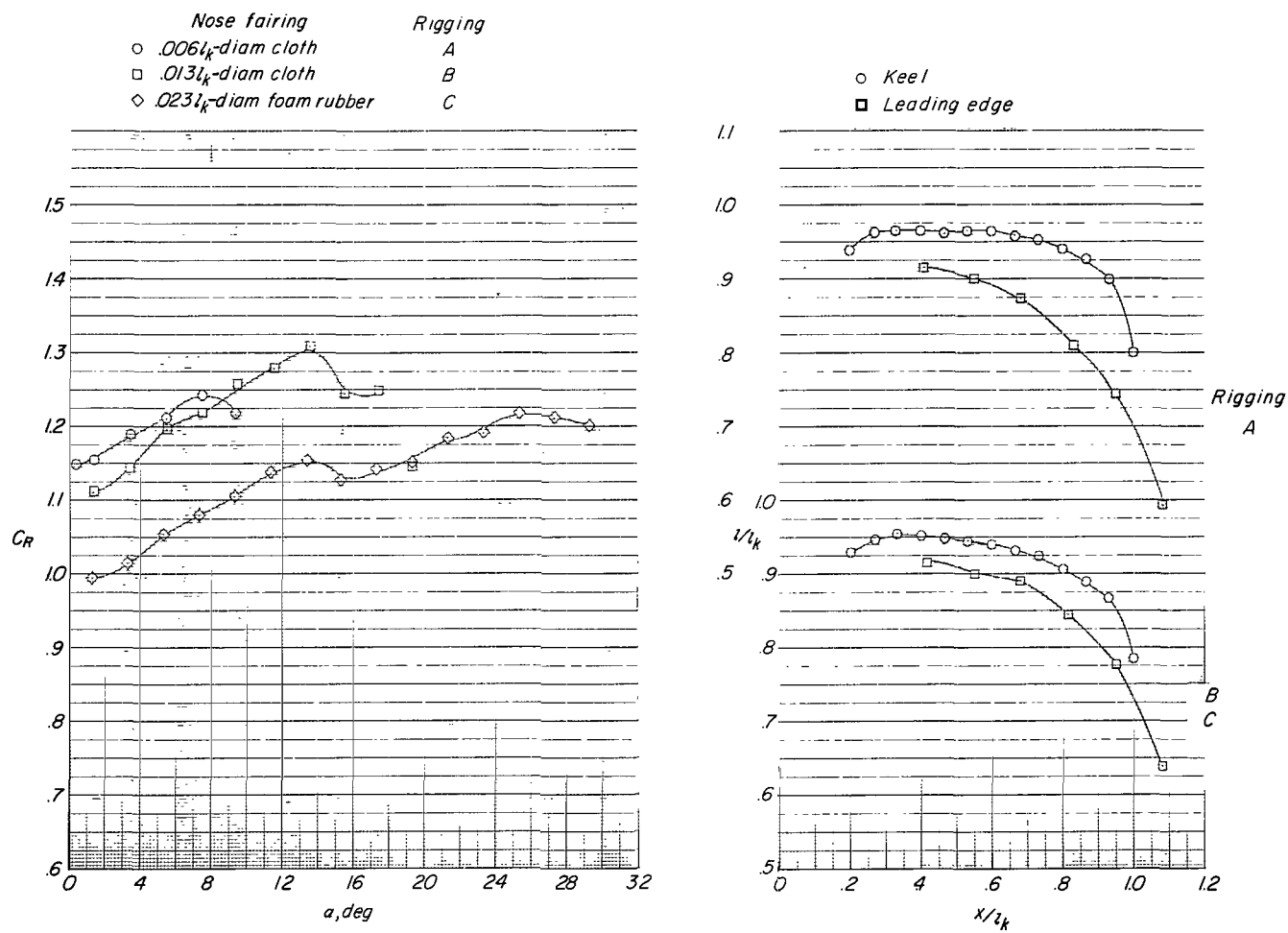
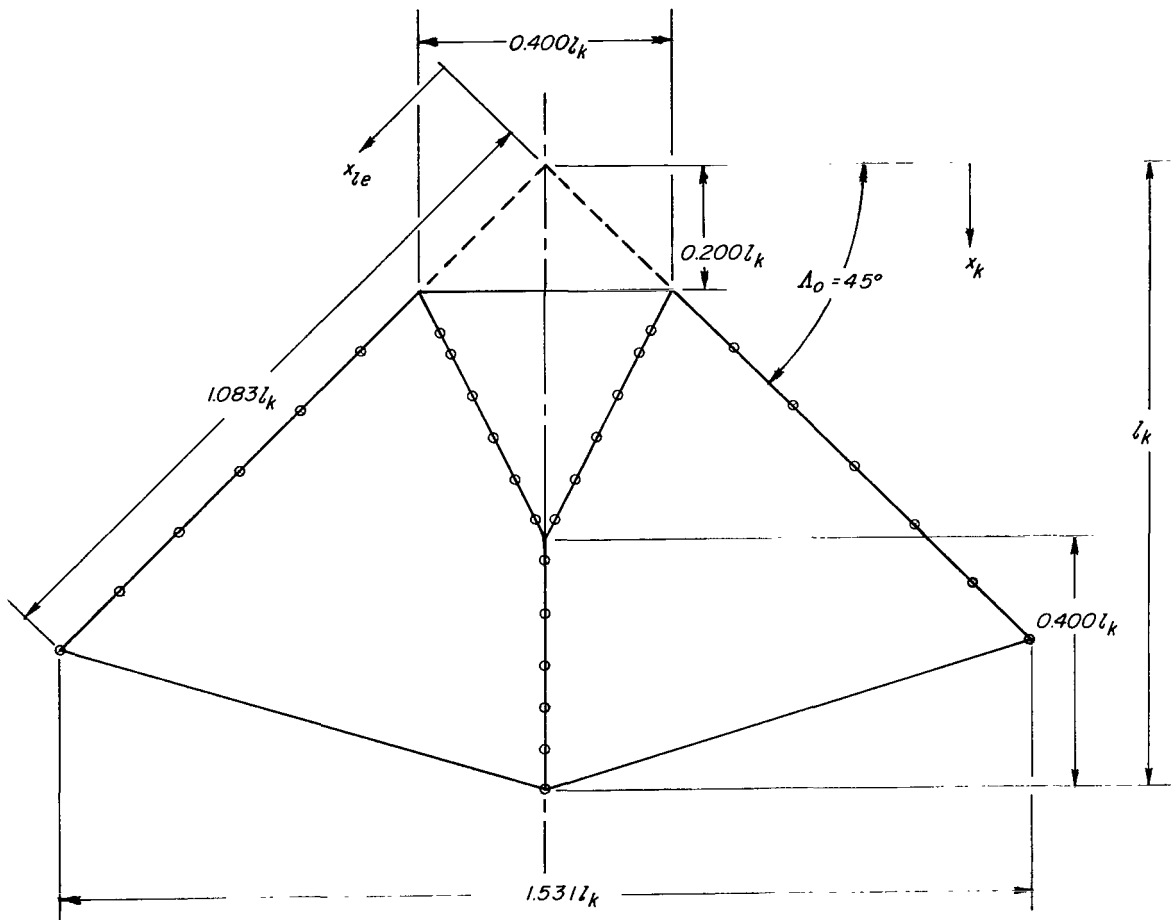


Figure 12.- Concluded.



*Line attachment locations*

$x/l_k$

<i>Kee<i></i></i>	<i>Leading edge<i></i></i>
.266	.416
.300	.549
.366	.683
.434	.816
.500	.949
.567	1.083
.634	
.716	
.800	
.866	
.934	
1.000	

Figure 13.- Flat-planform details of twin-keel parawing model 1.

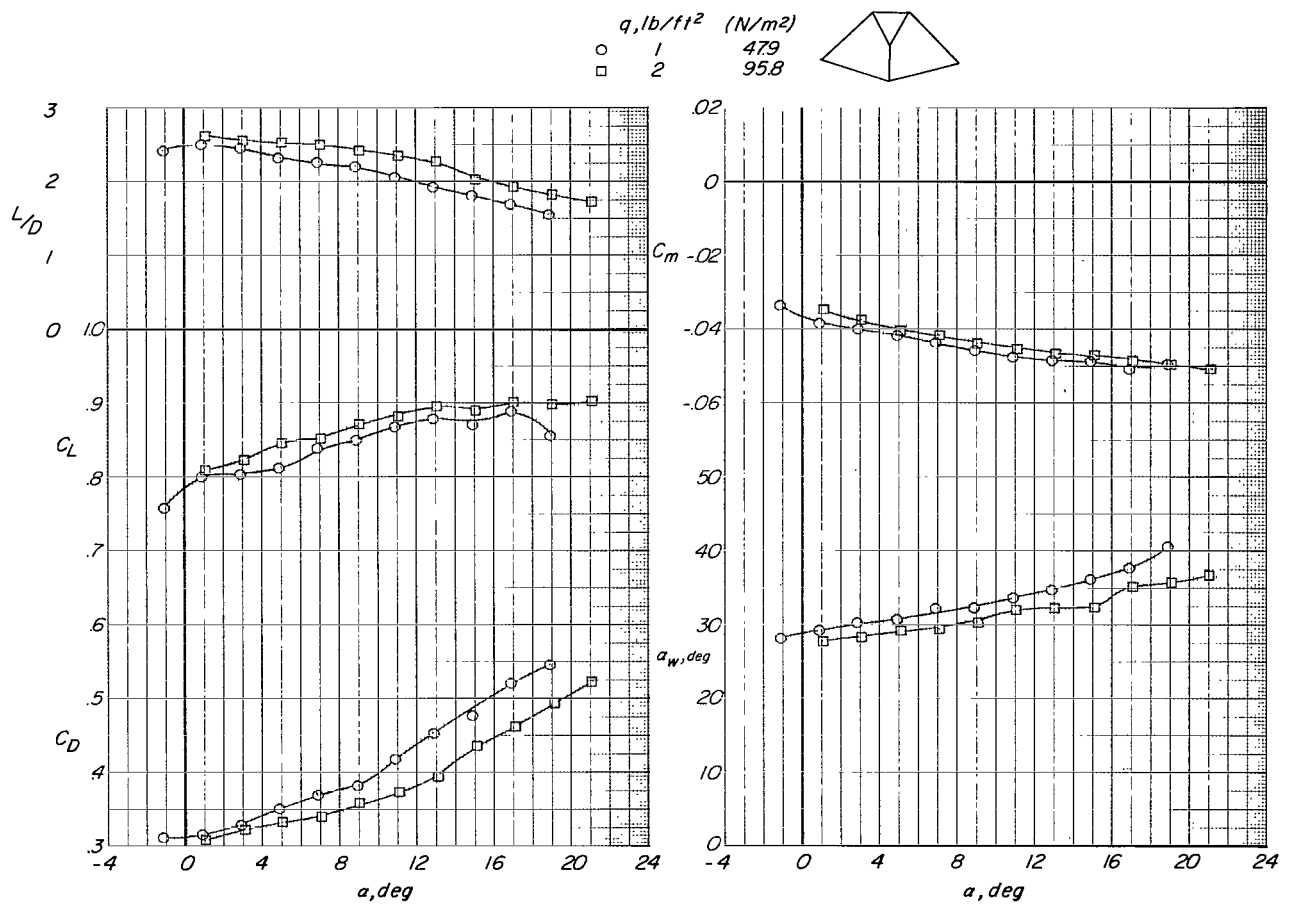


Figure 14.- Effect of dynamic pressure on the aerodynamic characteristics of twin-keel parawing model 1.

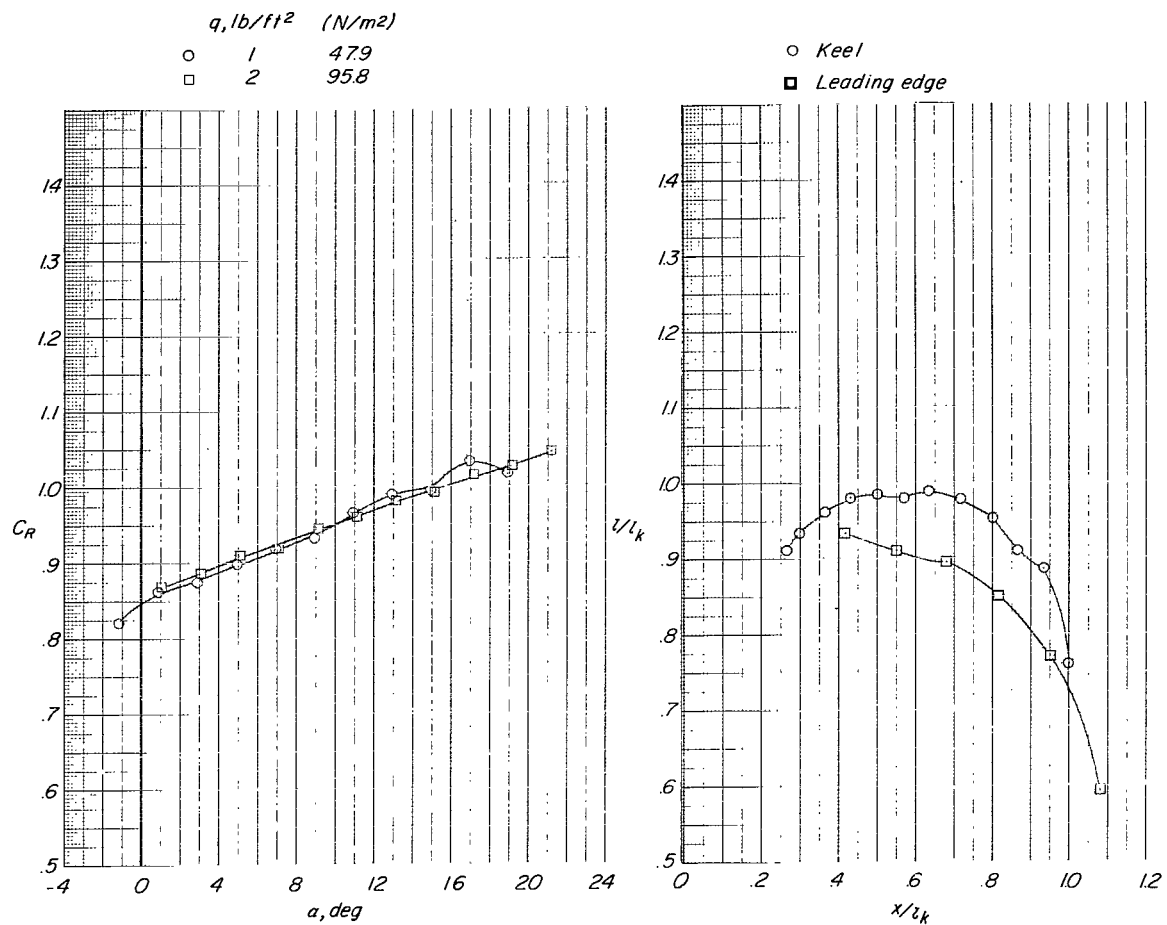


Figure 14.- Concluded.

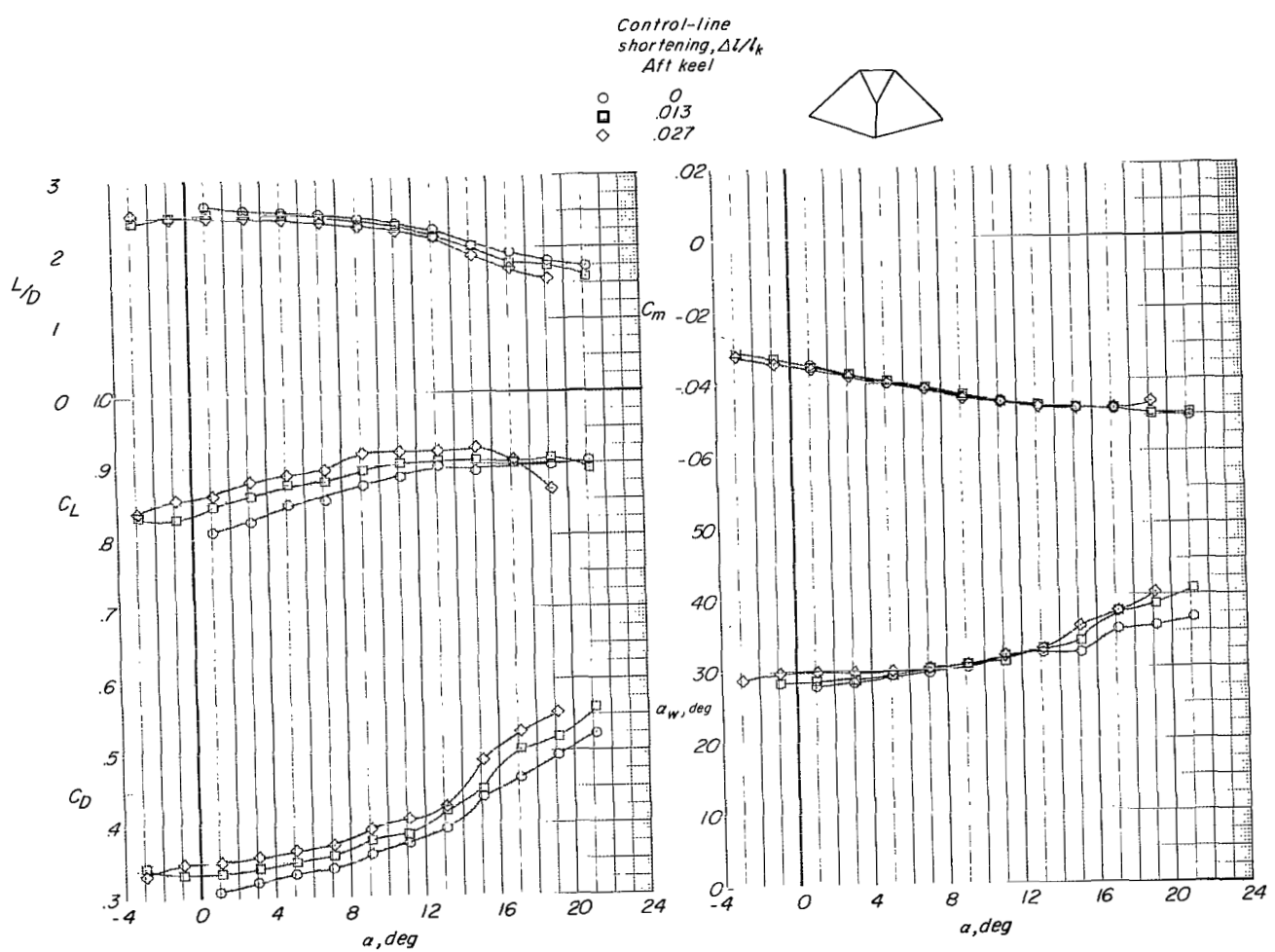


Figure 15.- Effect of aft-keel-line shortening on the aerodynamic characteristics of twin-keel parawing model 1.  $q = 2.0 \text{ lb/ft}^2 (95.8 \text{ N/m}^2)$ .

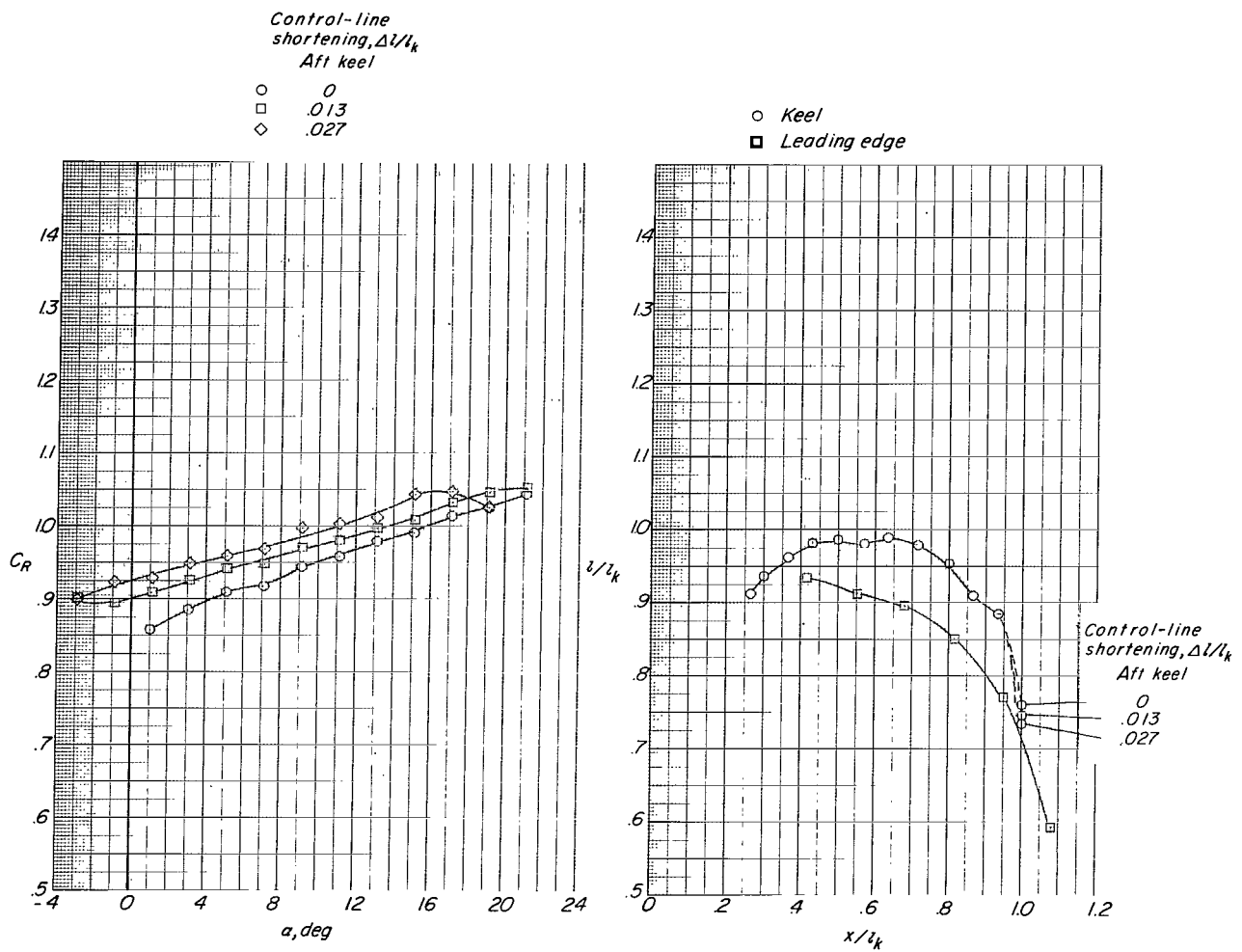


Figure 15.- Concluded.

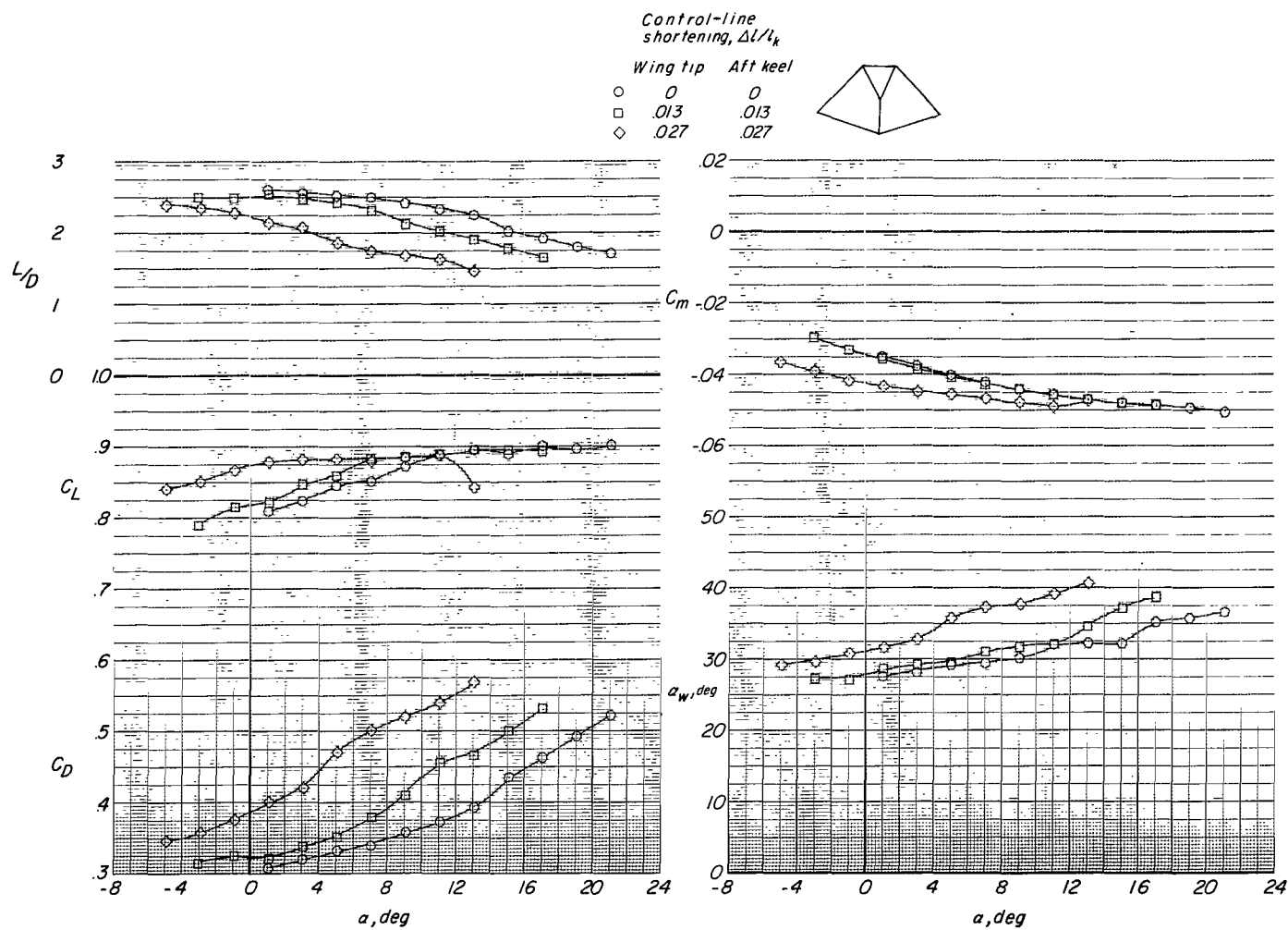


Figure 16.- Effect of tip-line and aft-keel-line shortening on the aerodynamic characteristics of twin-keel parawing model 1.  $q = 2.0 \text{ lb/ft}^2$  (95.8 N/m $^2$ ).

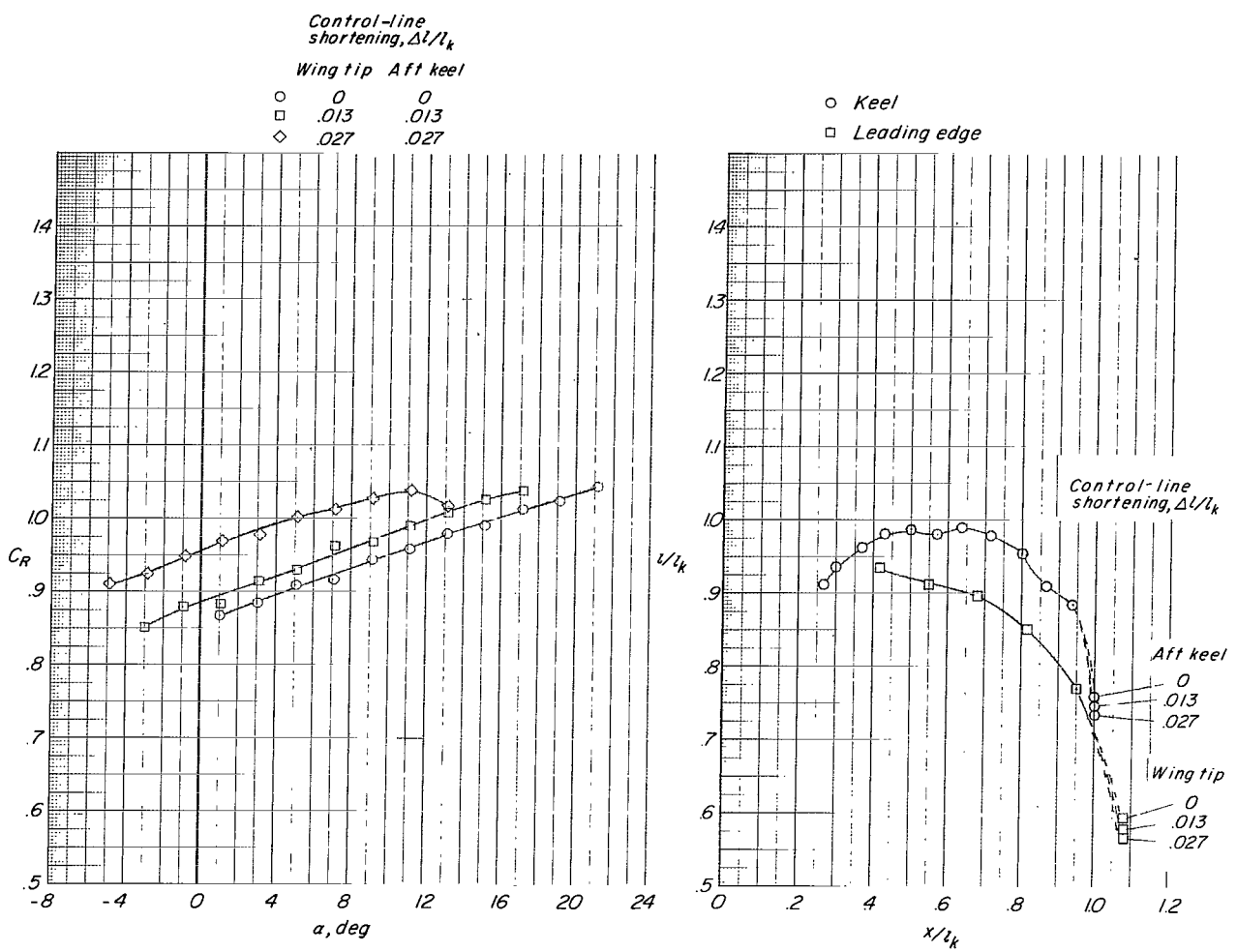
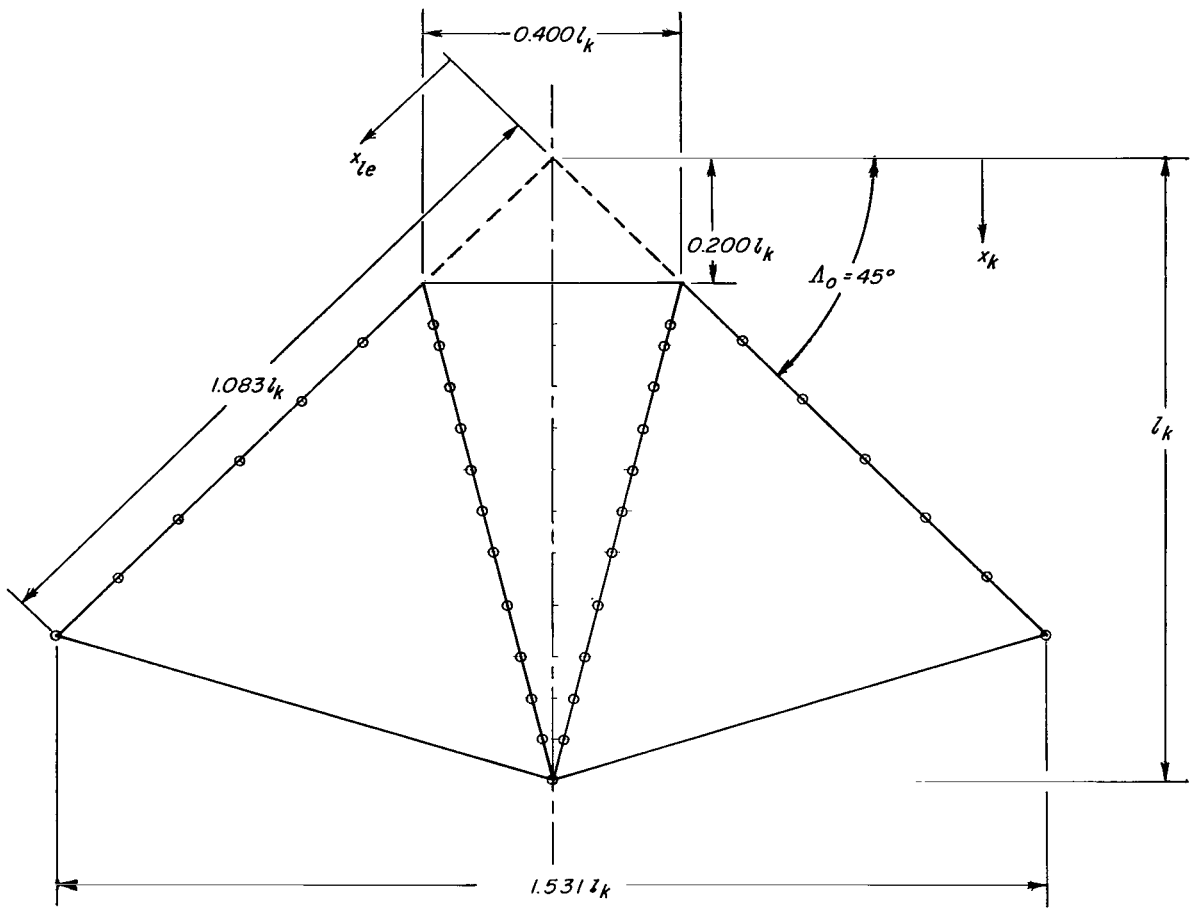


Figure 16.- Concluded.



*Line attachment locations*

$x/l_k$

<i>Keel</i>	<i>Leading edge</i>
.266	.416
.300	.549
.366	.683
.434	.816
.500	.949
.567	1.000
.634	
.716	
.800	
.866	
.934	
1.000	

Figure 17.- Flat-planform details of twin-keel parawing model 2.

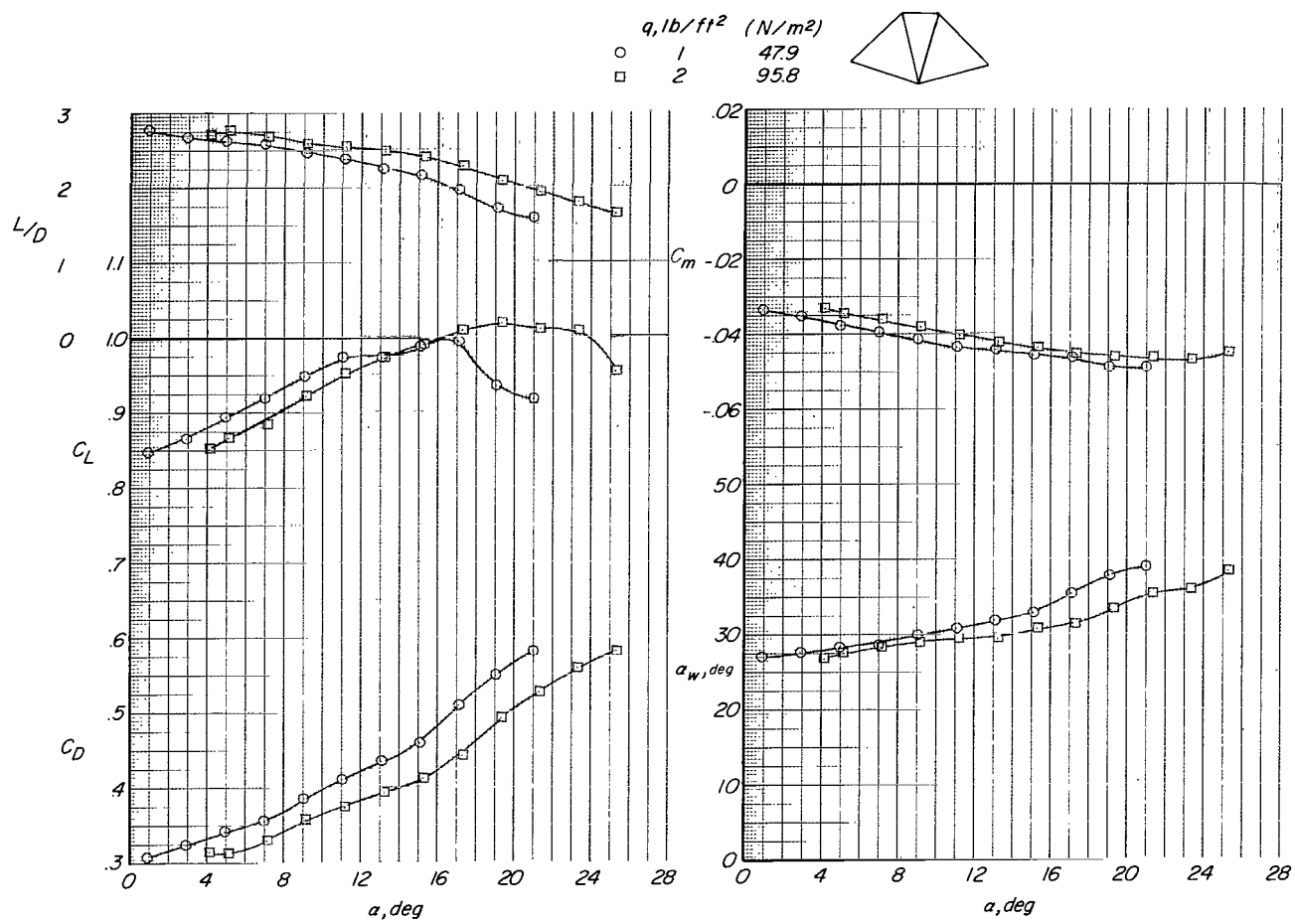


Figure 18.- Effect of dynamic pressure on the aerodynamic characteristics of twin-keel parawing model 2.

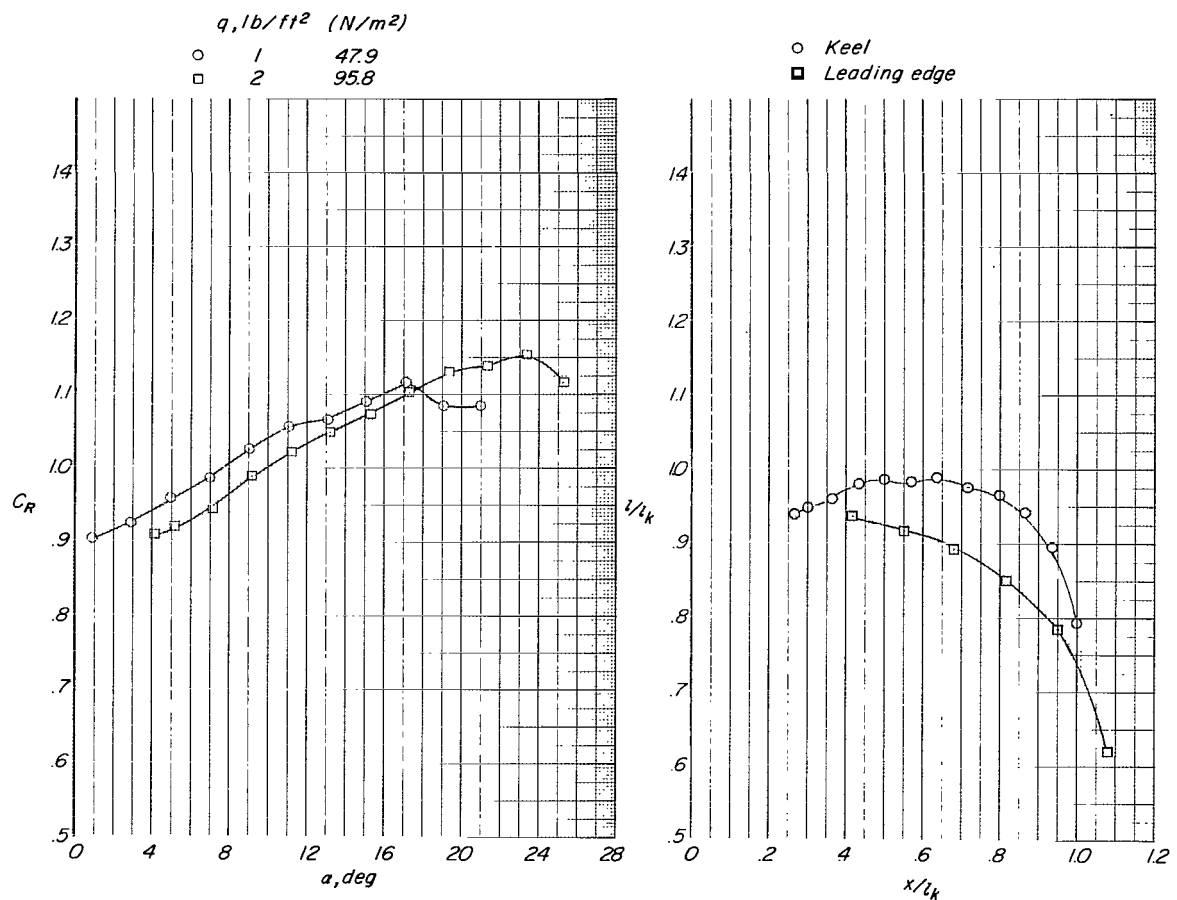


Figure 18.- Concluded.

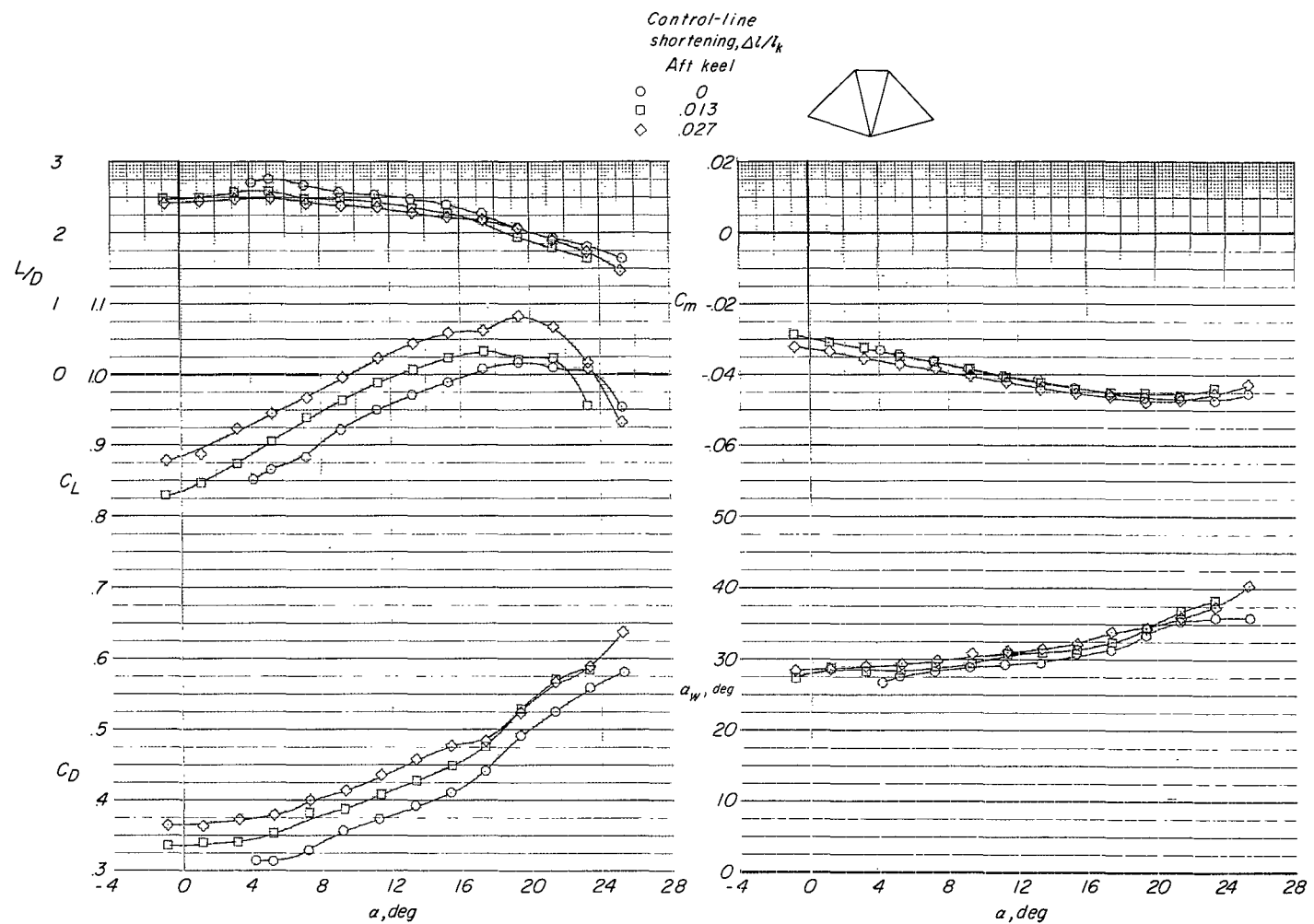


Figure 19.- Effect of aft-keel-line shortening on the aerodynamic characteristics of twin-keel parawing model 2.  $q = 2.0 \text{ lb/ft}^2 (95.8 \text{ N/m}^2)$ .

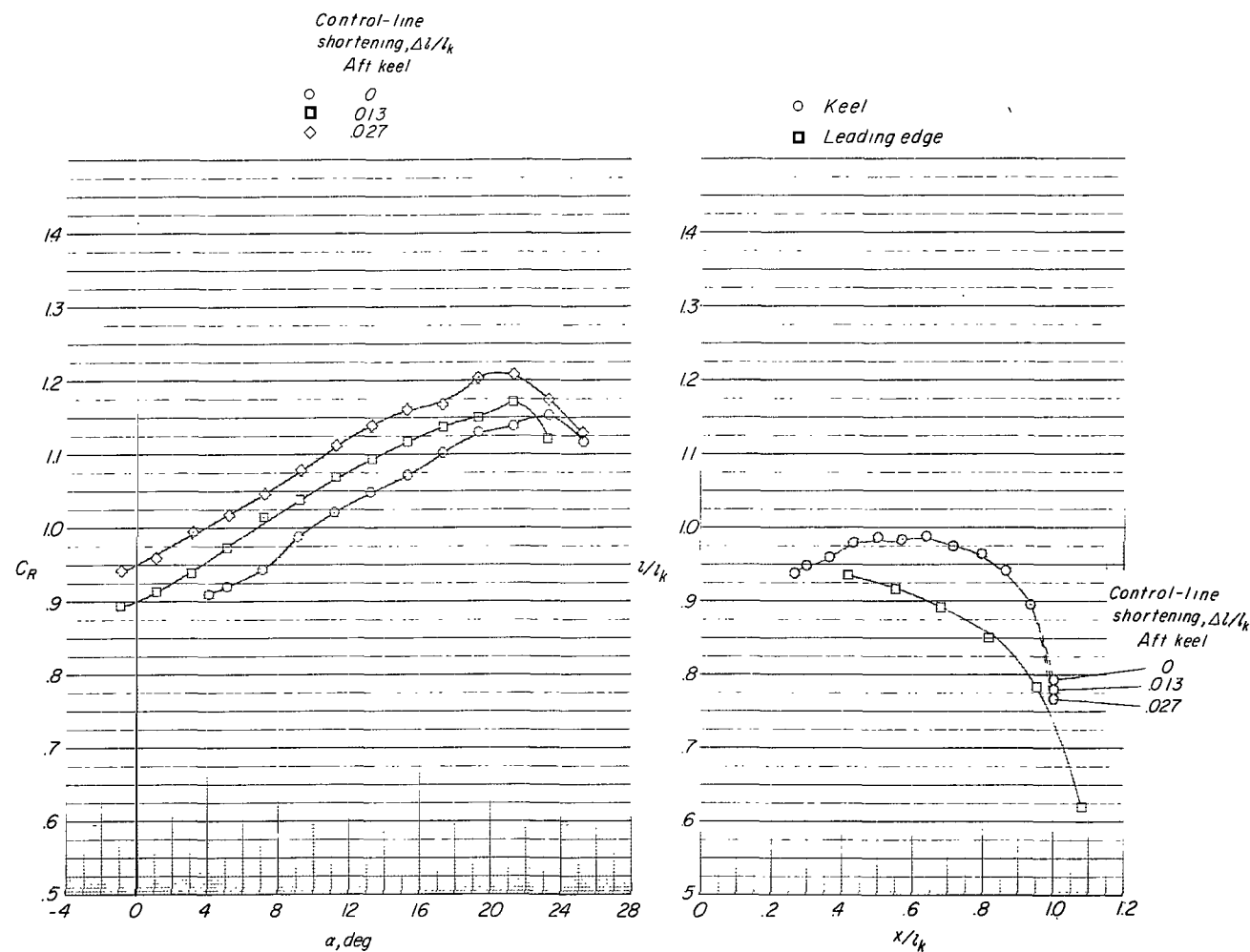


Figure 19.- Concluded.

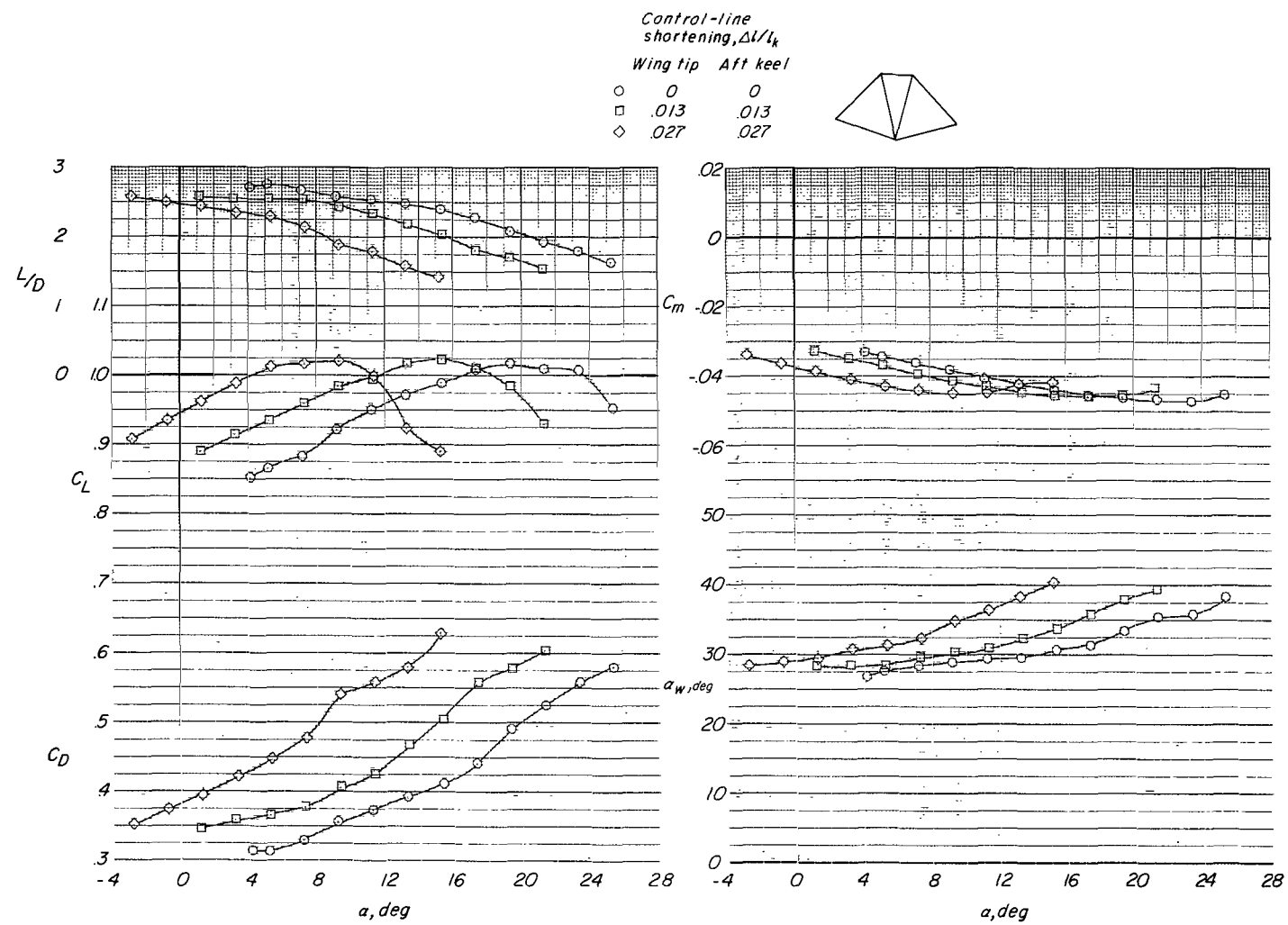


Figure 20.- Effect of tip-line and aft-keel-line shortening on the aerodynamic characteristics of twin-keel parawing model 2.  $q = 2.0 \text{ lb/ft}^2$  ( $95.8 \text{ N/m}^2$ ).

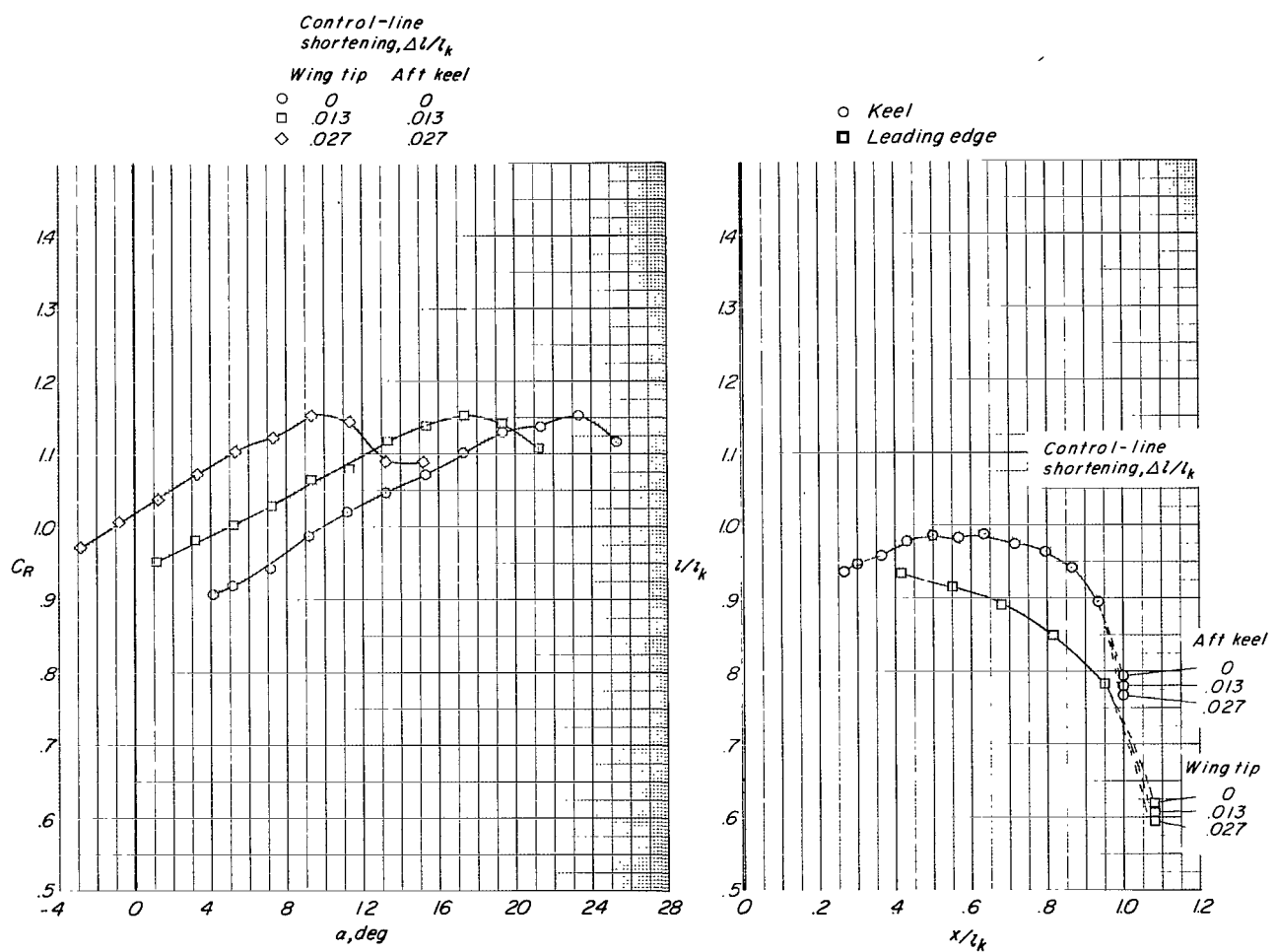
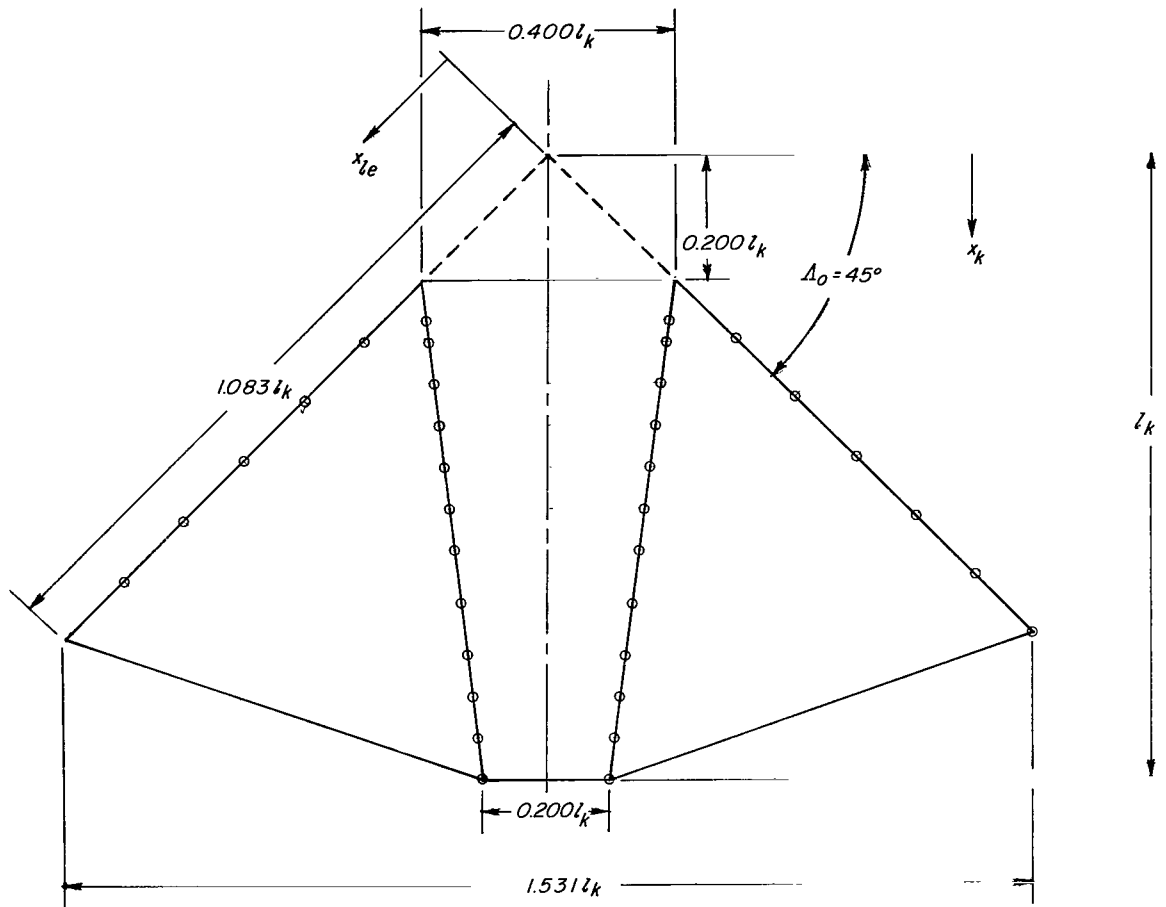


Figure 20.- Concluded.



*Line attachment locations*

$x/l_k$

<i>Kee<i>l</i></i>	<i>Leading edge</i>
.266	.416
.300	.549
.366	.683
.434	.816
.500	.949
.567	1.083
.634	
.716	
.800	
.866	
.934	
1.000	

Figure 21.- Flat-planform details of twin-keel parawing model 3.

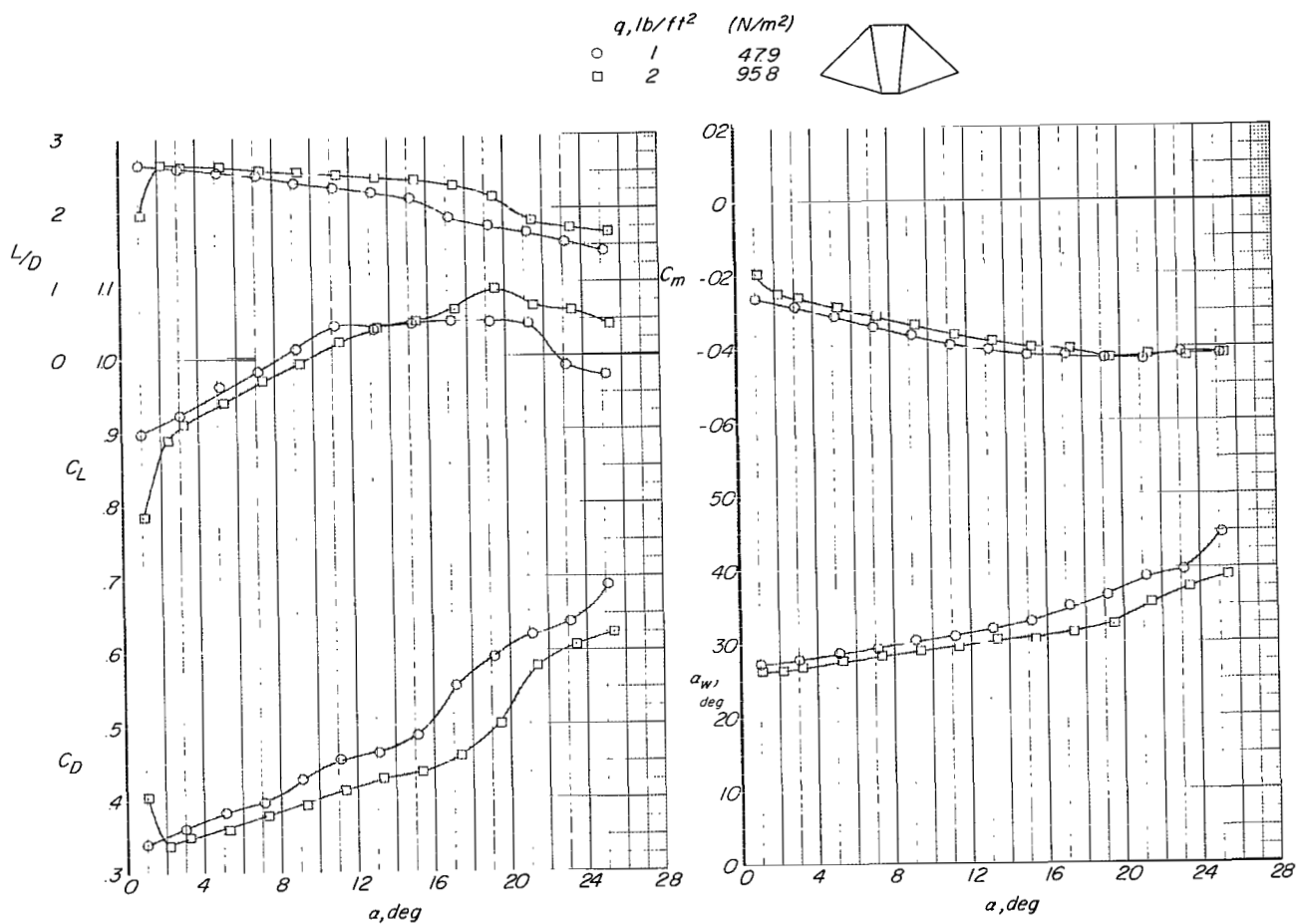


Figure 22.- Effect of dynamic pressure on the aerodynamic characteristics of twin-keel parawing model 3.

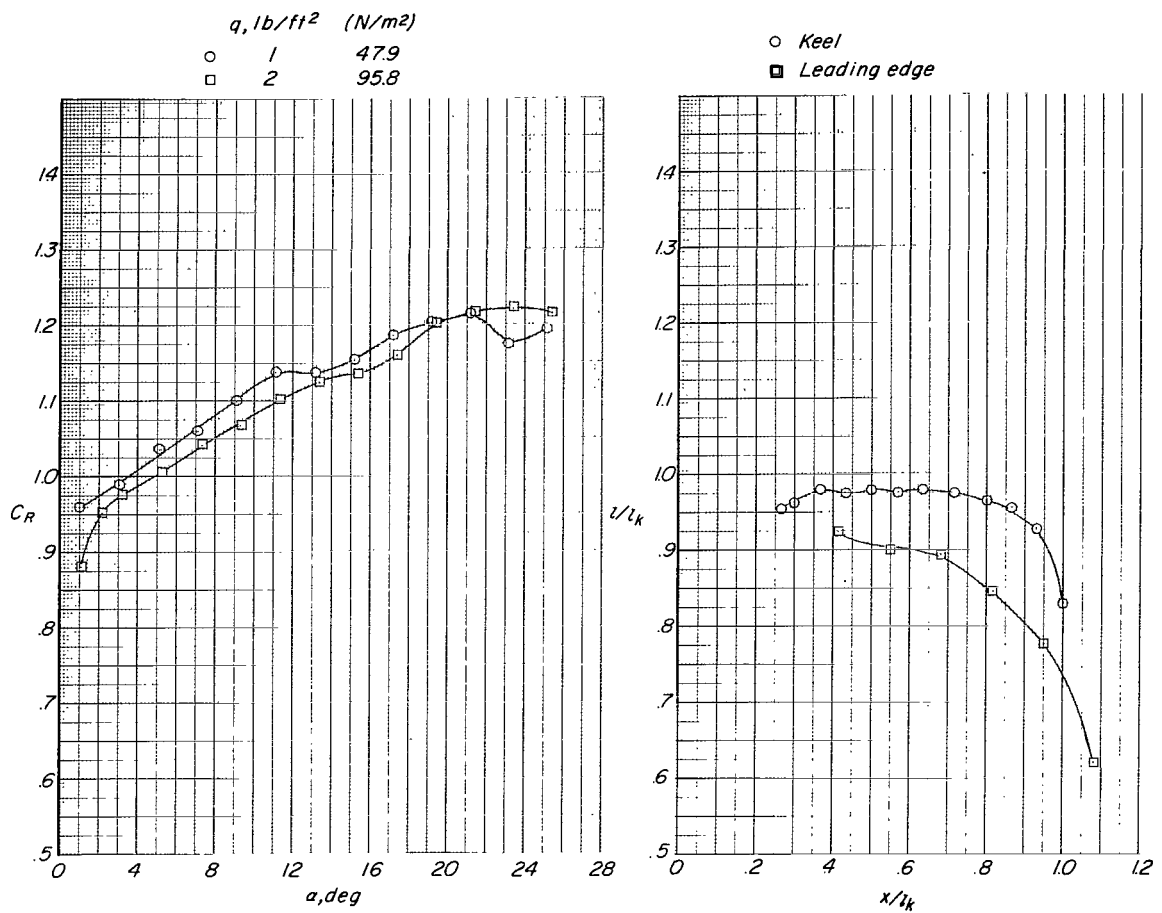


Figure 22.- Concluded.

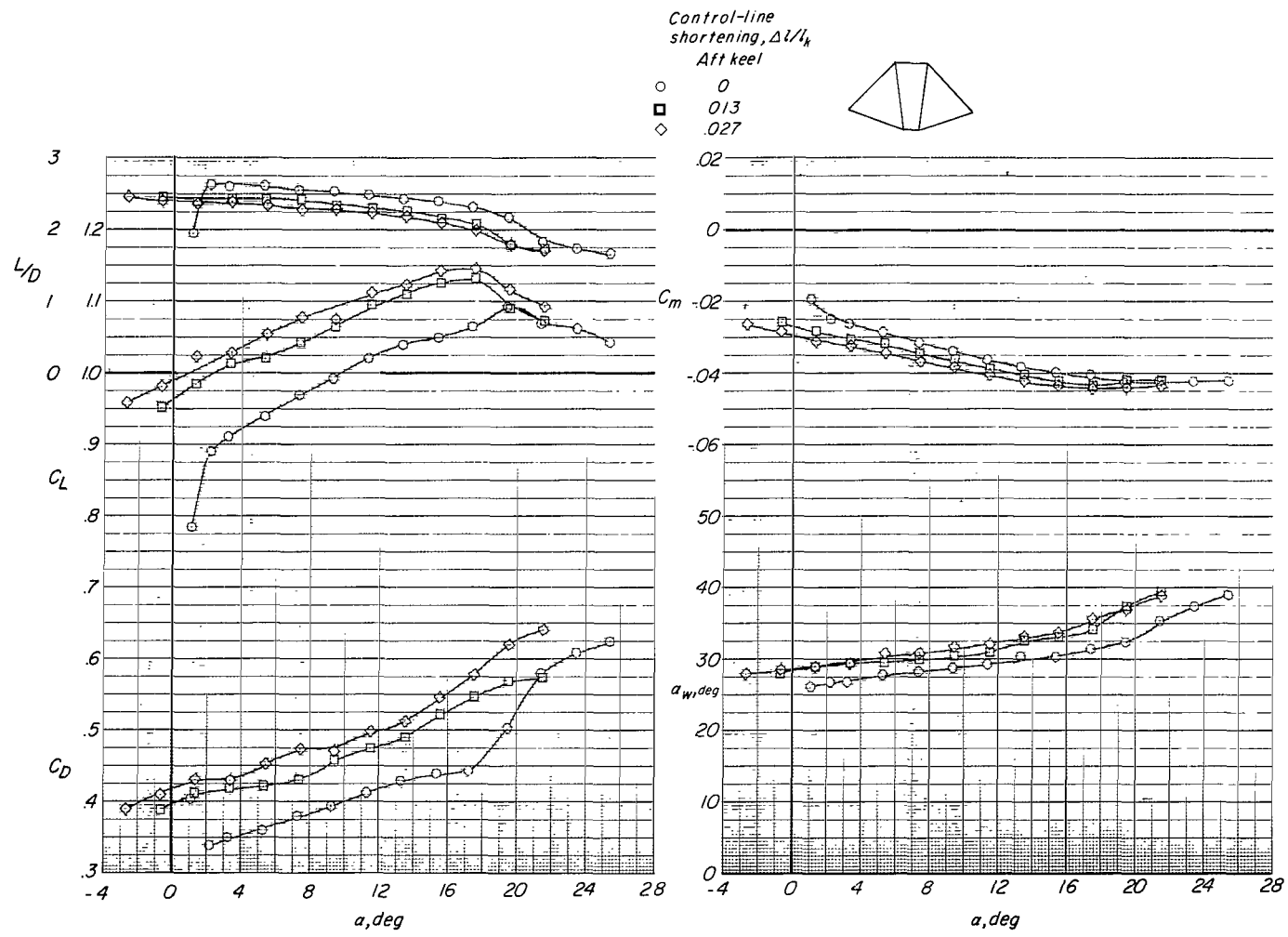


Figure 23.- Effect of aft-keel-line shortening on the aerodynamic characteristics of twin-keel parawing model 3.  $q = 2.0 \text{ lb/ft}^2$  (95.8 N/m<sup>2</sup>).

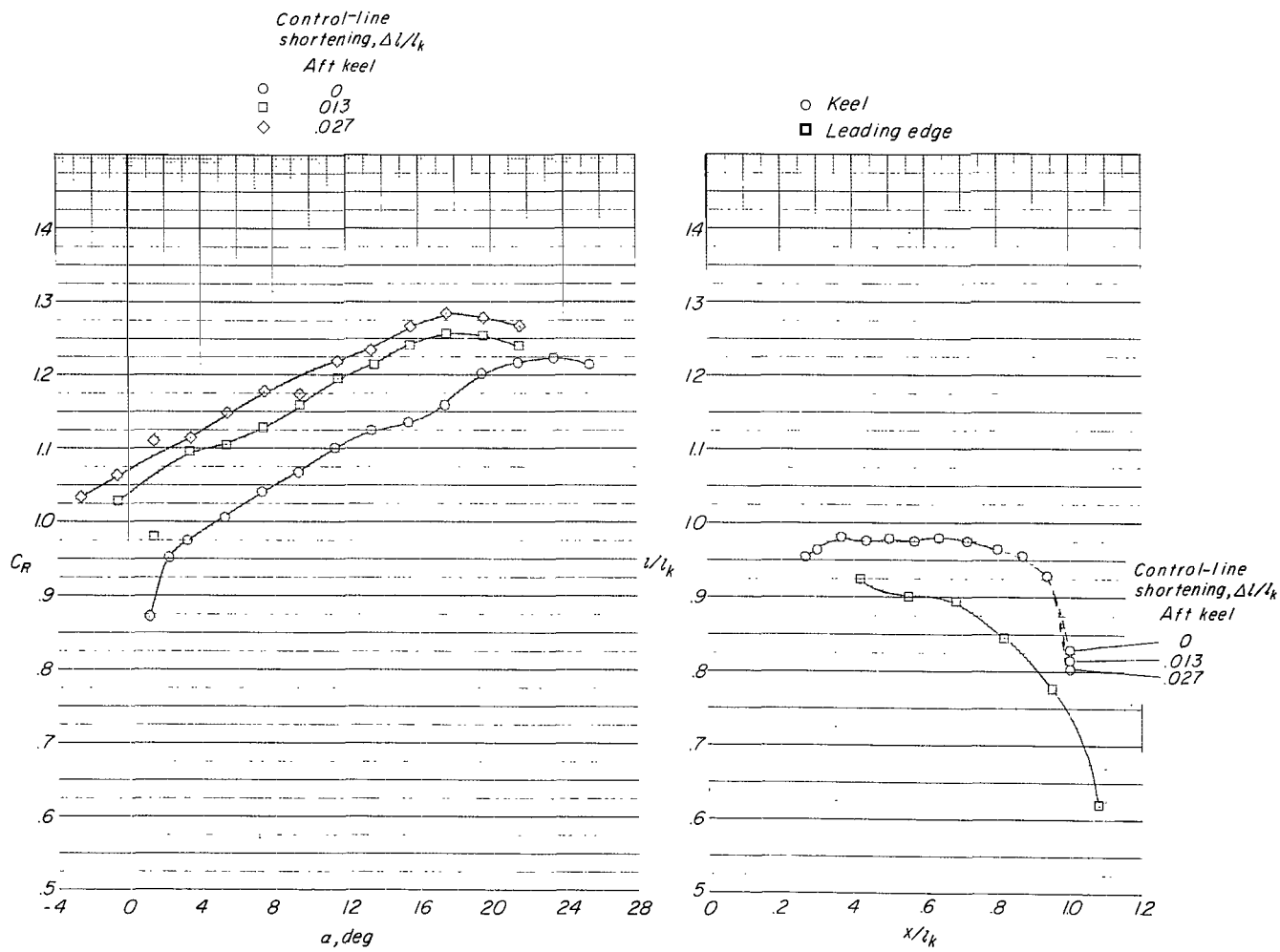


Figure 23.- Concluded.

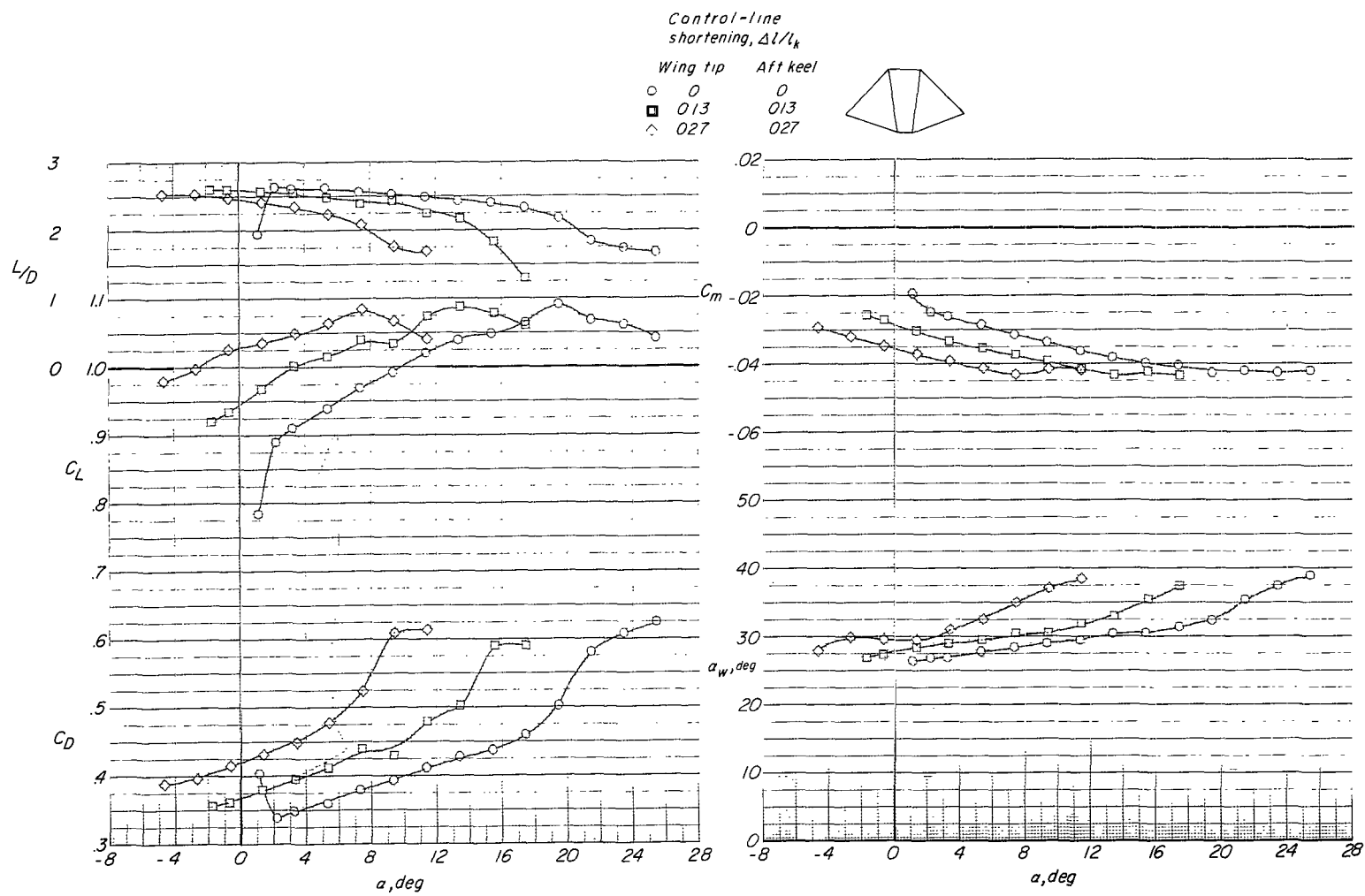


Figure 24.- Effect of tip-line and aft-keel-line shortening on the aerodynamic characteristics of twin-keel parawing model 3.  $q = 2.0 \text{ lb/ft}^2 (95.8 \text{ N/m}^2)$ .

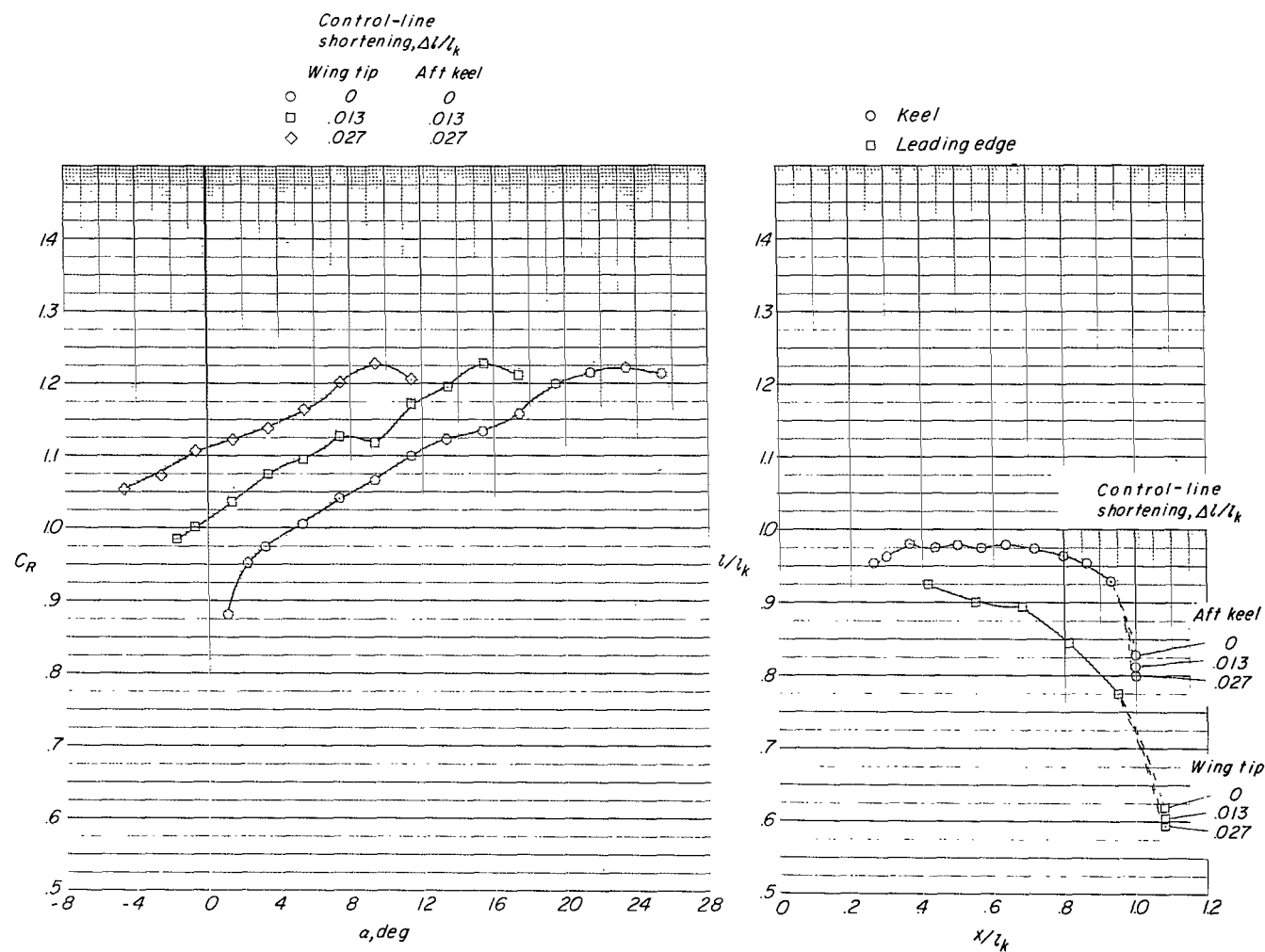
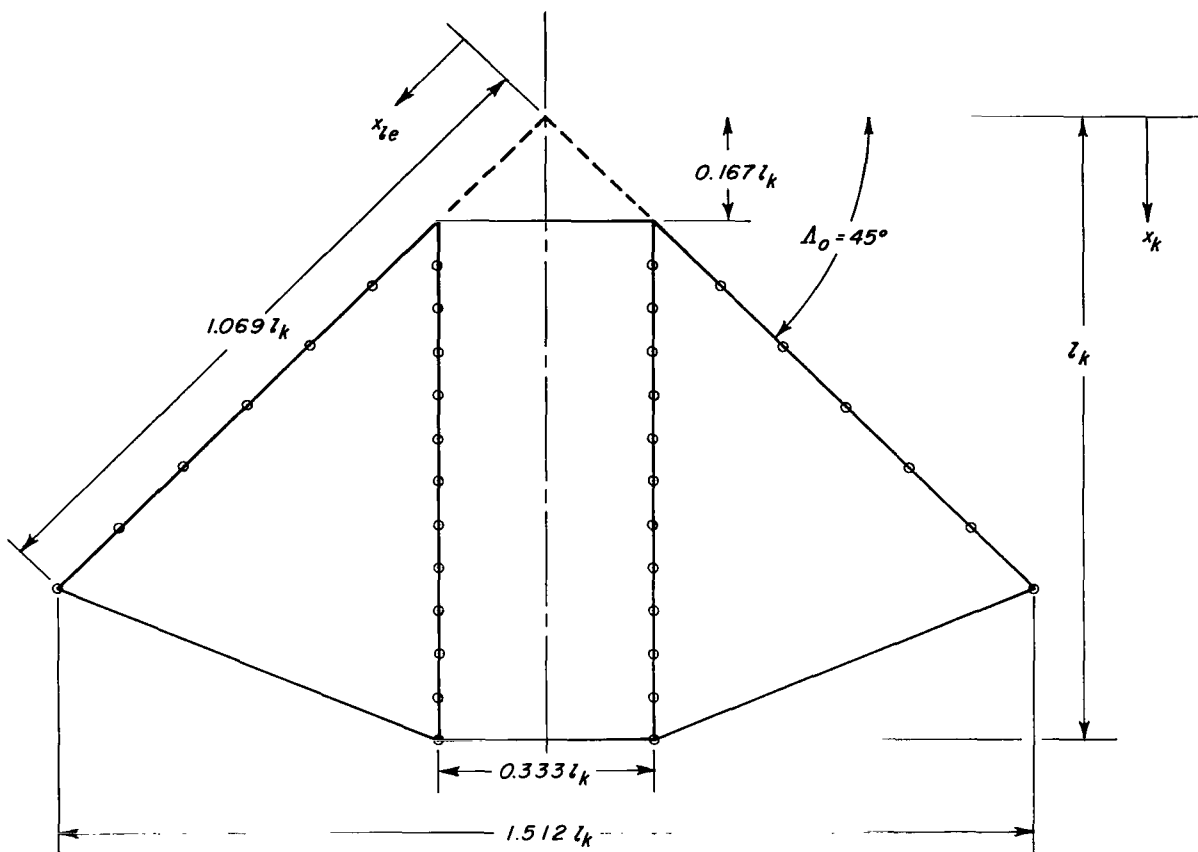


Figure 24.- Concluded.



*Line attachment locations*

$x/l_k$

<i>Kee l</i>	<i>Leading edge</i>
.236	.375
.306	.513
.375	.652
.444	.791
.514	.930
.583	1.069
.653	
.722	
.792	
.861	
.931	
1.000	

Figure 25.- Flat-planform details of twin-keel parawing model 4.

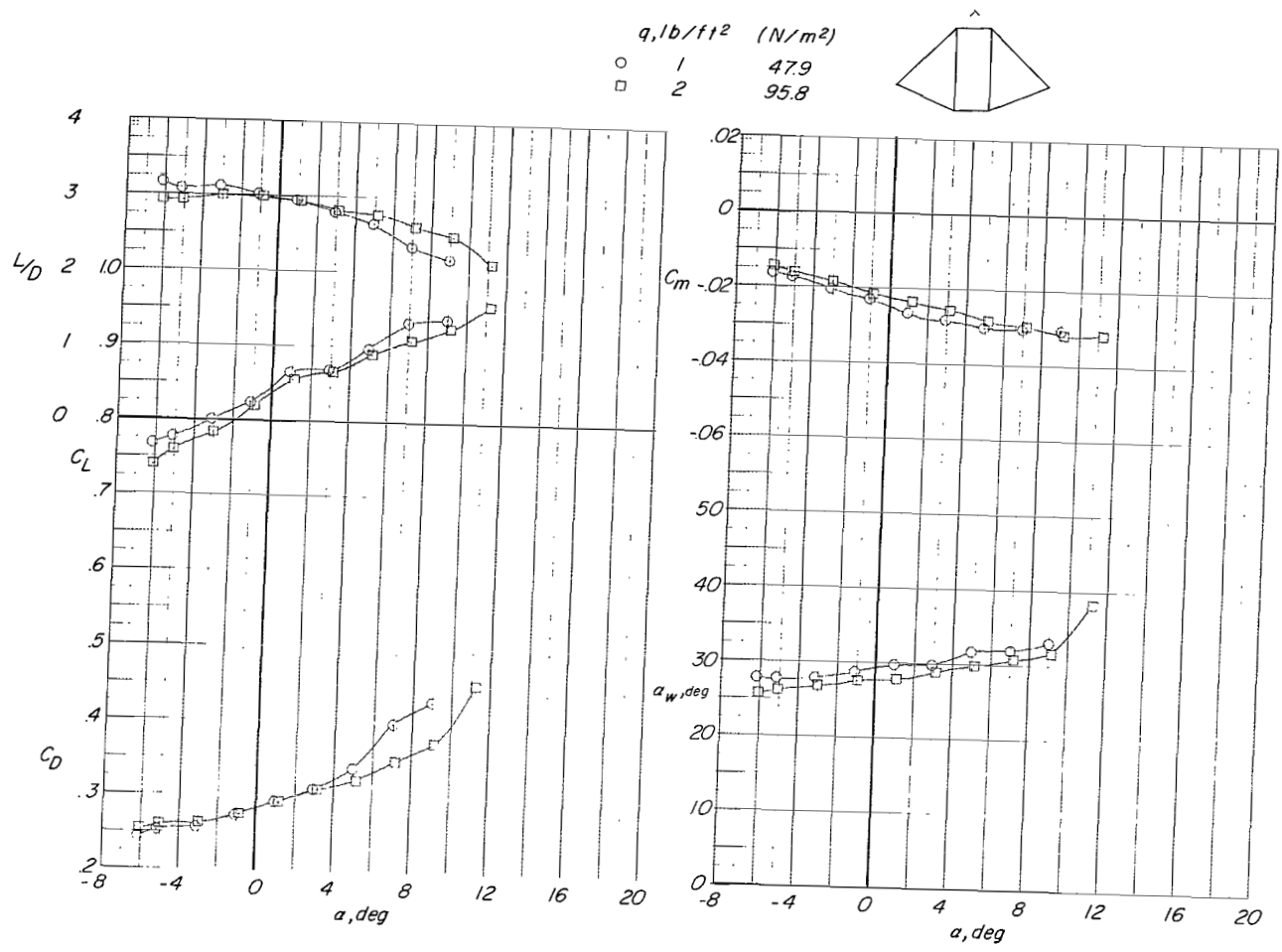


Figure 26.- Effect of dynamic pressure on the aerodynamic characteristics of twin-keel parawing model 4.

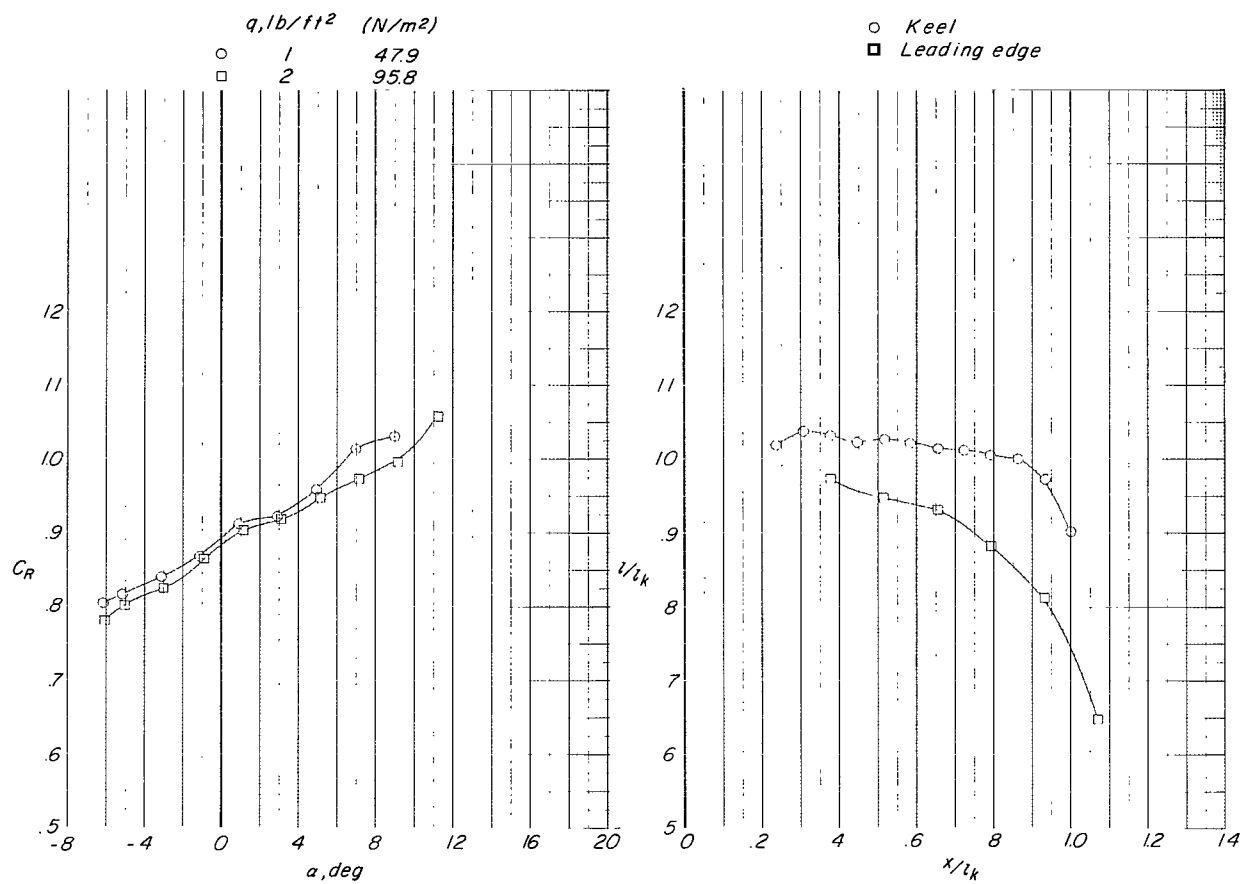
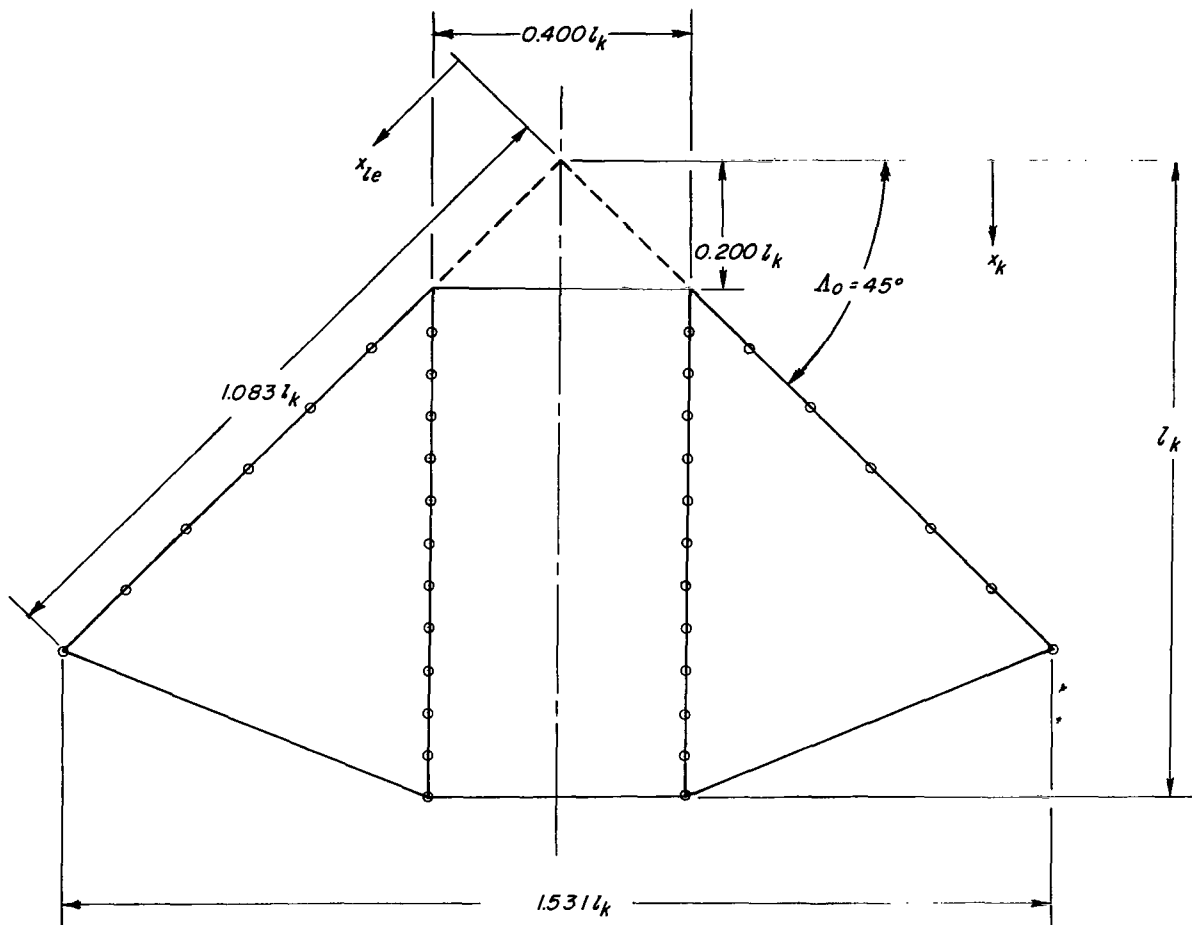


Figure 26.- Concluded.



*Line attachment locations*

$x/l_k$

<i>Kee<i>l</i></i>	<i>Leading edge</i>
.267	.416
.333	.549
.400	.683
.466	.816
.533	.949
.600	1.083
.666	
.733	
.799	
.866	
.933	
1.000	

Figure 27.- Flat-planform details of twin-keel parawing model 5.

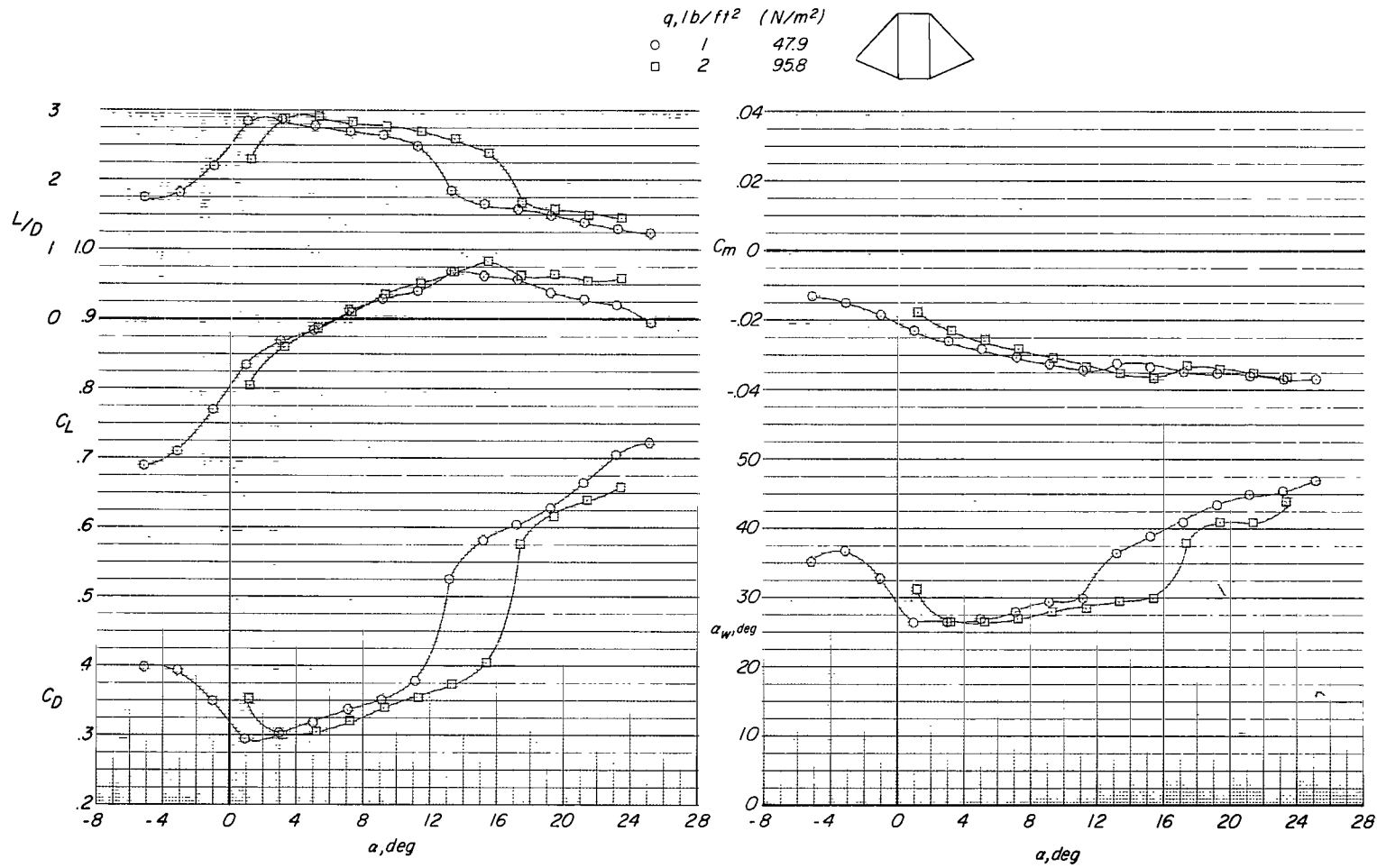


Figure 28.- Effect of dynamic pressure on the aerodynamic characteristics of twin-keel parawing model 5.

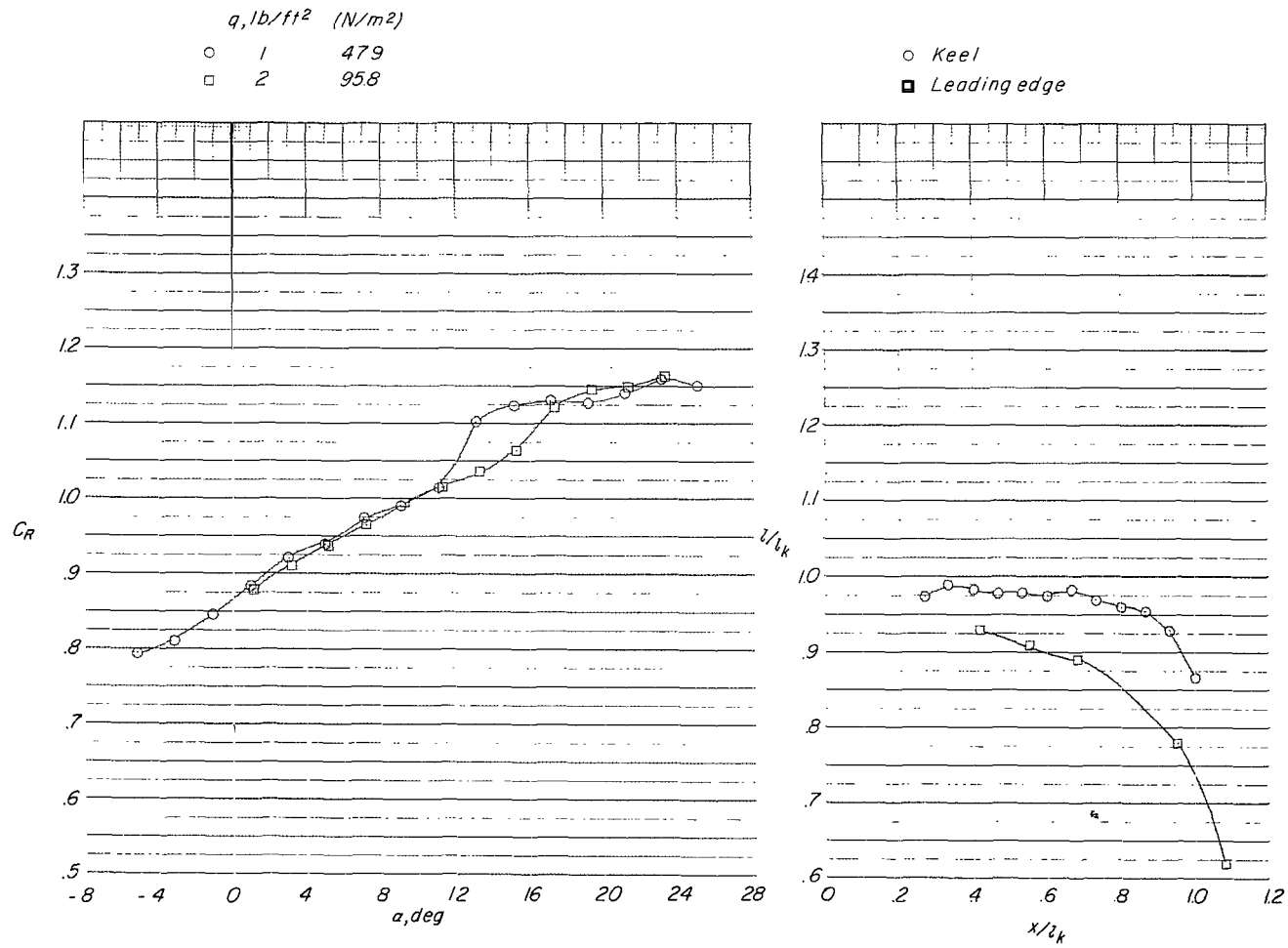


Figure 28.- Concluded.

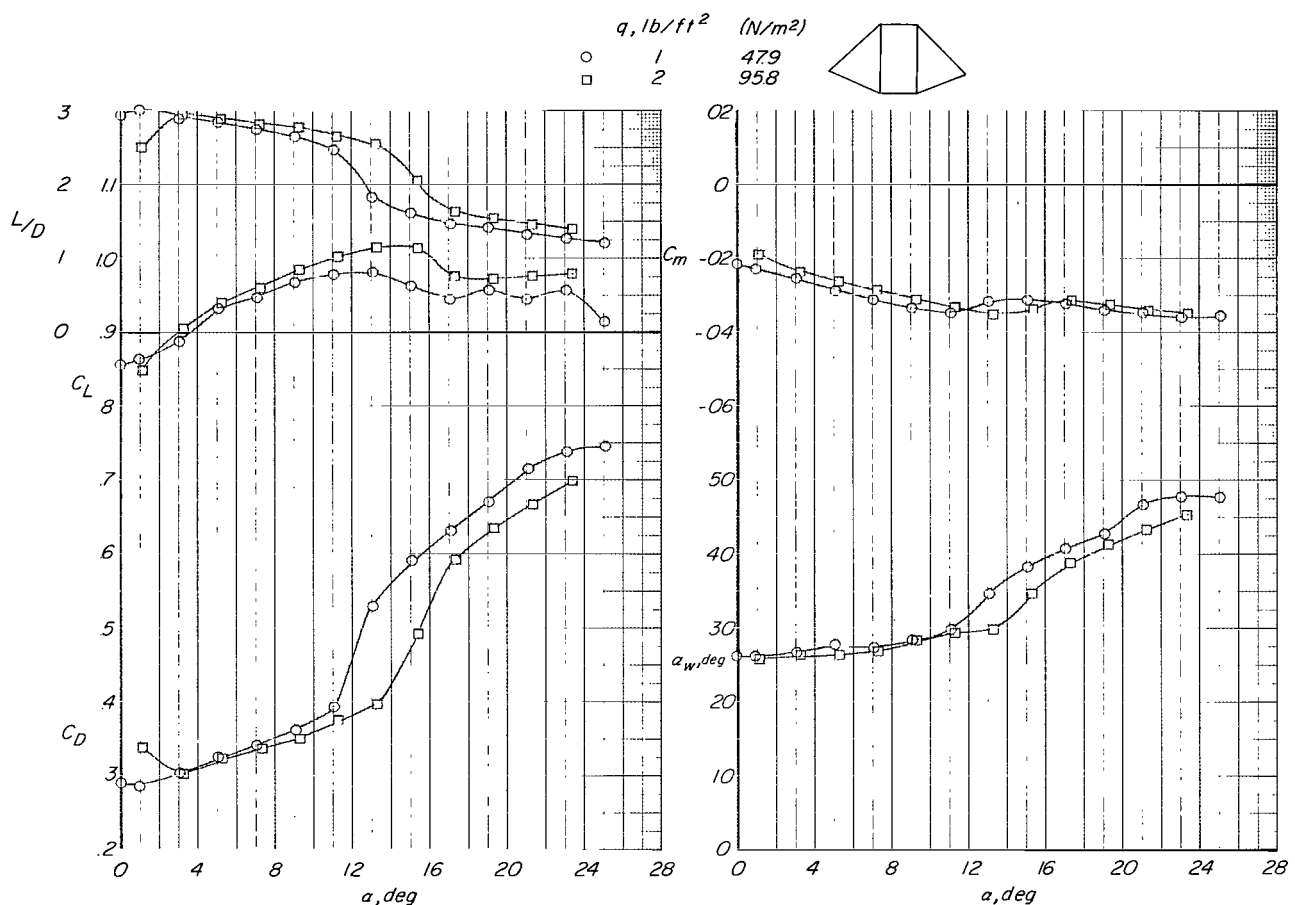


Figure 29.- Effect of dynamic pressure on the aerodynamic characteristics of twin-keel parawing model 5. Check tests.

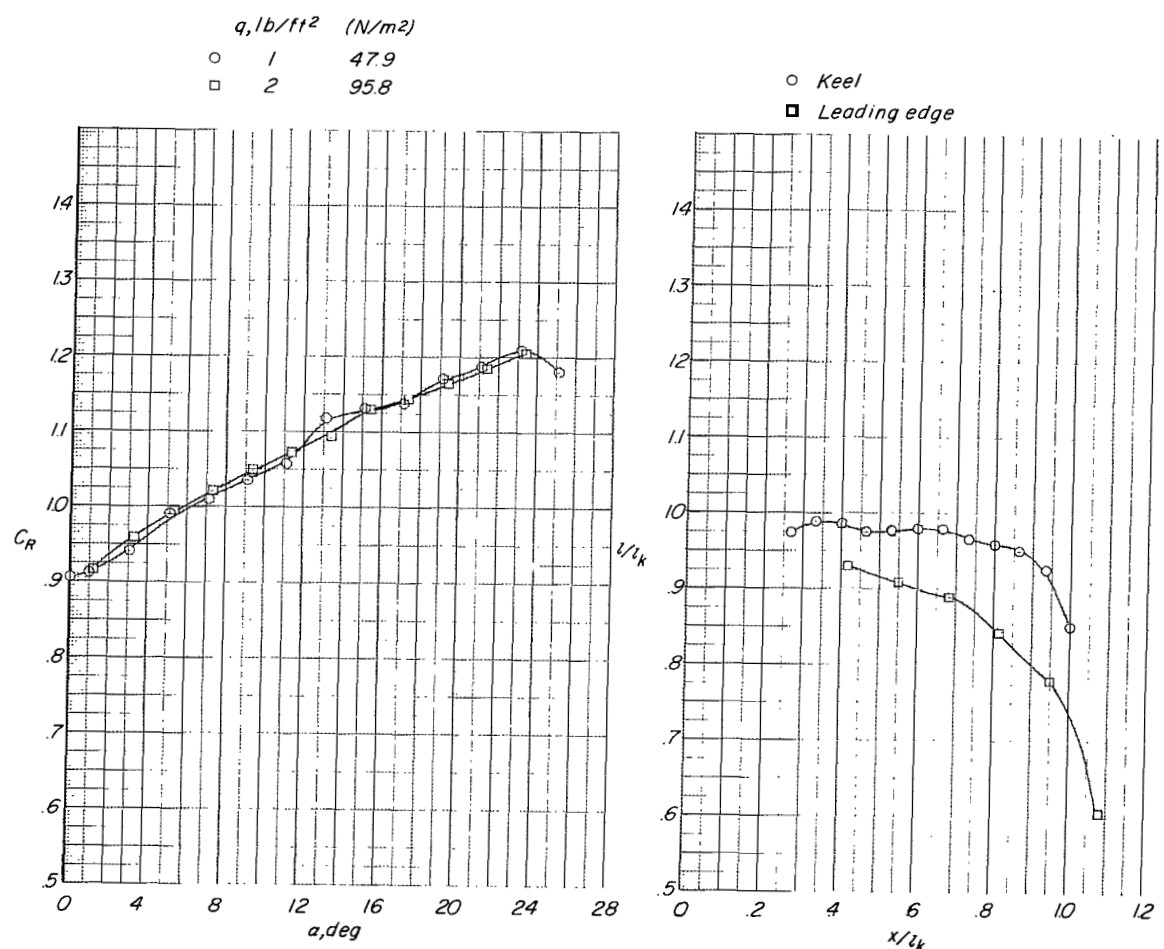


Figure 29.- Concluded.

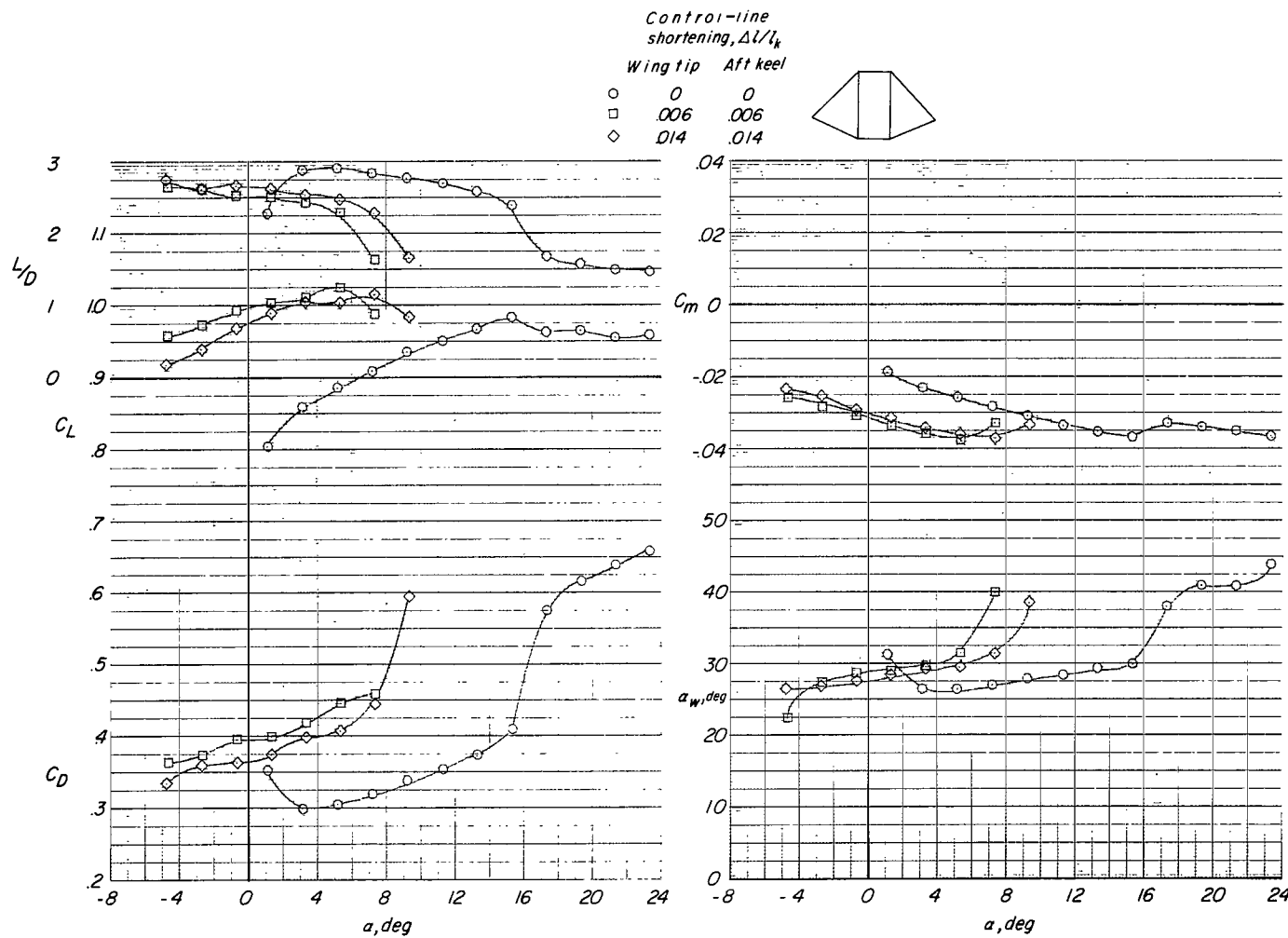


Figure 30.- Effect of tip-line and aft-keel-line shortening on the aerodynamic characteristics of twin-keel parawing model 5.  $q = 2.0 \text{ lb/ft}^2$  ( $95.8 \text{ N/m}^2$ ).

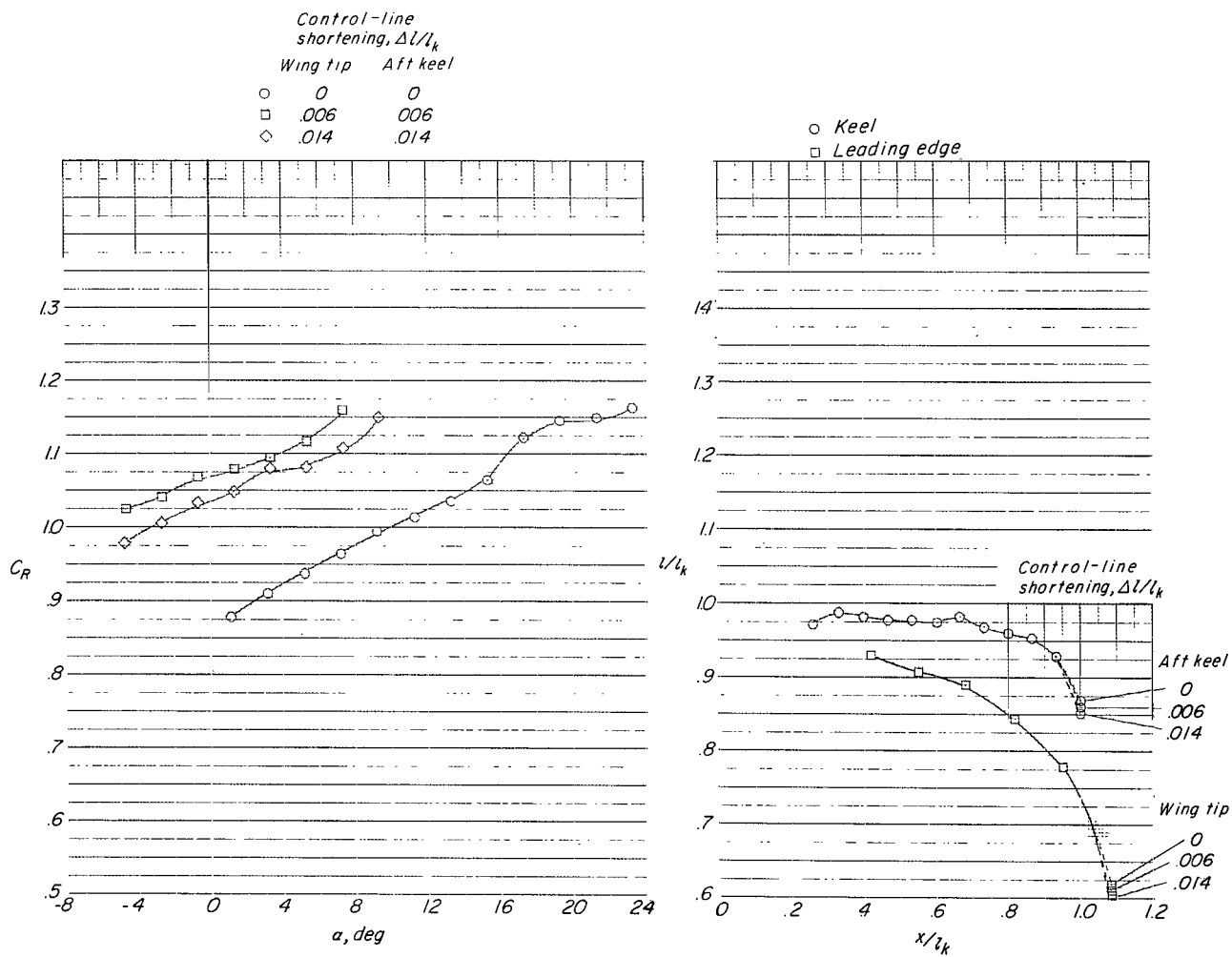


Figure 30.- Continued.

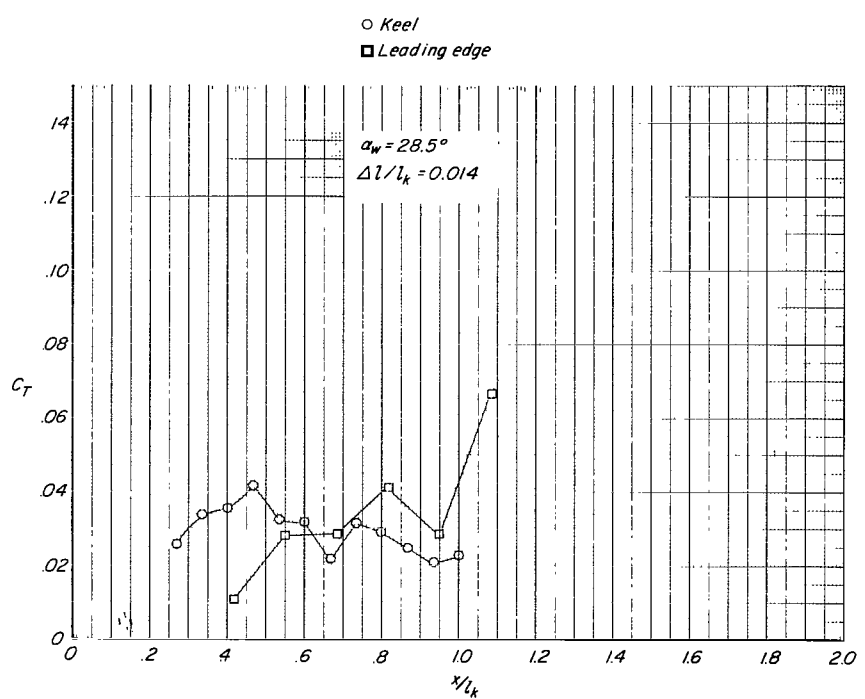
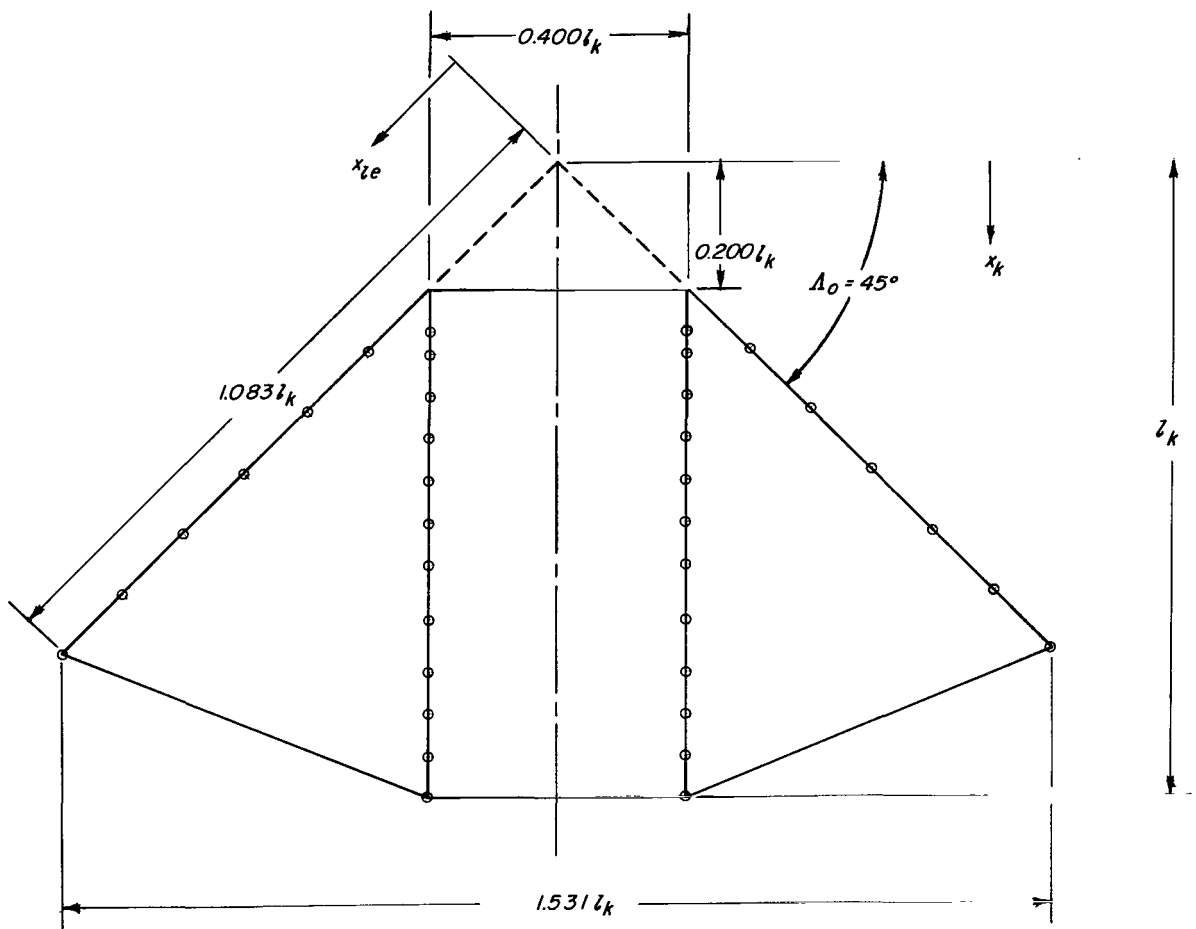


Figure 30.- Concluded.



*Line attachment locations*

$x/l_k$

<i>Keel</i>	<i>Leading edge</i>
.266	.416
.300	.549
.366	.683
.434	.816
.500	.949
.567	1.083
.634	
.716	
.800	
.866	
.934	
1.000	

Figure 31.- Flat-planform details of twin-keel parawing model 6.

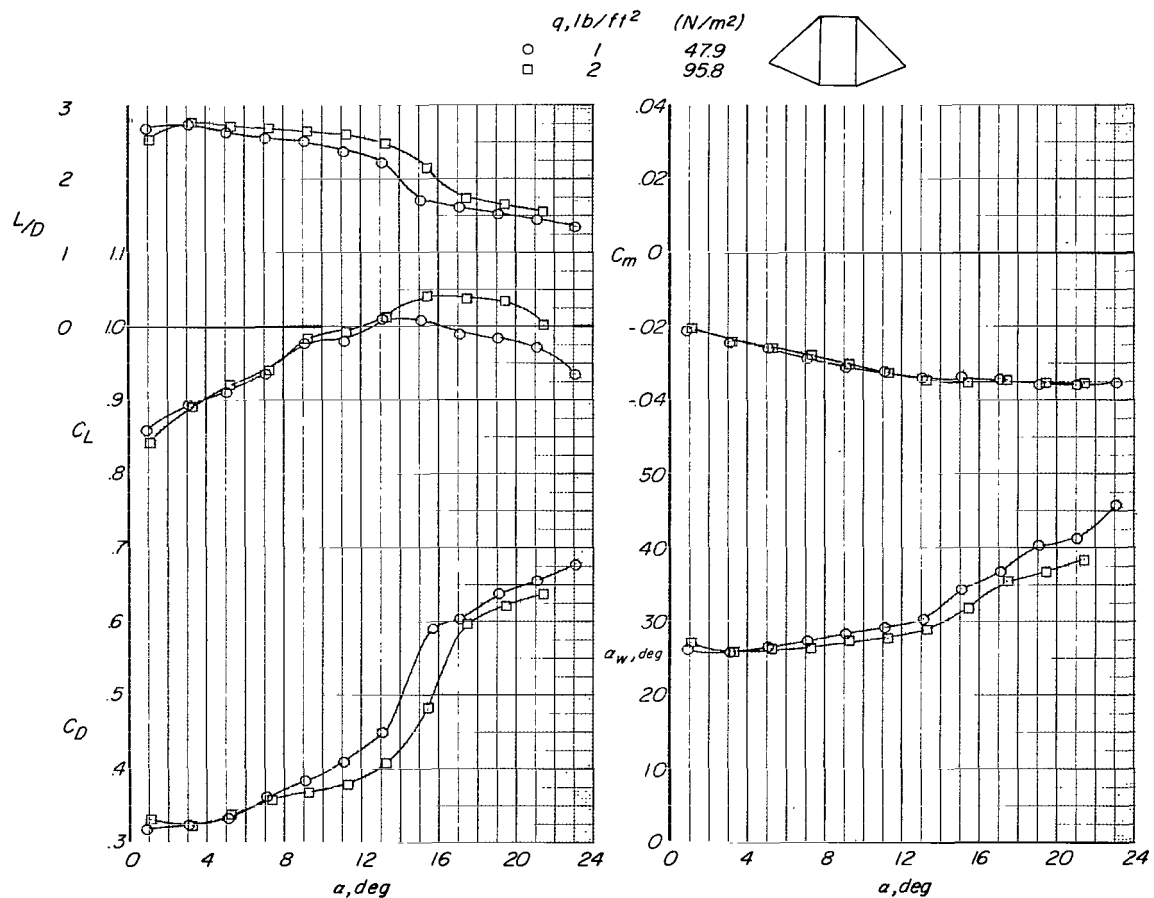


Figure 32.- Effect of dynamic pressure on the aerodynamic characteristics of twin-keel parawing model 6.

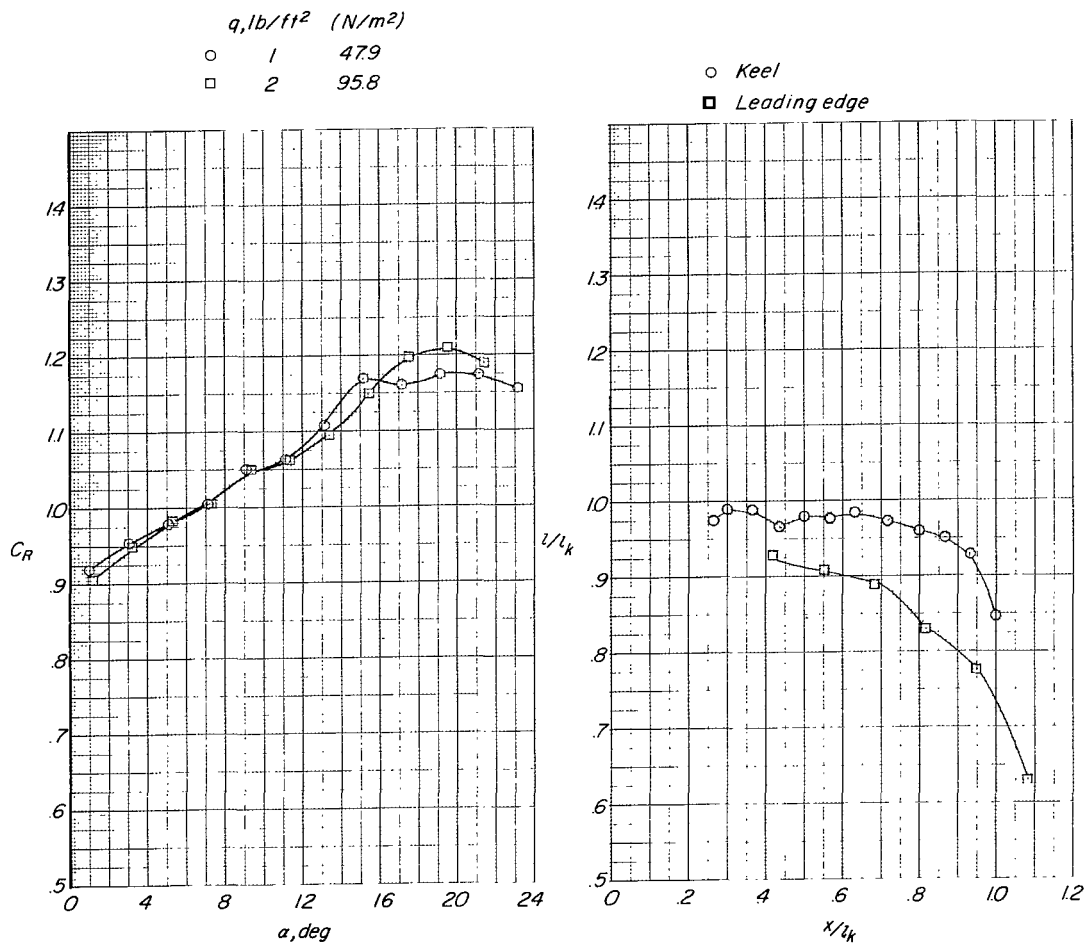


Figure 32.- Concluded.

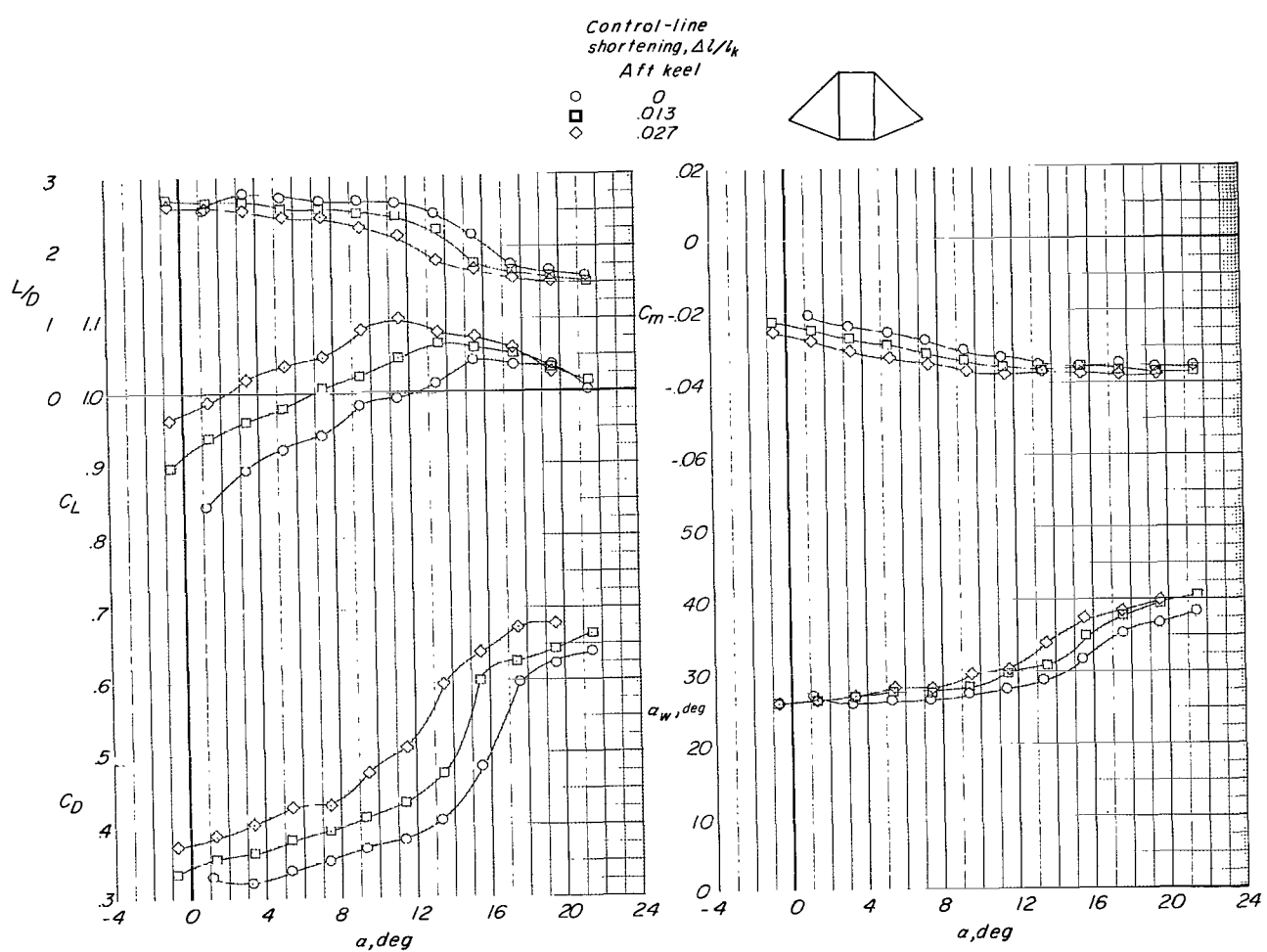


Figure 33.- Effect of aft-keel-line shortening on the aerodynamic characteristics of twin-keel parawing model 6.  $q = 2.0 \text{ lb}/\text{ft}^2$  ( $95.8 \text{ N}/\text{m}^2$ ).

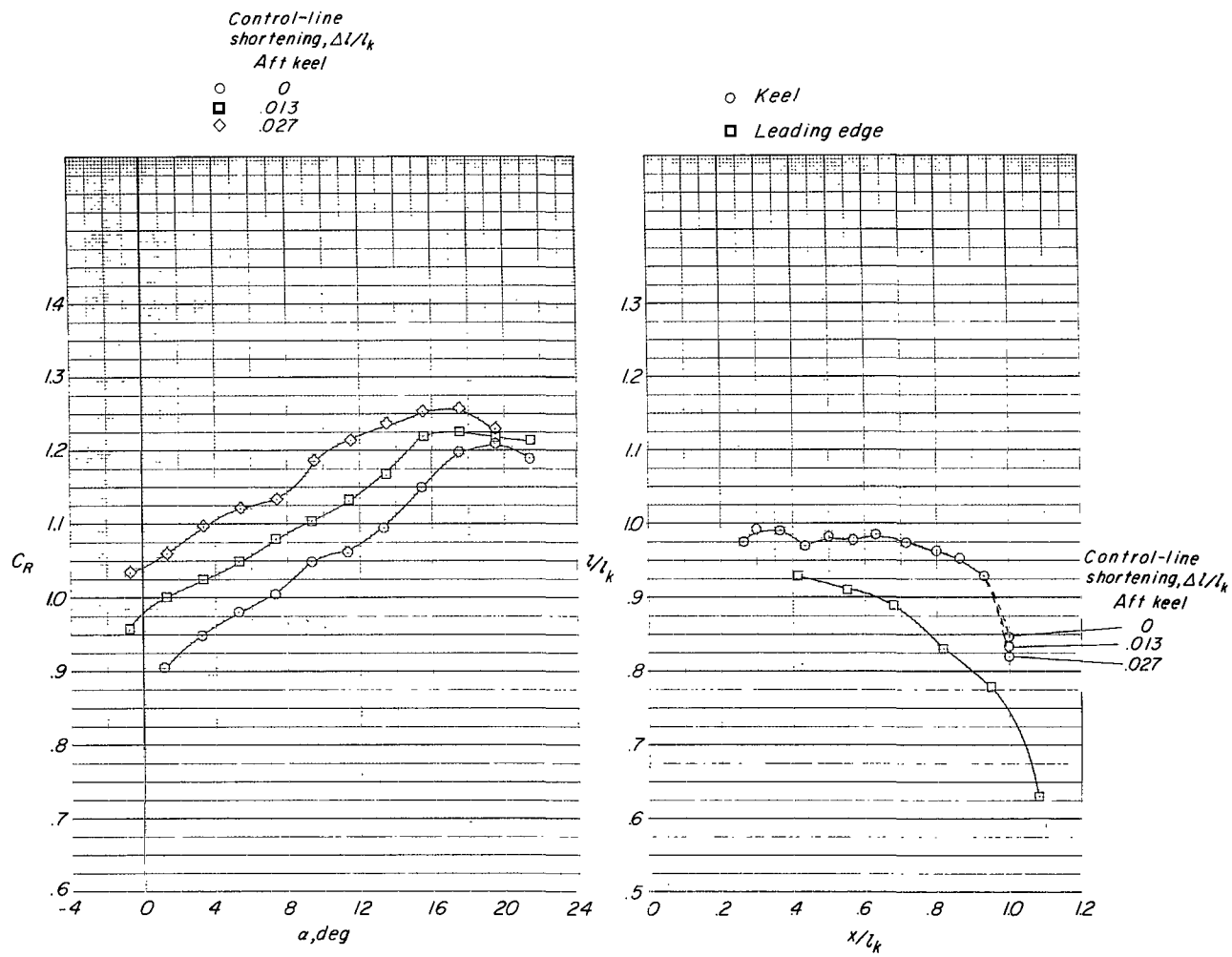


Figure 33.- Concluded.

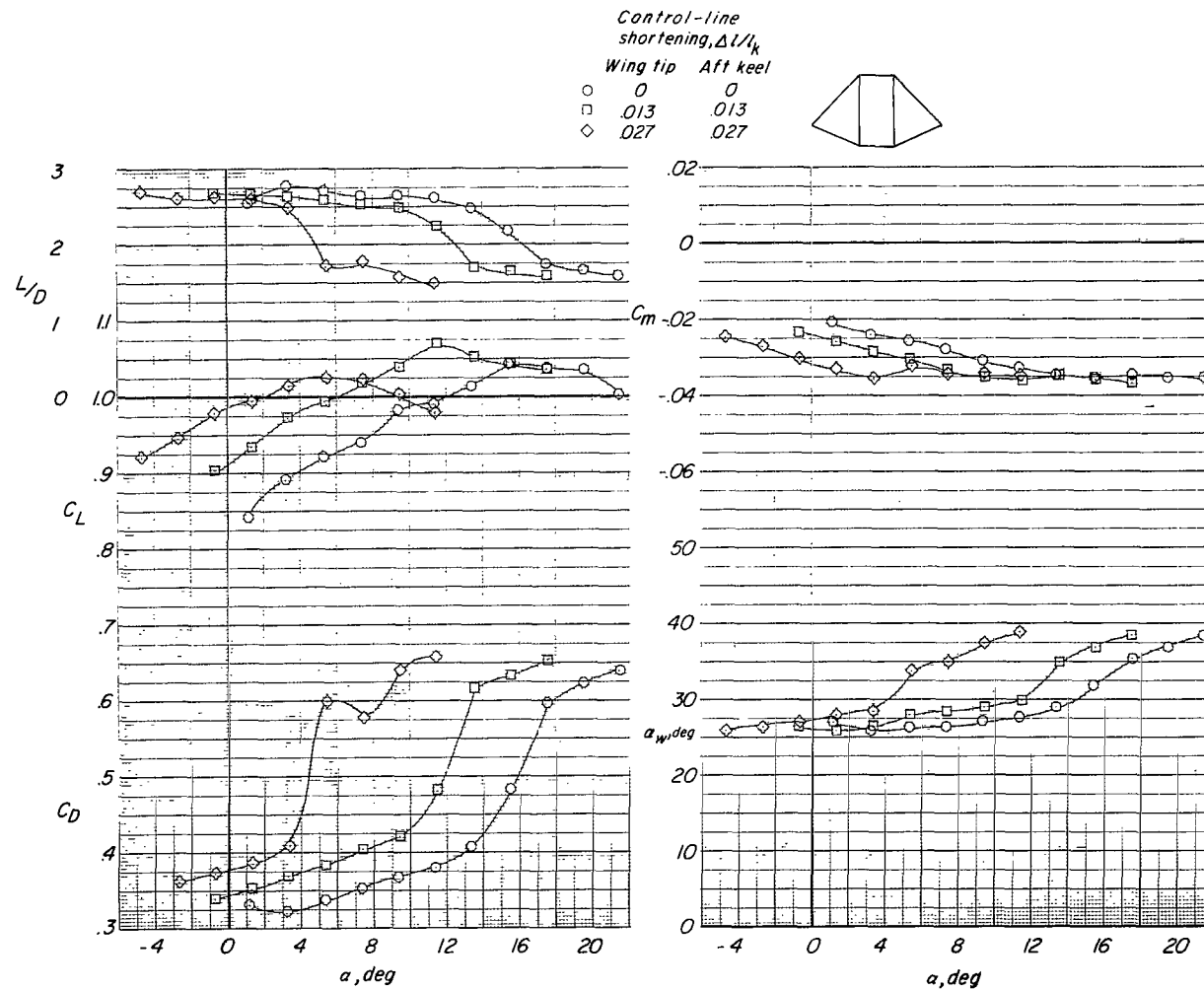


Figure 34.- Effect of tip-line and aft-keel-line shortening on the aerodynamic characteristics of twin-keel parawing model 6.  $q = 2.0 \text{ lb/ft}^2 (95.8 \text{ N/m}^2)$ .

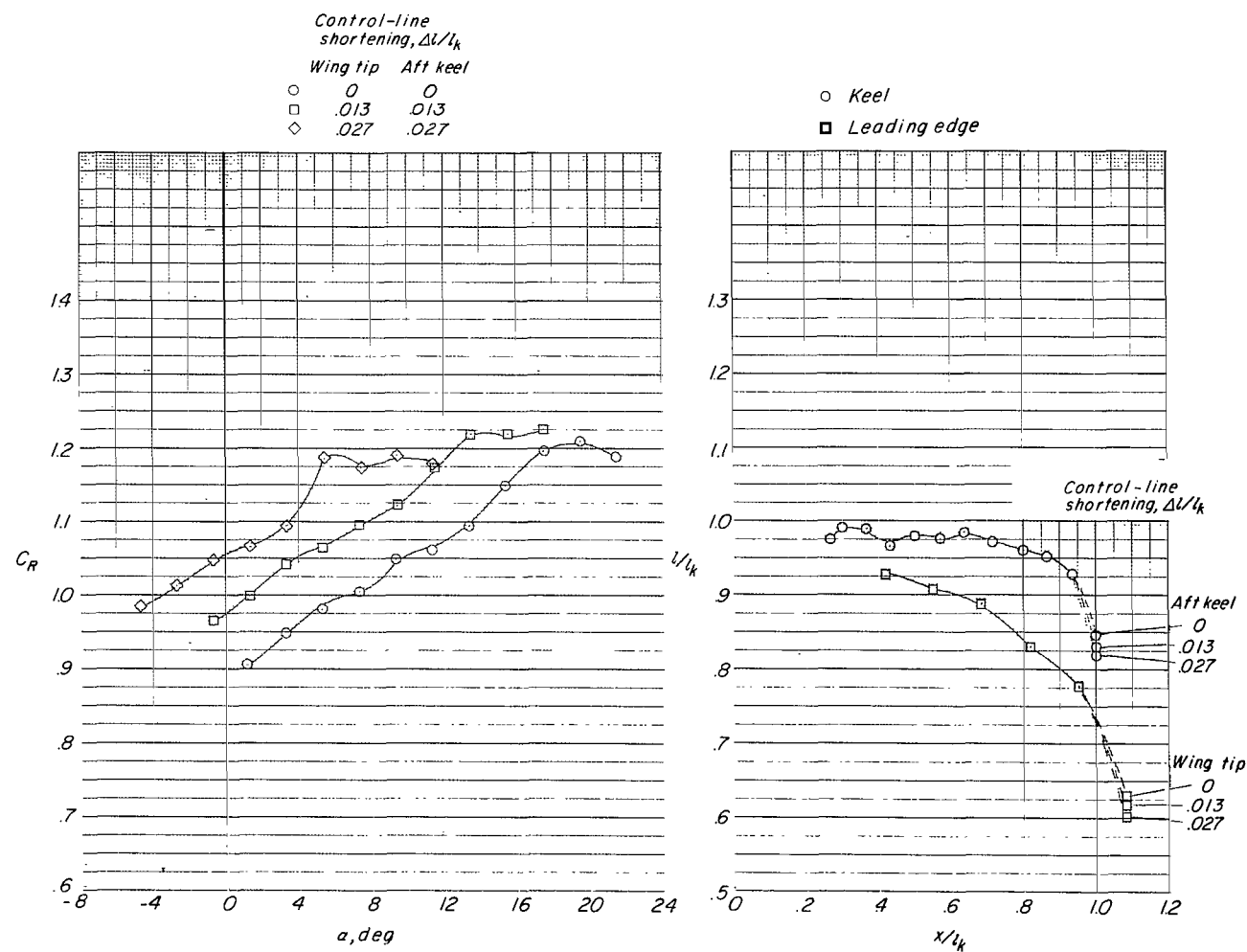


Figure 34.- Concluded.

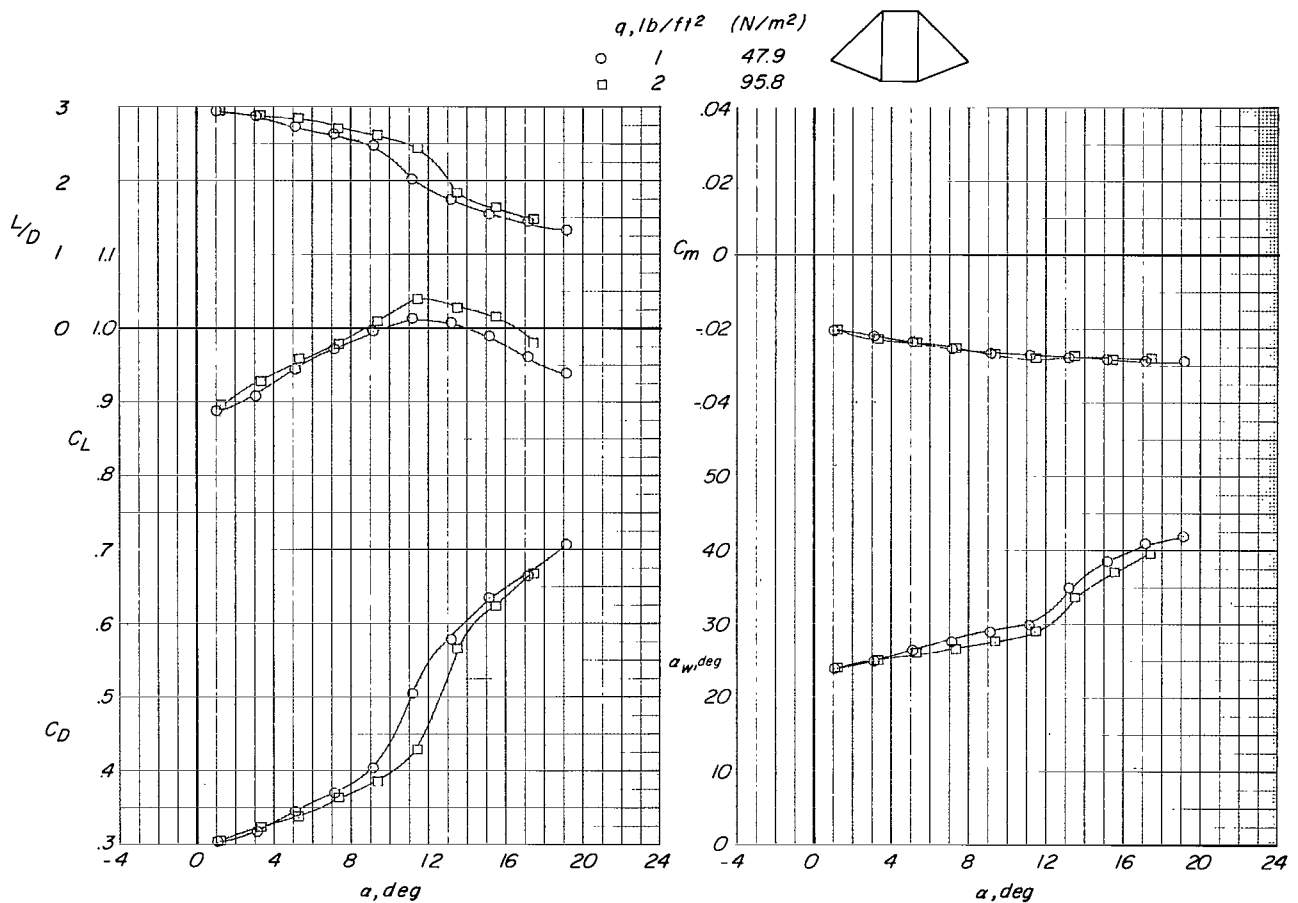


Figure 35.- Effect of dynamic pressure on the aerodynamic characteristics of twin-keel parawing model 6, rerigged.

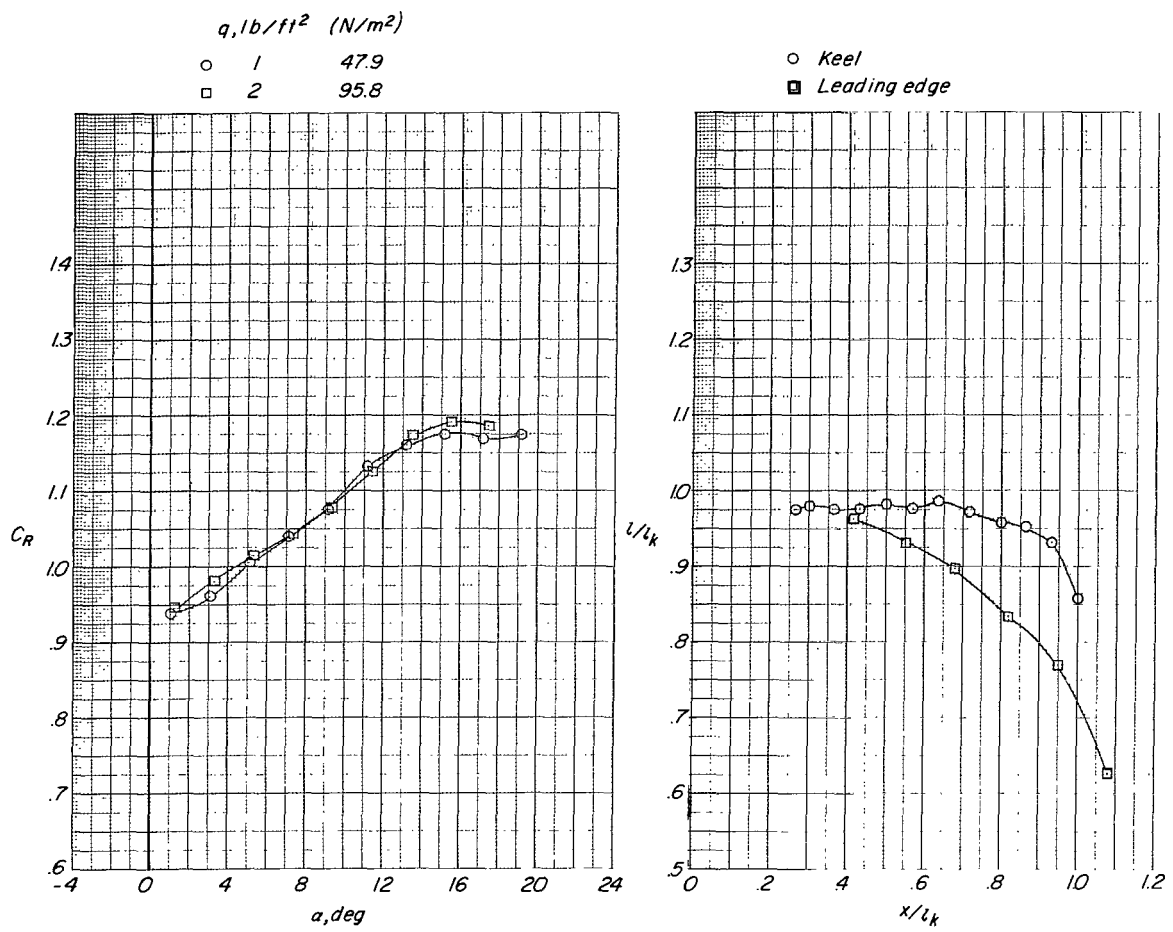
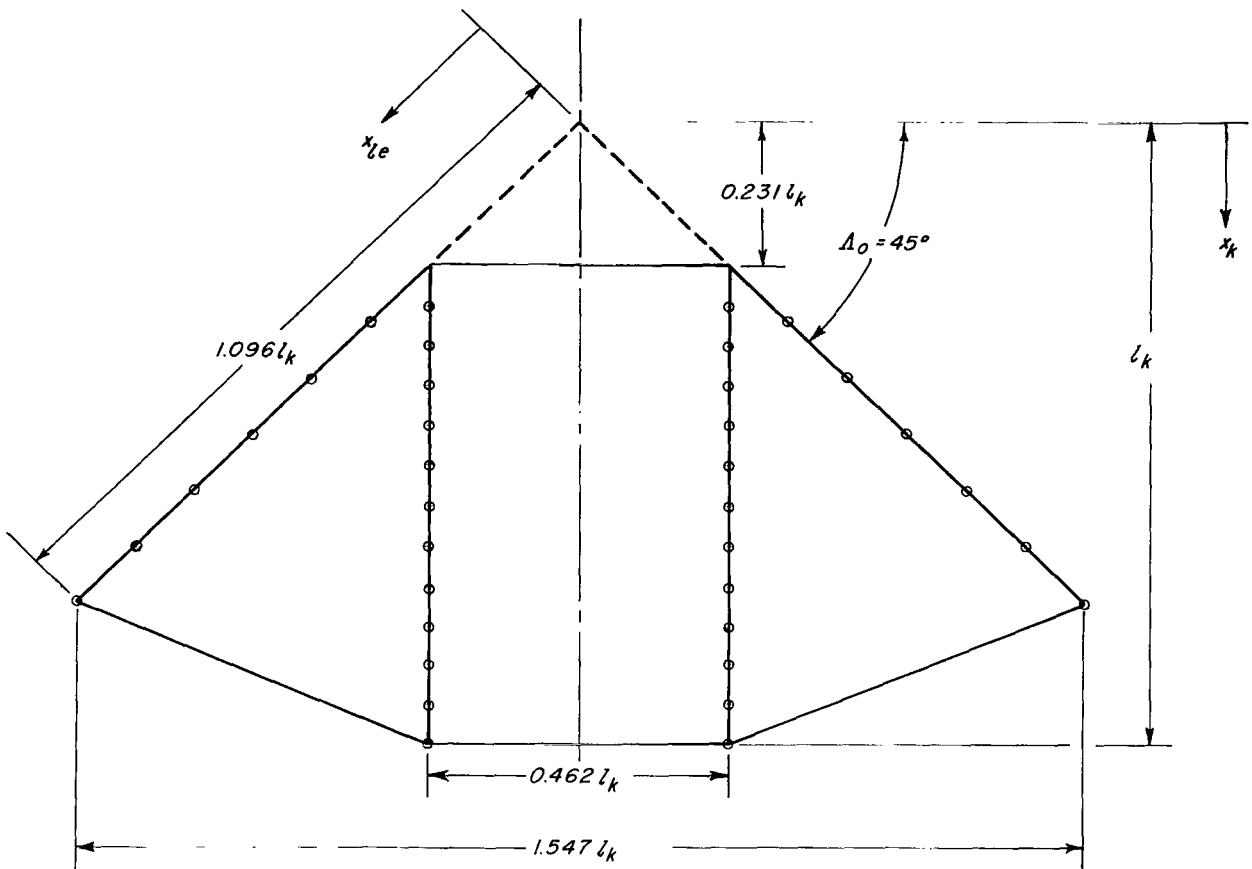


Figure 35.- Concluded.



*Line attachment locations*

$x/l_k$

<i>KeeI</i>	<i>Leading edge</i>	
	<i>A</i>	<i>B</i>
.295	.455	.480
.359	.583	.634
.423	.711	.788
.487	.839	.942
.551	.967	1.096
.615	1.096	
.680		
.744	<i>A: Six-line leading-edge arrangement</i>	
.808		
.872	<i>B: Five-line leading-edge arrangement</i>	
.936		
1.000		

Figure 36.- Flat-planform details of twin-keel parawing model 7.

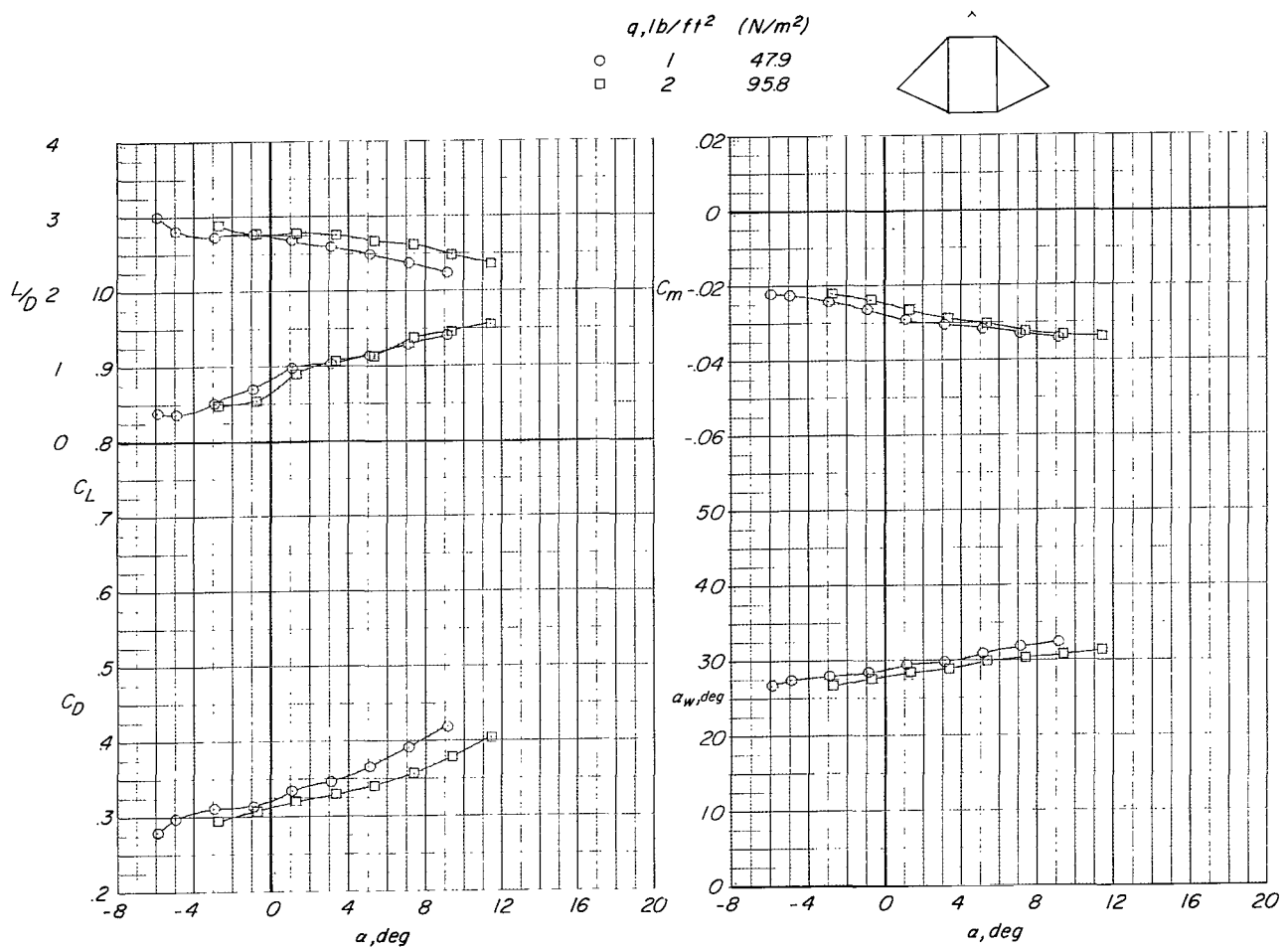


Figure 37.- Effect of dynamic pressure on the aerodynamic characteristics of twin-keel parawing model 7 with six lines on each leading edge.

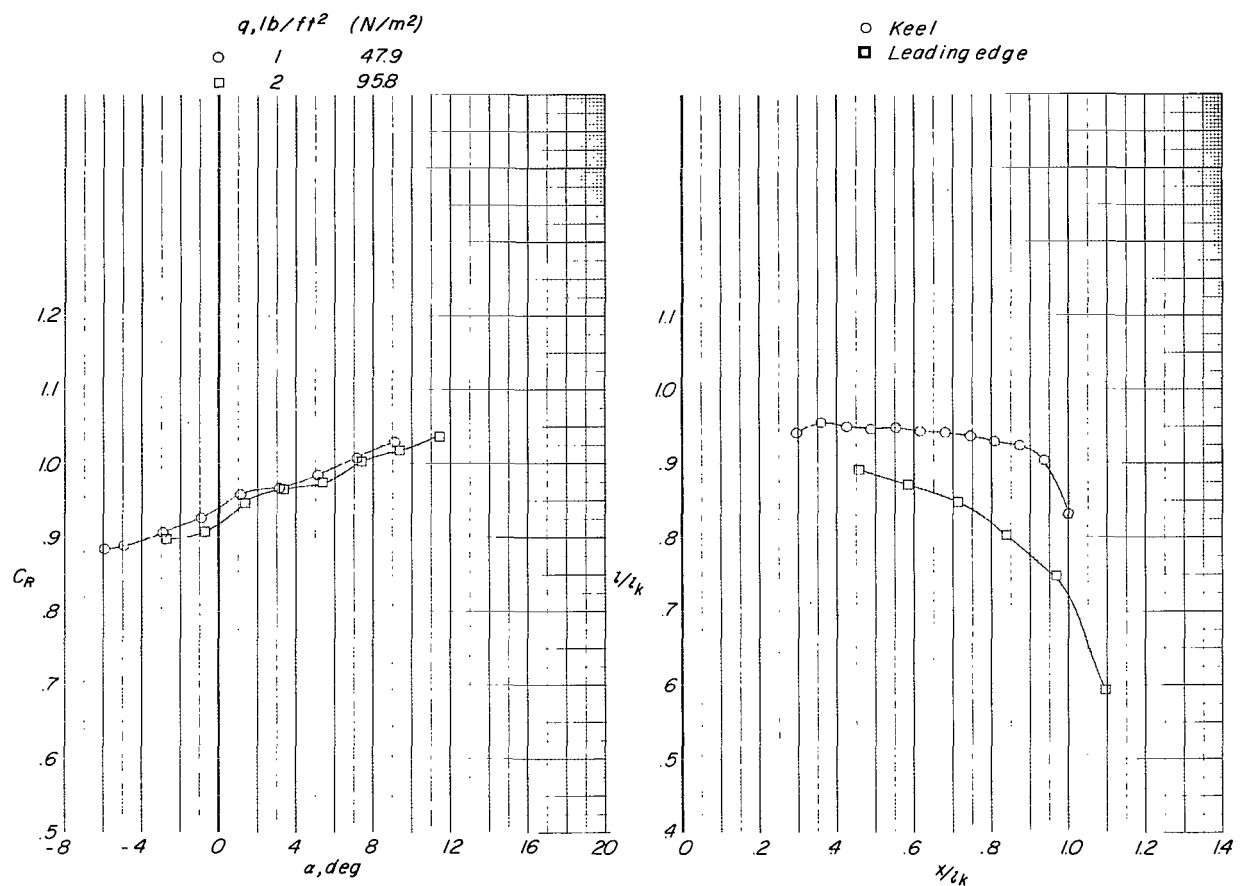


Figure 37.- Concluded.

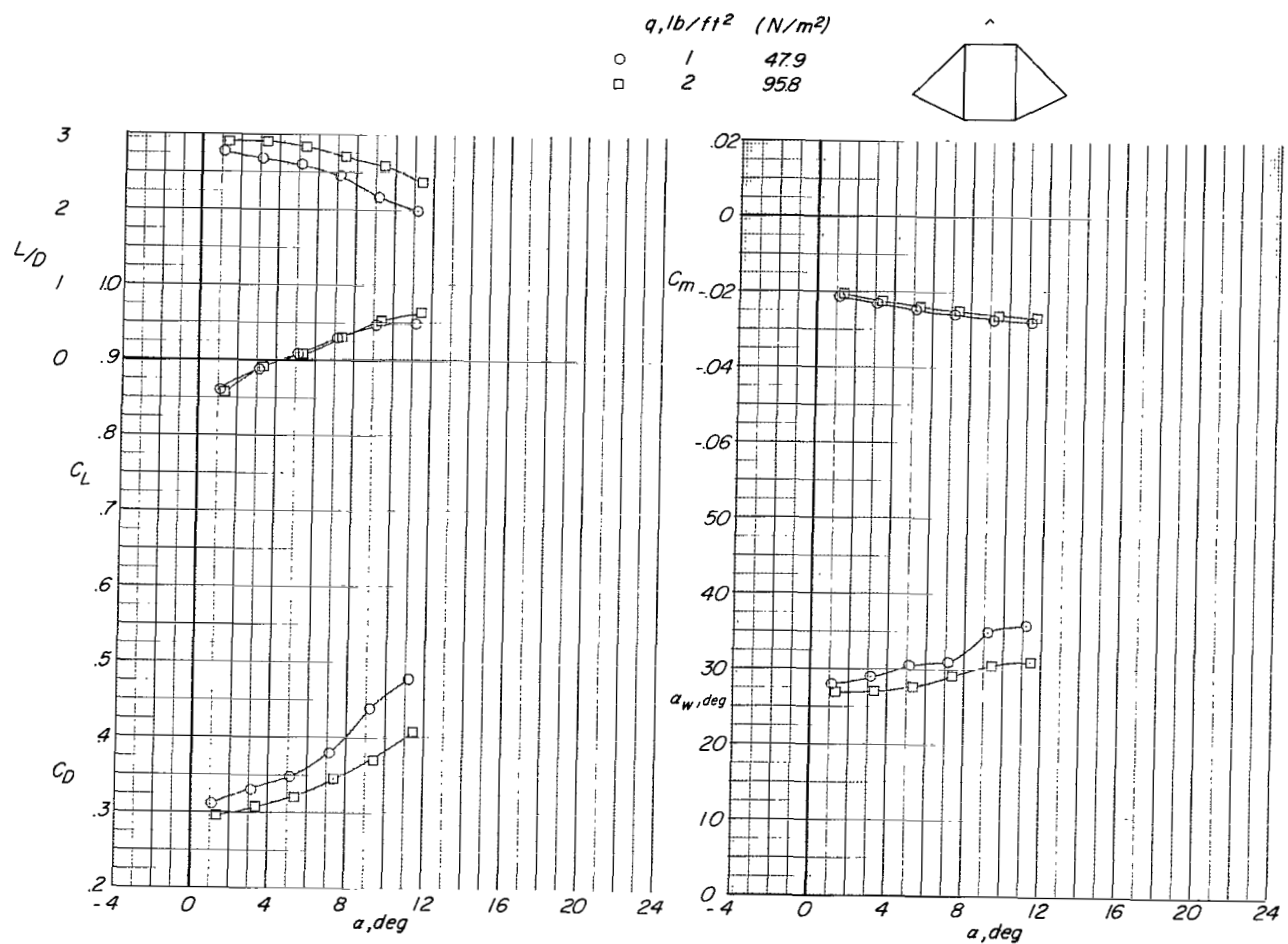


Figure 38.- Effect of dynamic pressure on the aerodynamic characteristics of twin-keel parawing model 7 with five lines on each leading edge.

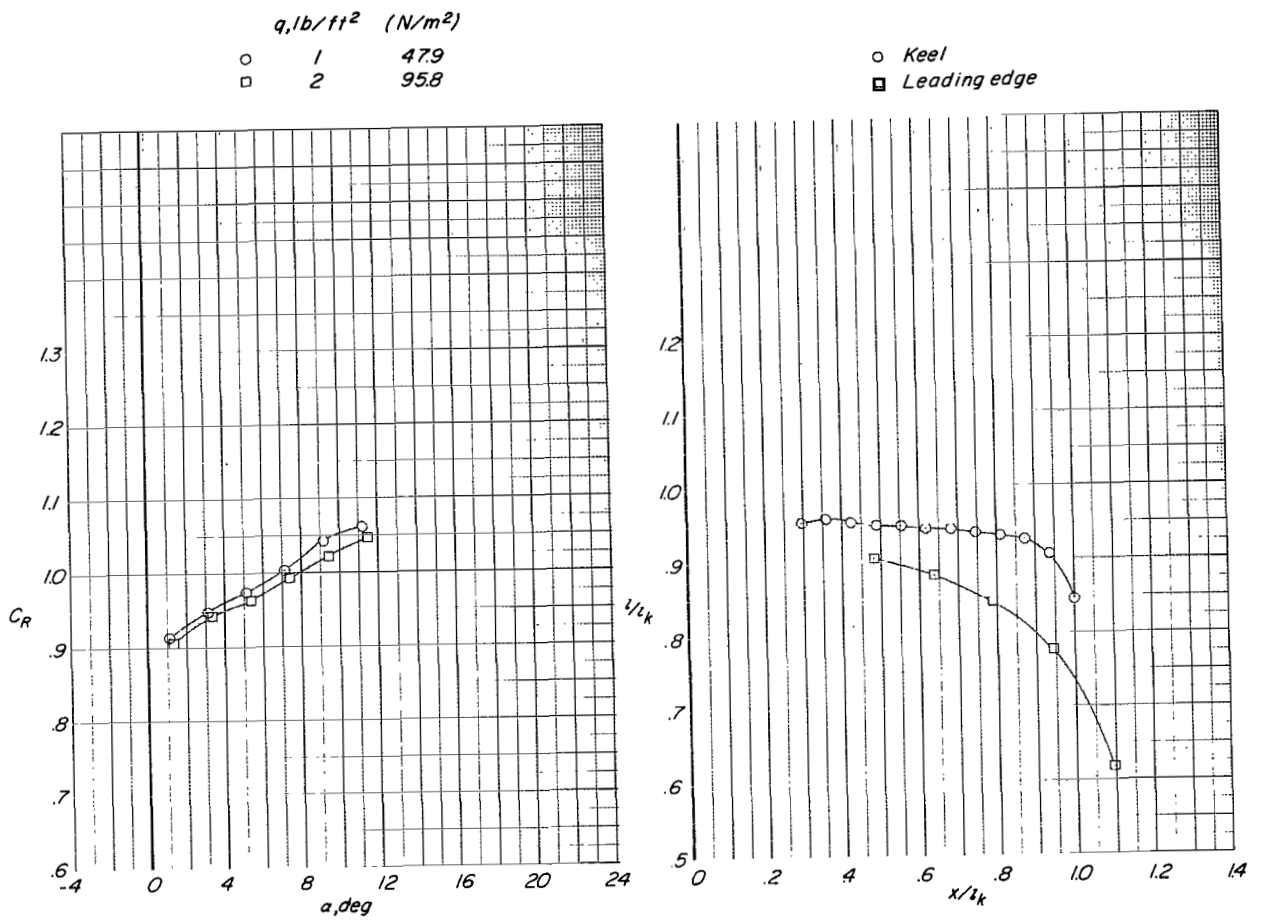
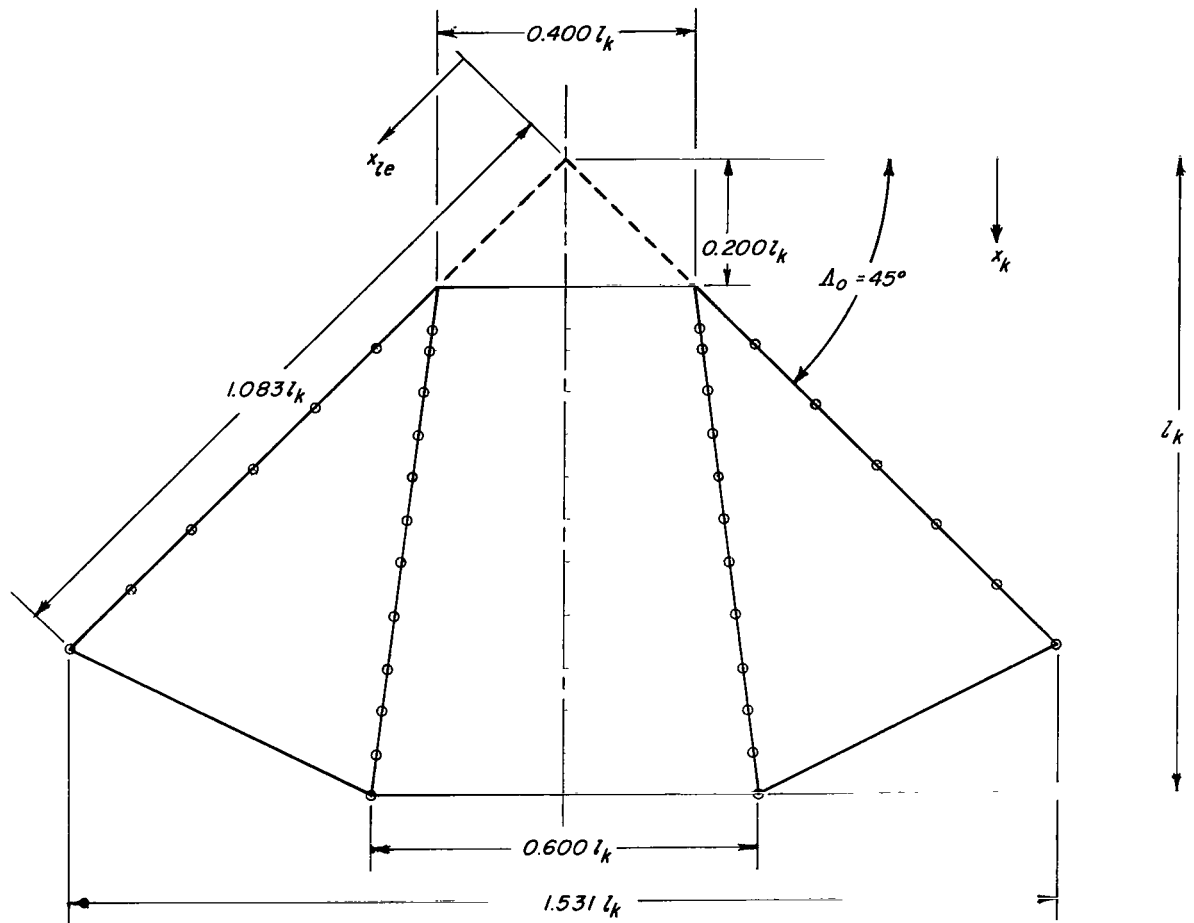


Figure 38.- Concluded.



*Line attachment locations*

$x/l_k$

<i>Keel</i>	<i>Leading edge</i>
.266	.416
.300	.549
.366	.683
.434	.816
.500	.949
.567	1.083
.634	
.716	
.800	
.866	
.934	
1.000	

Figure 39.- Flat-planform details of twin-keel parawing model 8.

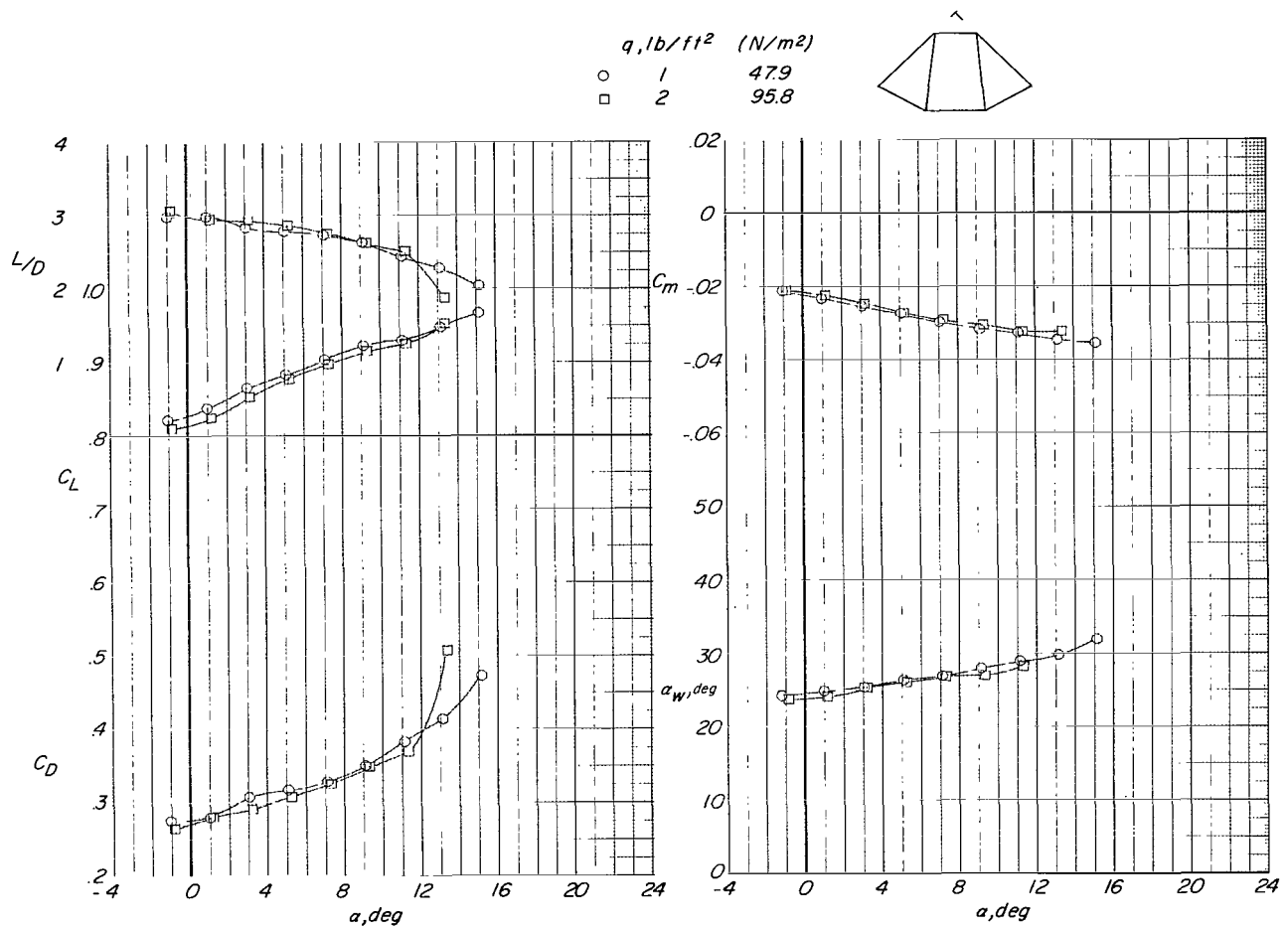


Figure 40.- Effect of dynamic pressure on the aerodynamic characteristics of twin-keel parawing model 8.

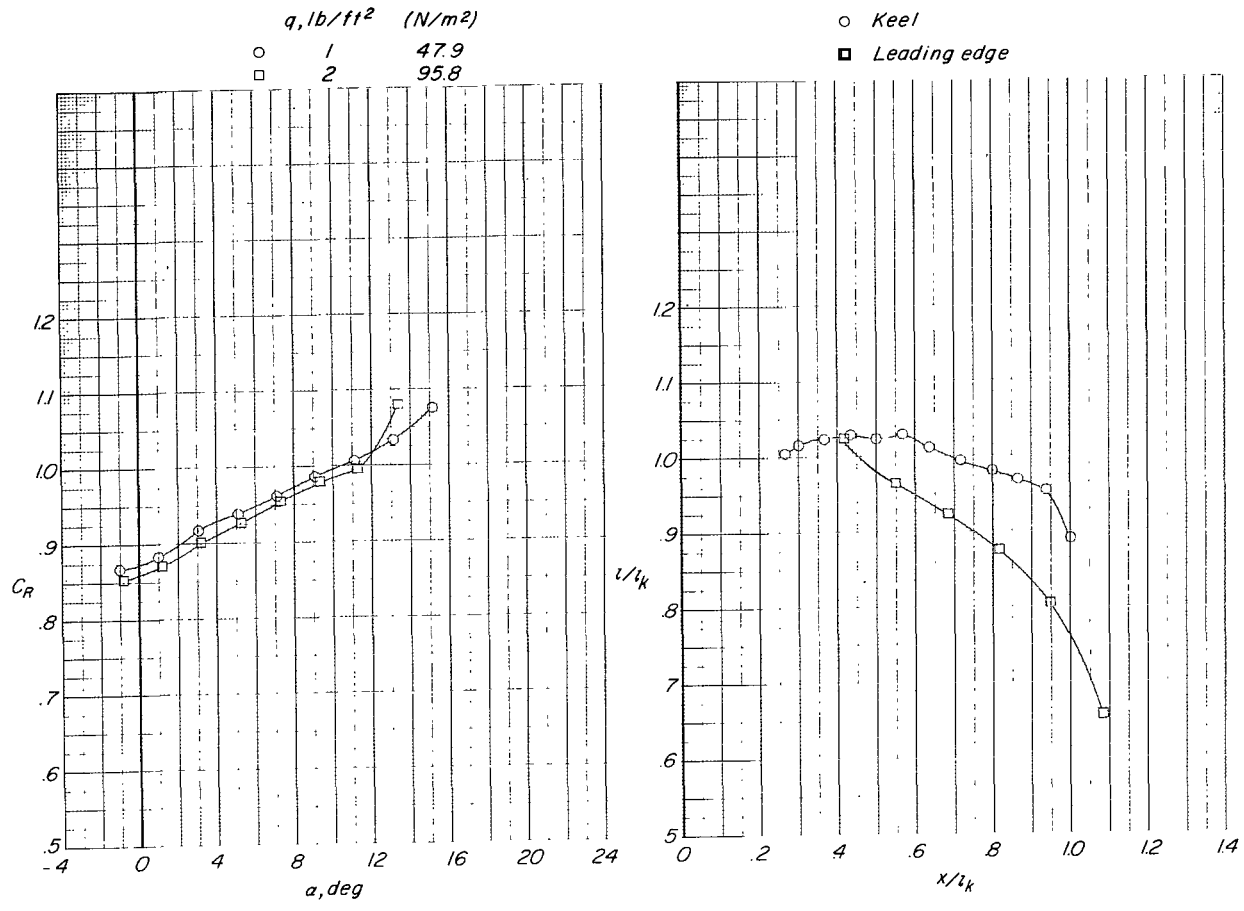
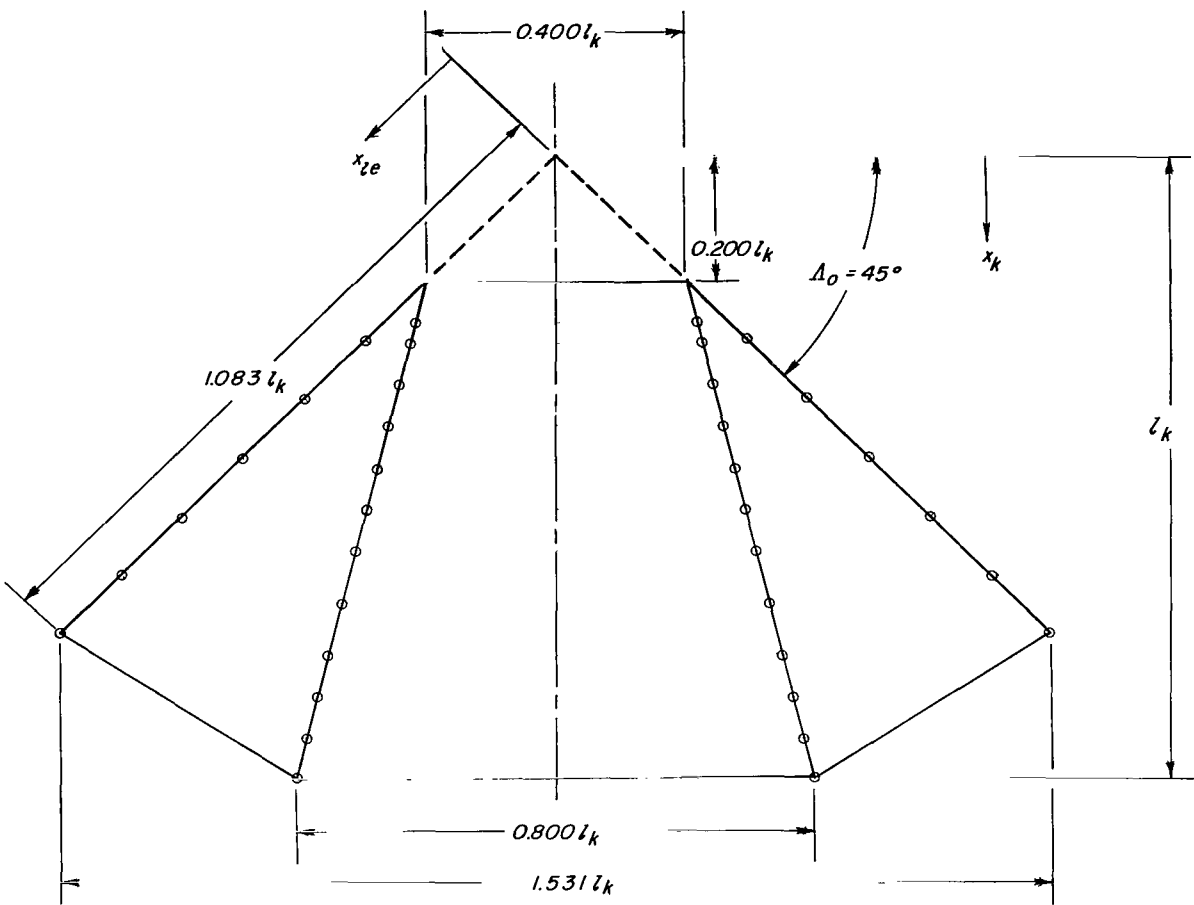


Figure 40.- Concluded.



*Line attachment locations*

$x/l_k$

<i>Keel</i>	<i>Leading edge</i>
.266	.416
.300	.549
.366	.683
.434	.816
.500	.949
.567	1.083
.634	
.716	
.800	
.866	
.934	
1.000	

Figure 41.- Flat-planform details of twin-keel parawing model 9.

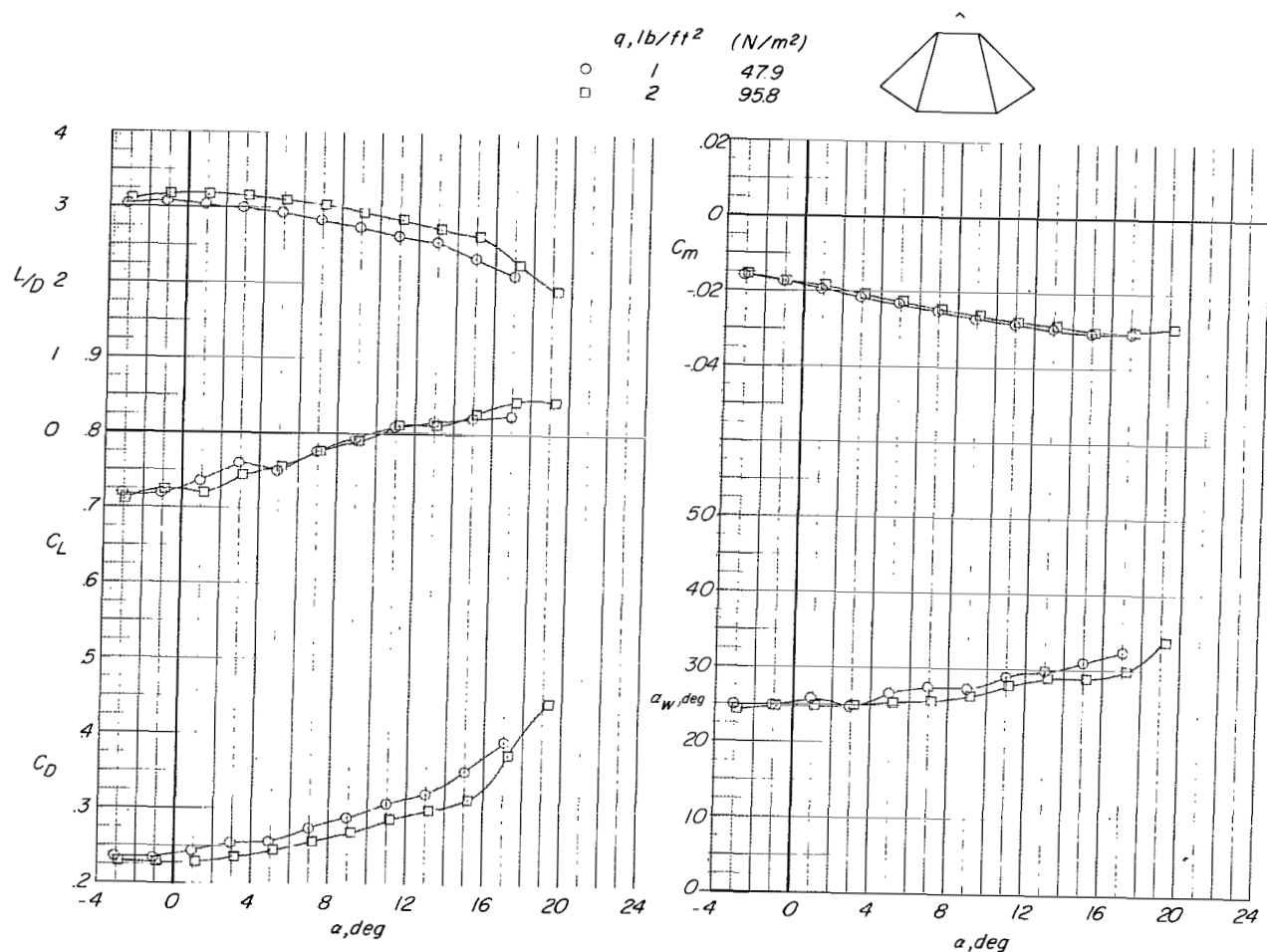


Figure 42.- Effect of dynamic pressure on the aerodynamic characteristics of twin-keel parawing model 9.

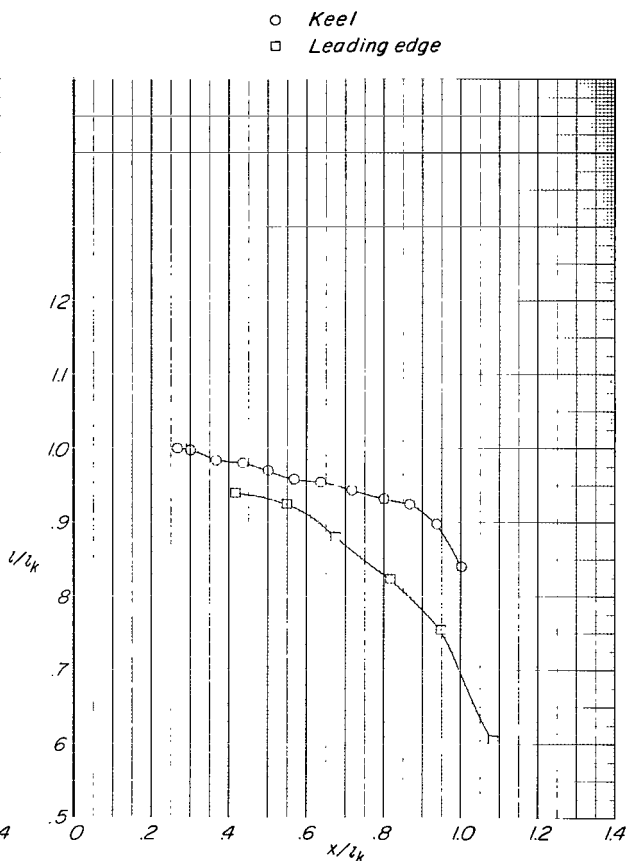
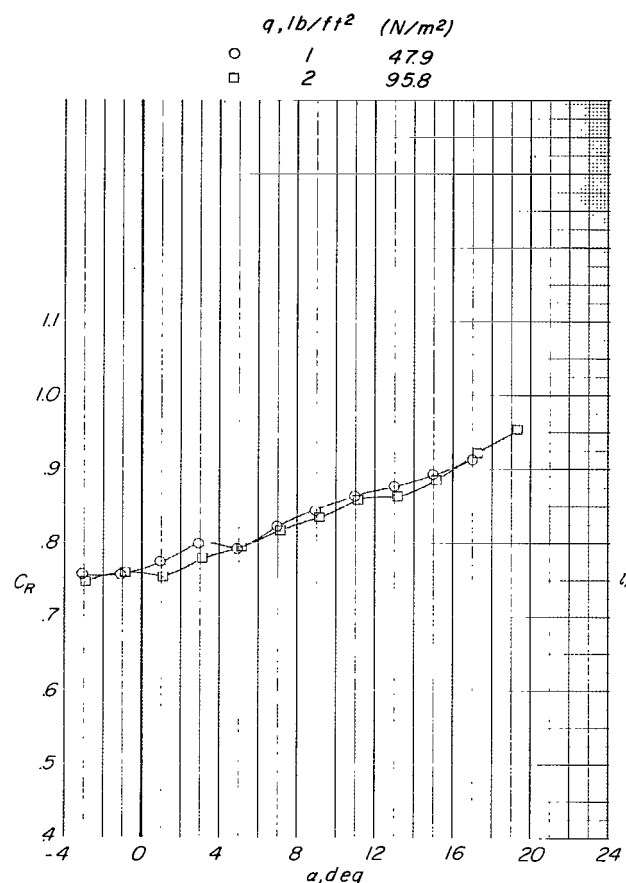


Figure 42.- Continued.

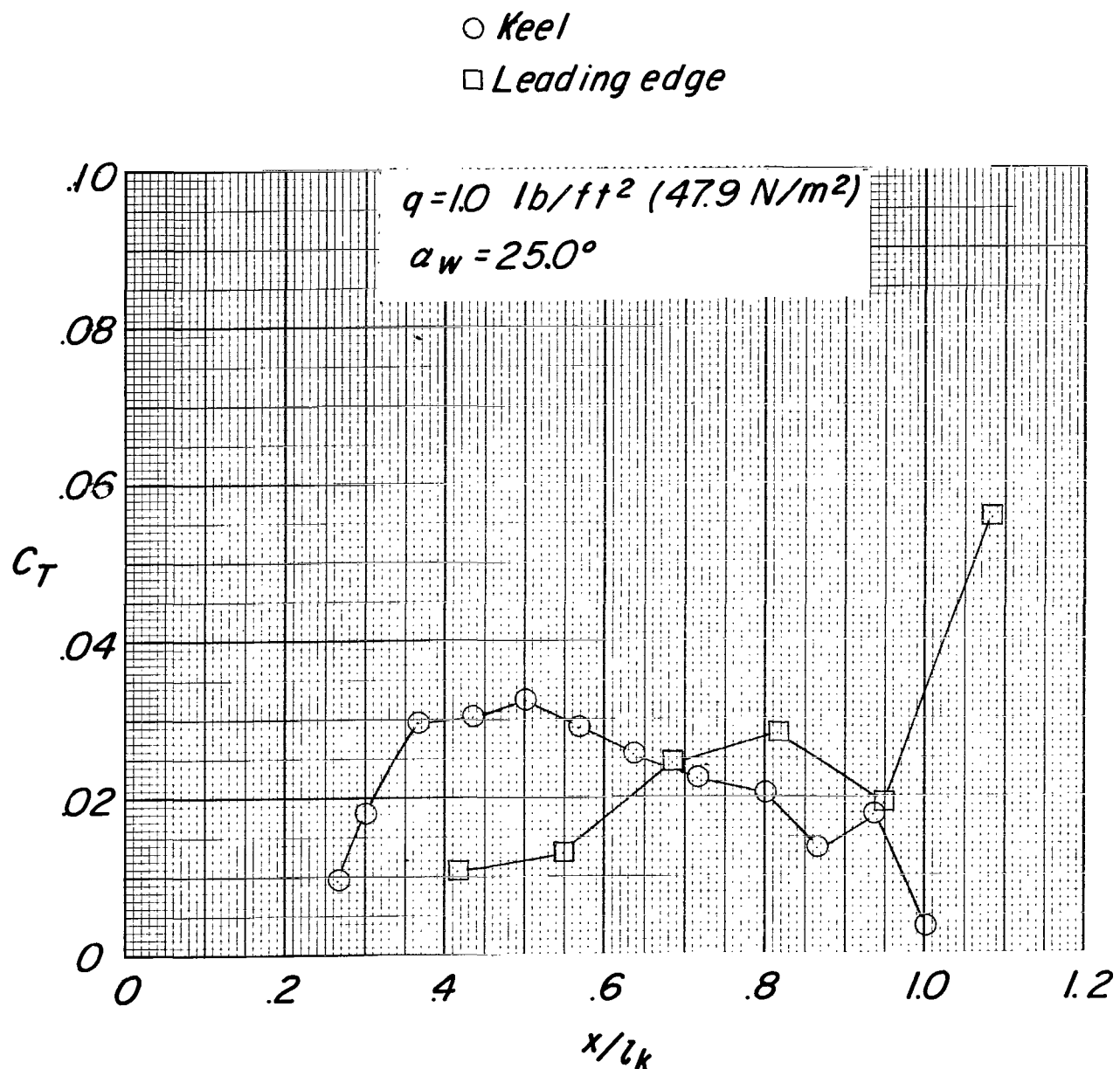
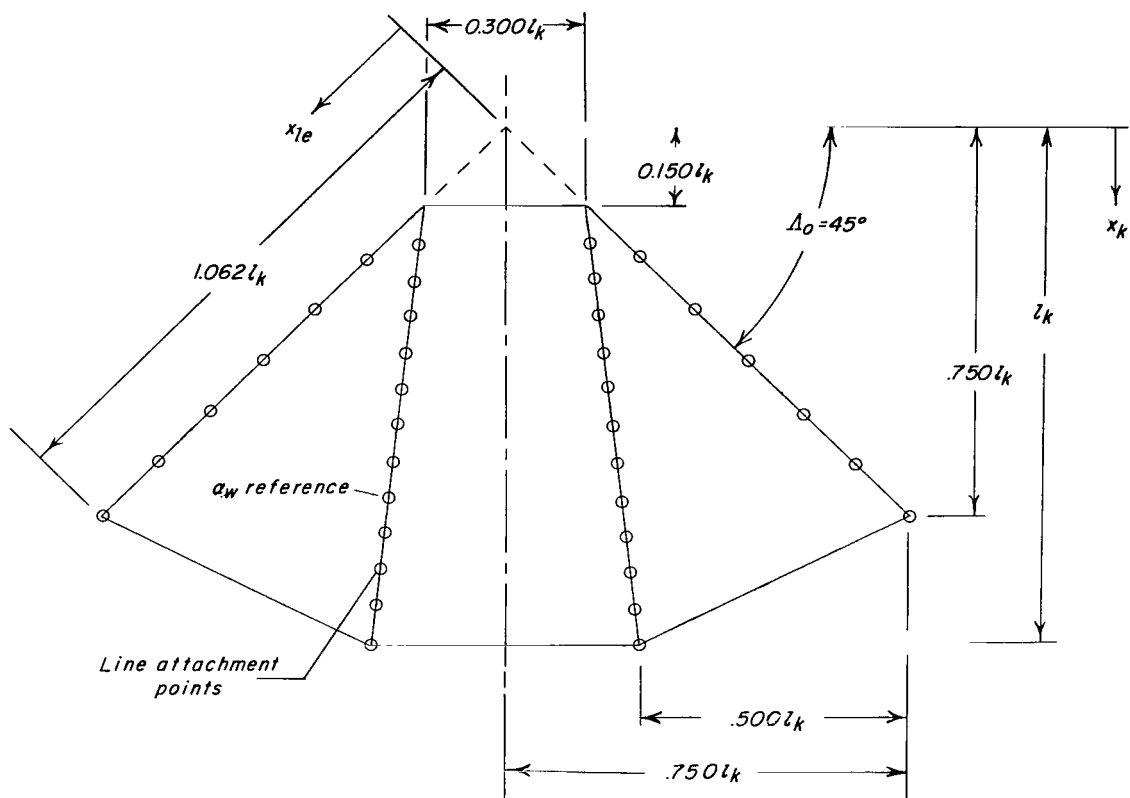


Figure 42.- Concluded.



Line attachment locations

$x/l_k$

Keel

Leading edge

.221	.354
.292	.433
.363	.637
.433	.779
.504	.920
.575	1.062
.646	
.717	
.788	
.858	
.929	
1.000	

Figure 43.- Flat-planform details of twin-keel parawing model 10.

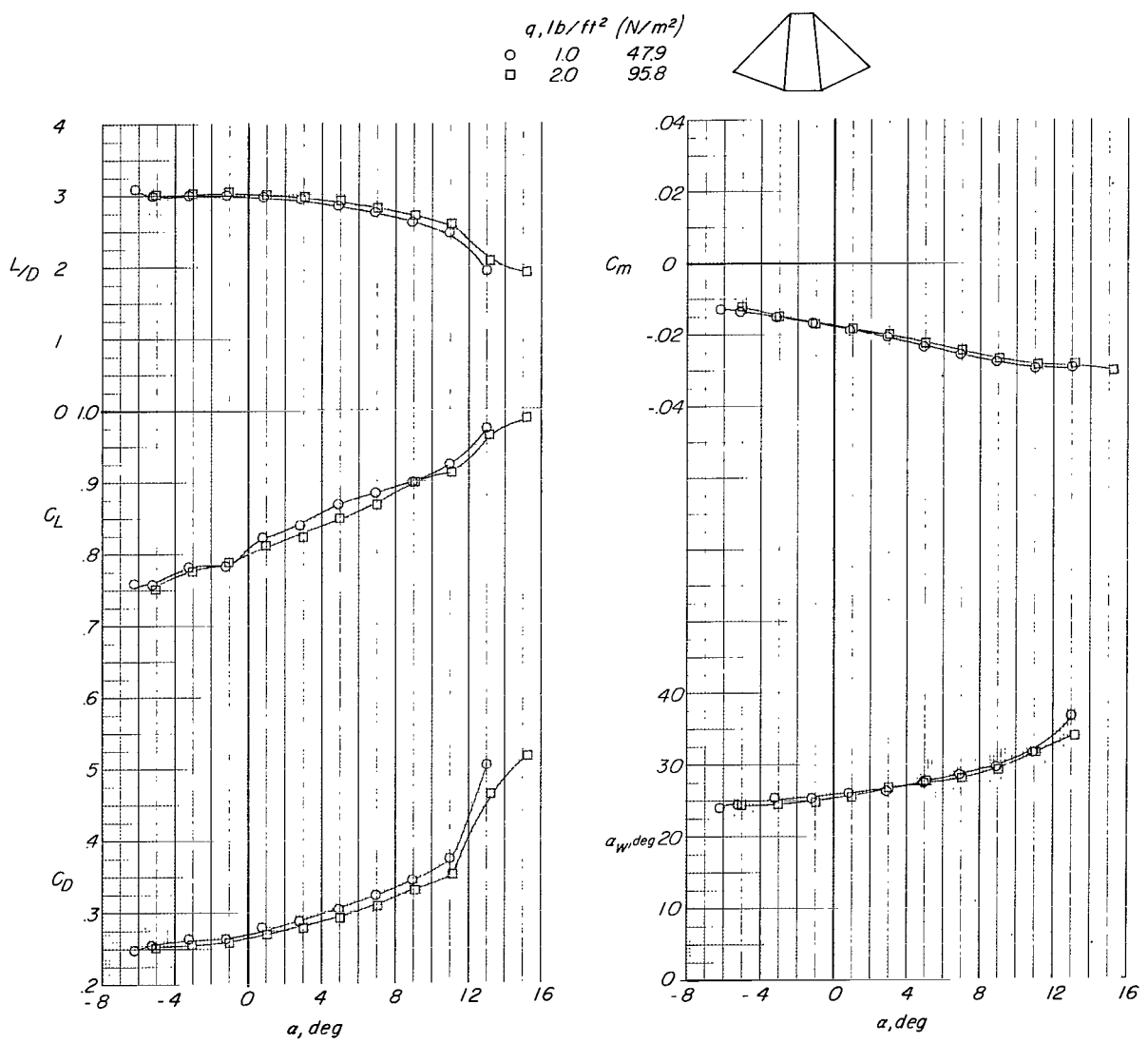


Figure 44.- Effect of dynamic pressure on the aerodynamic characteristics of twin-keel parawing model 10.

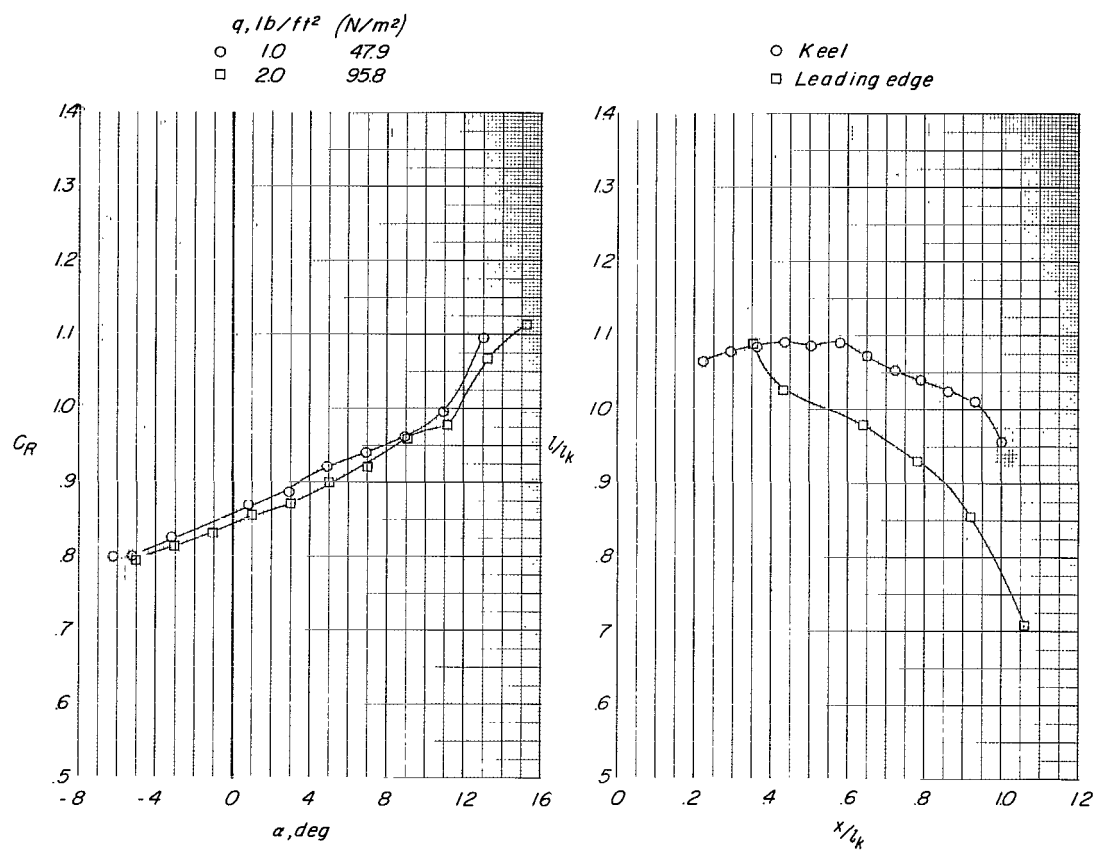


Figure 44.- Concluded.

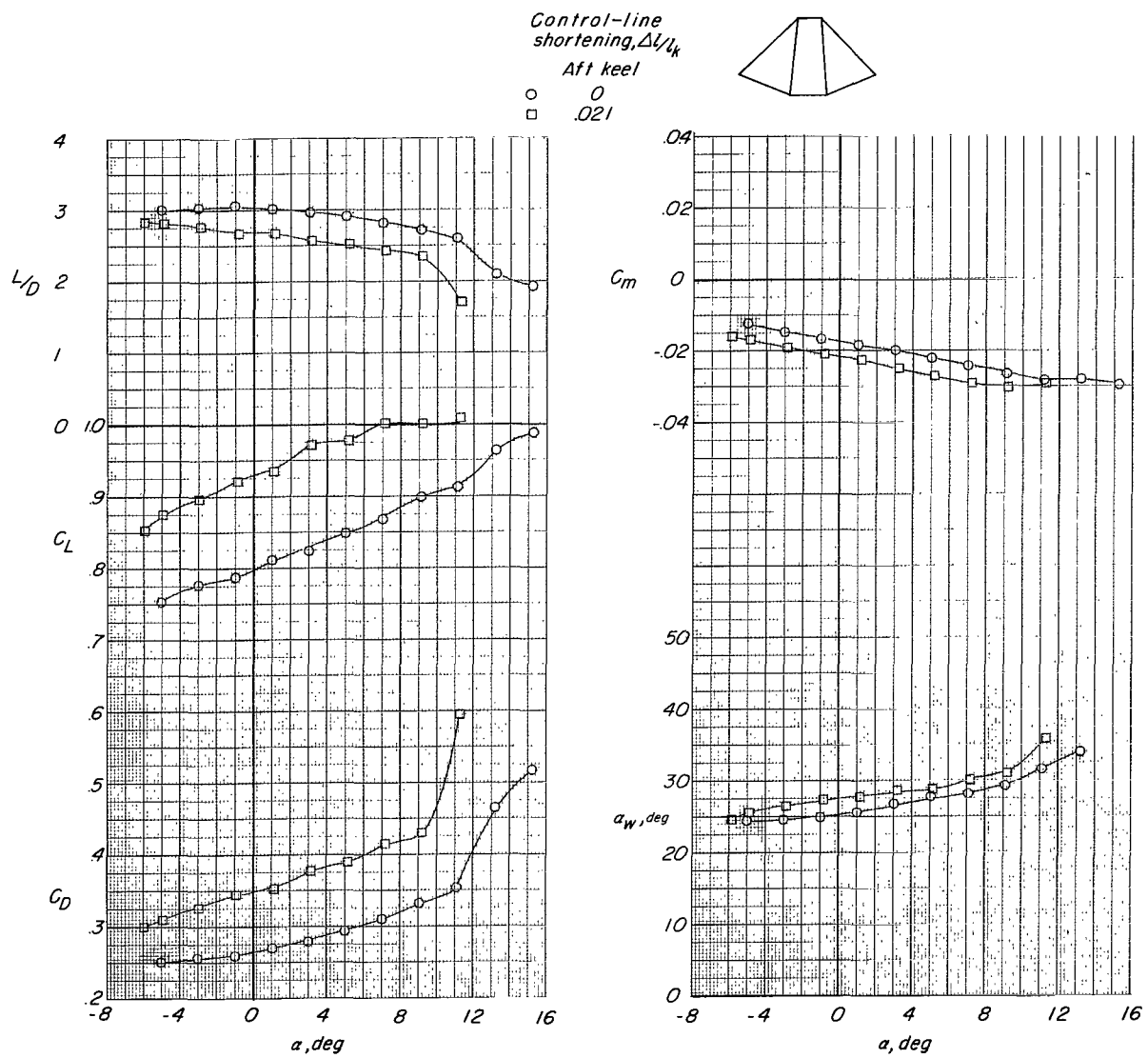


Figure 45.- Effect of aft-keel-line shortening on the aerodynamic characteristics of twin-keel parawing model 10.  $q = 2.0 \text{ lb/ft}^2$  (95.8 N/m<sup>2</sup>).

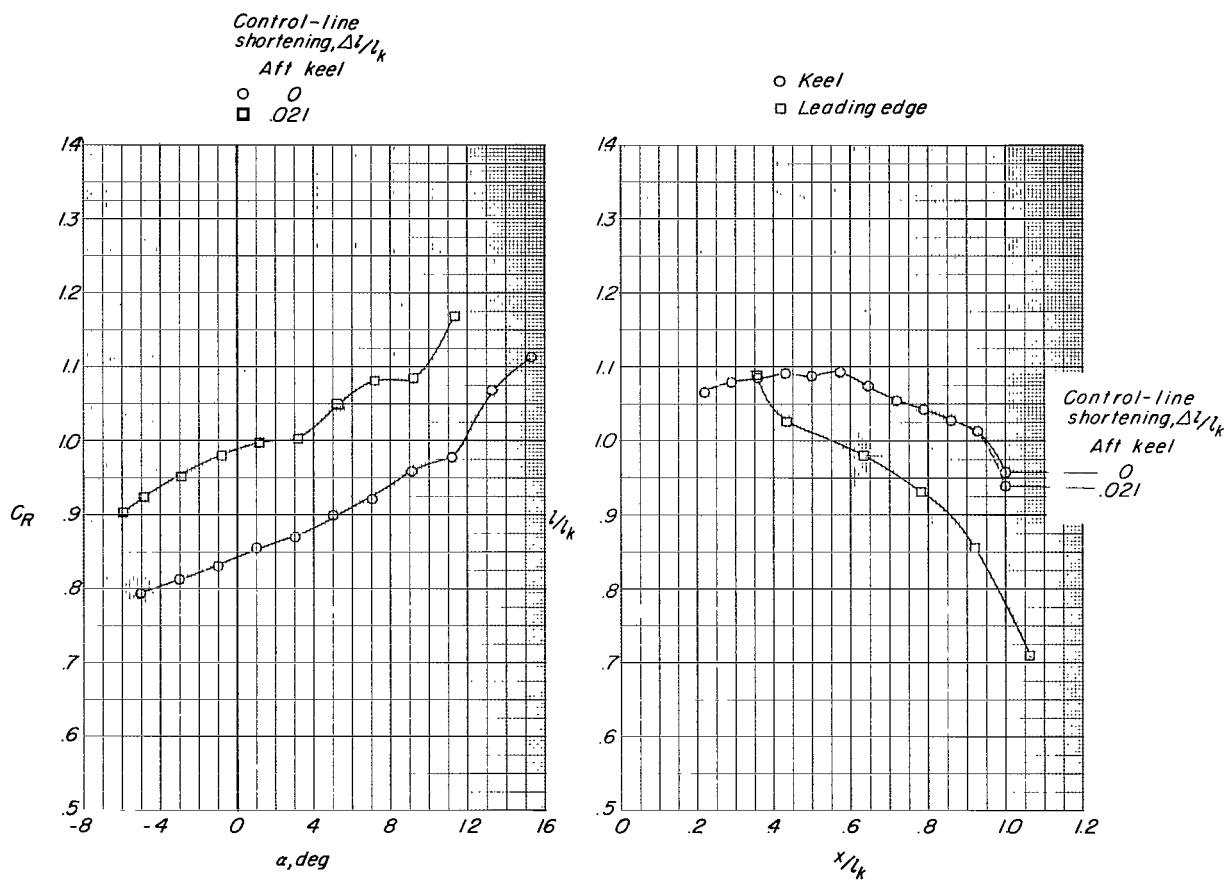


Figure 45.- Concluded.

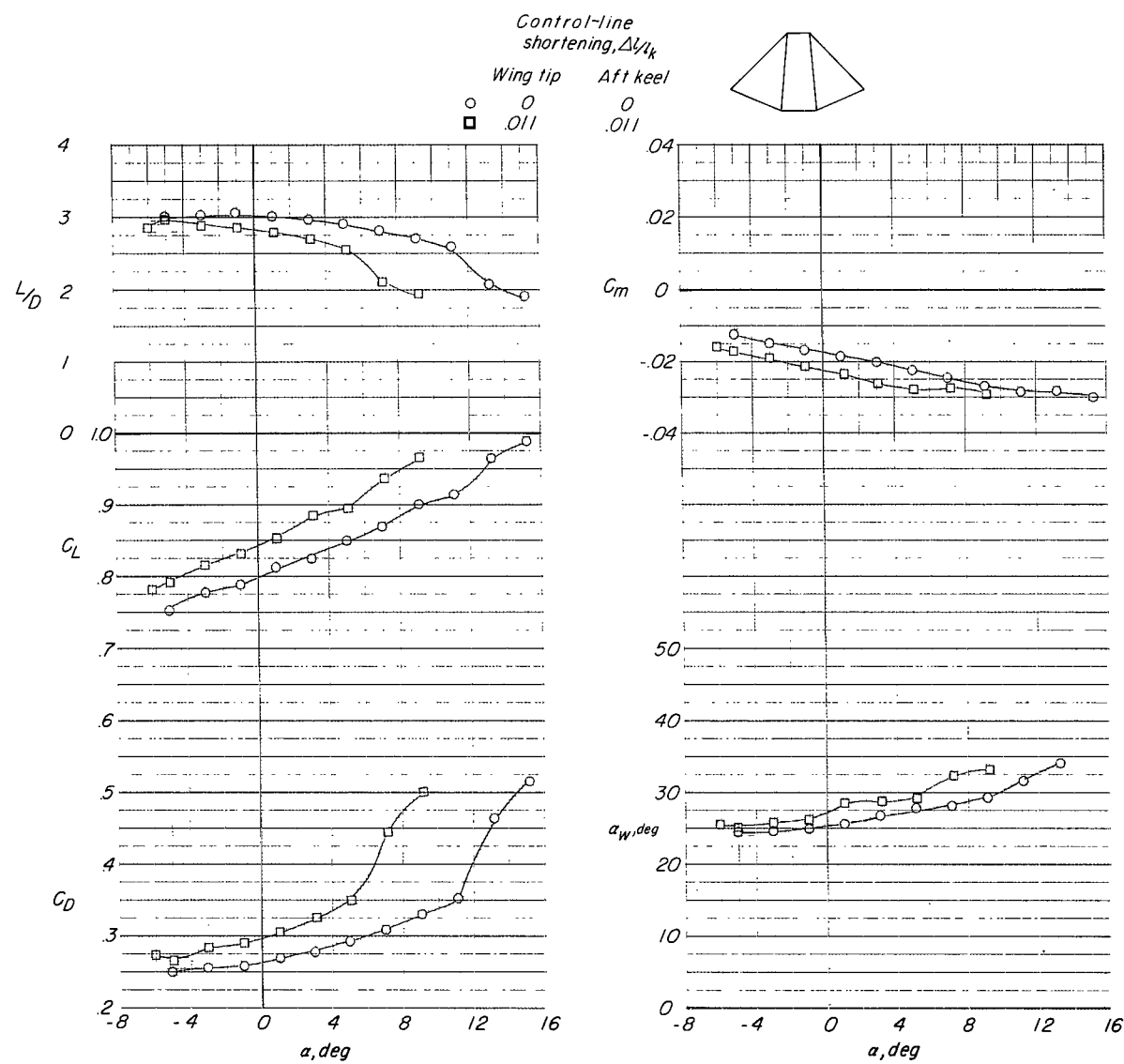


Figure 46.- Effect of tip-line and aft-keel-line shortening on the aerodynamic characteristics of twin-keel parawing model 10.  $q = 2.0 \text{ lb/ft}^2$  ( $95.8 \text{ N/m}^2$ ).

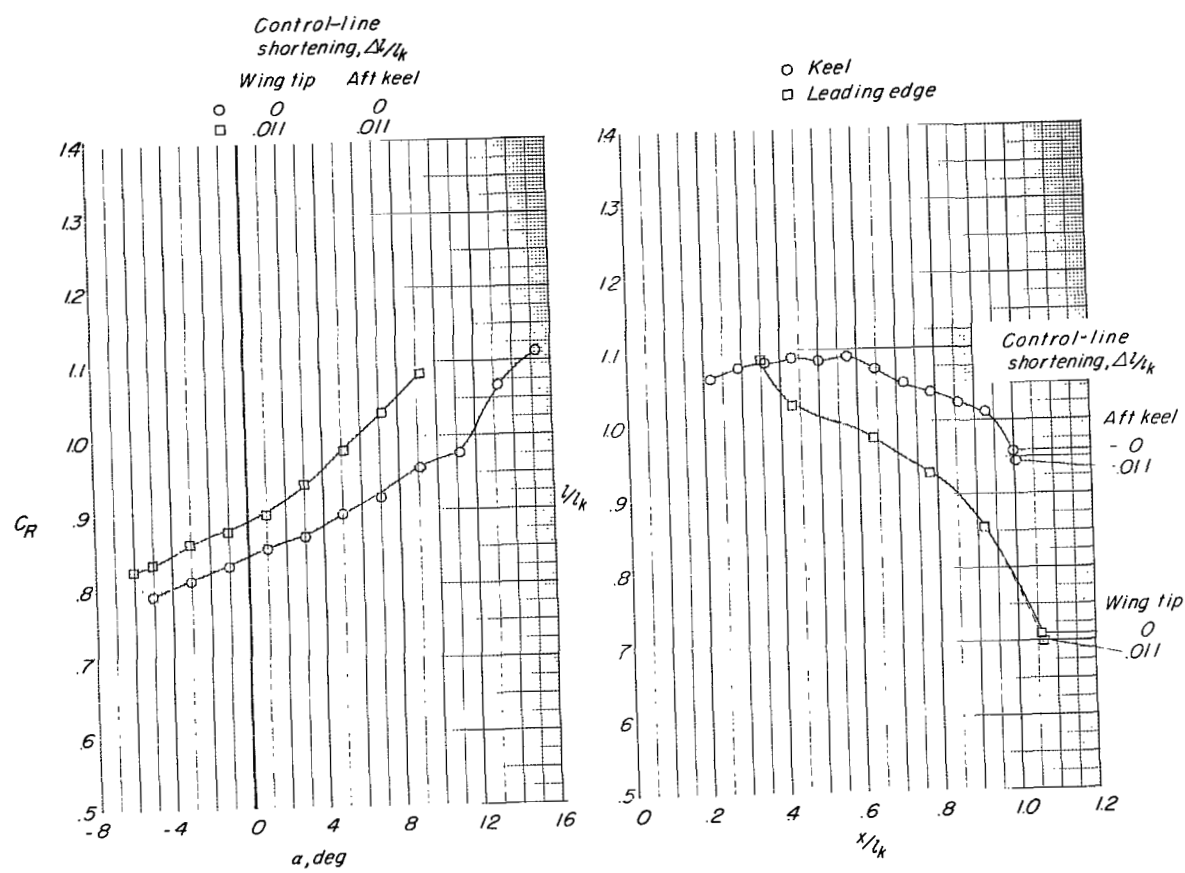


Figure 46.- Concluded.

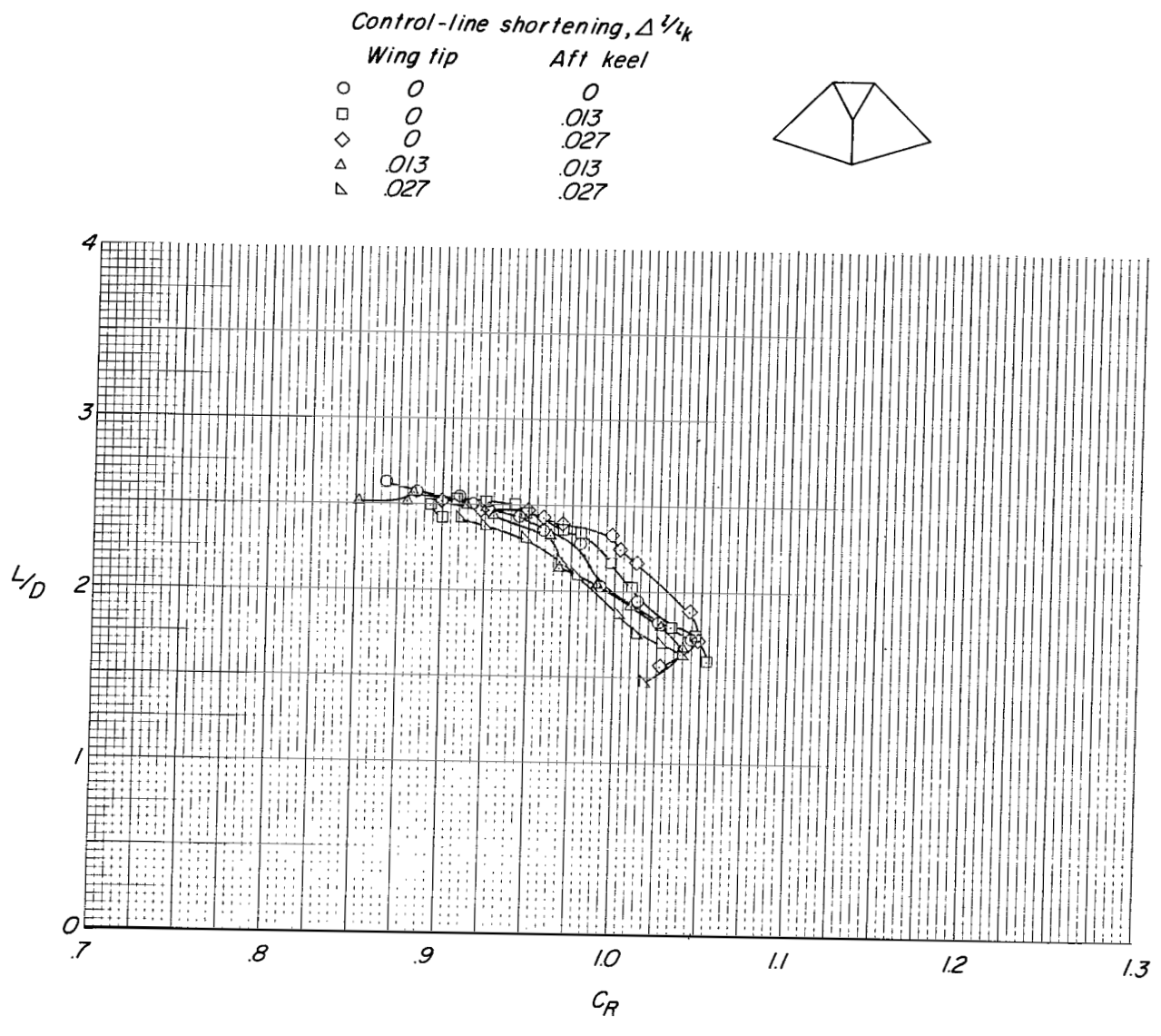
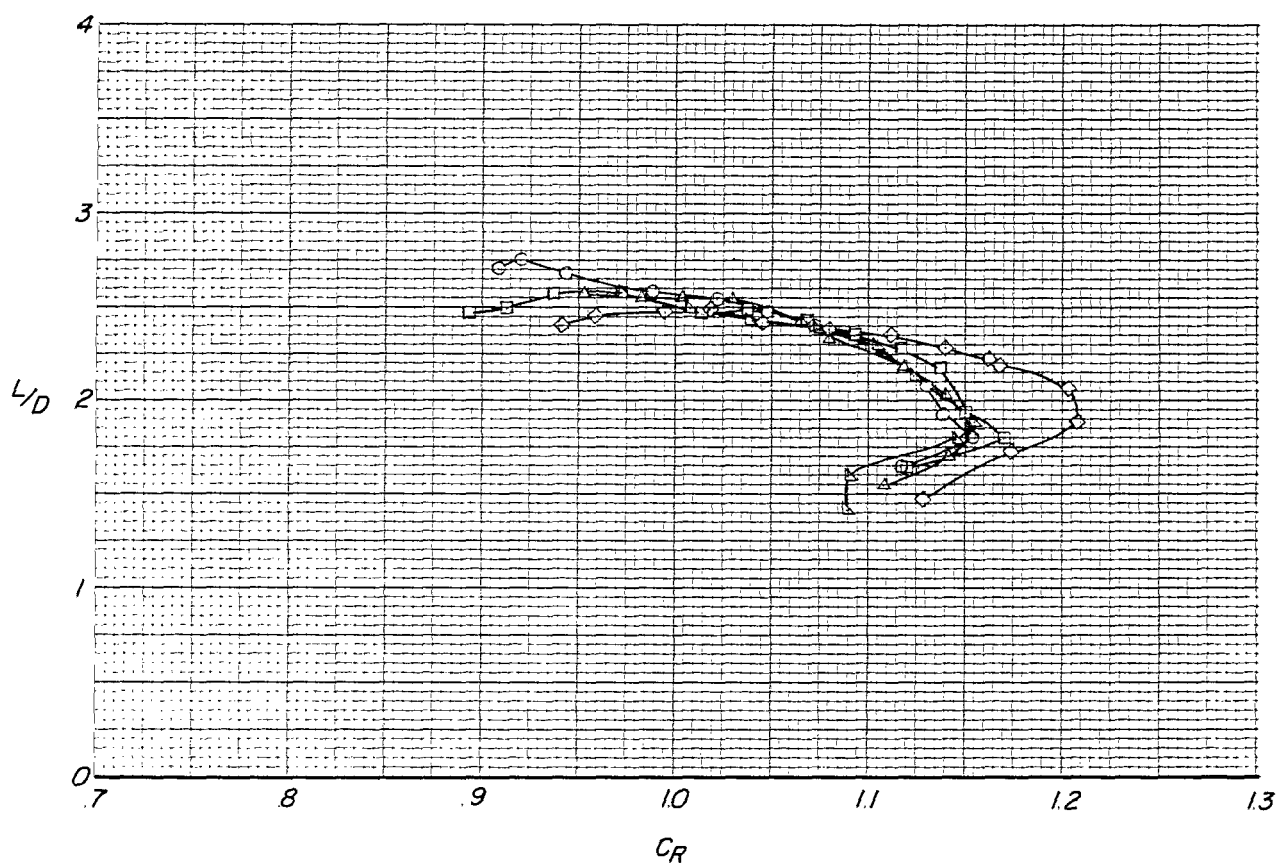
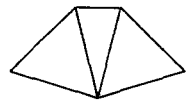


Figure 47.- Effect of control-line shortening on the variation of  $L/D$  with  $C_L$ .  $q = 2.0 \text{ lb/ft}^2$  ( $95.8 \text{ N/m}^2$ ).

Control-line shortening,  $\Delta l/l_k$

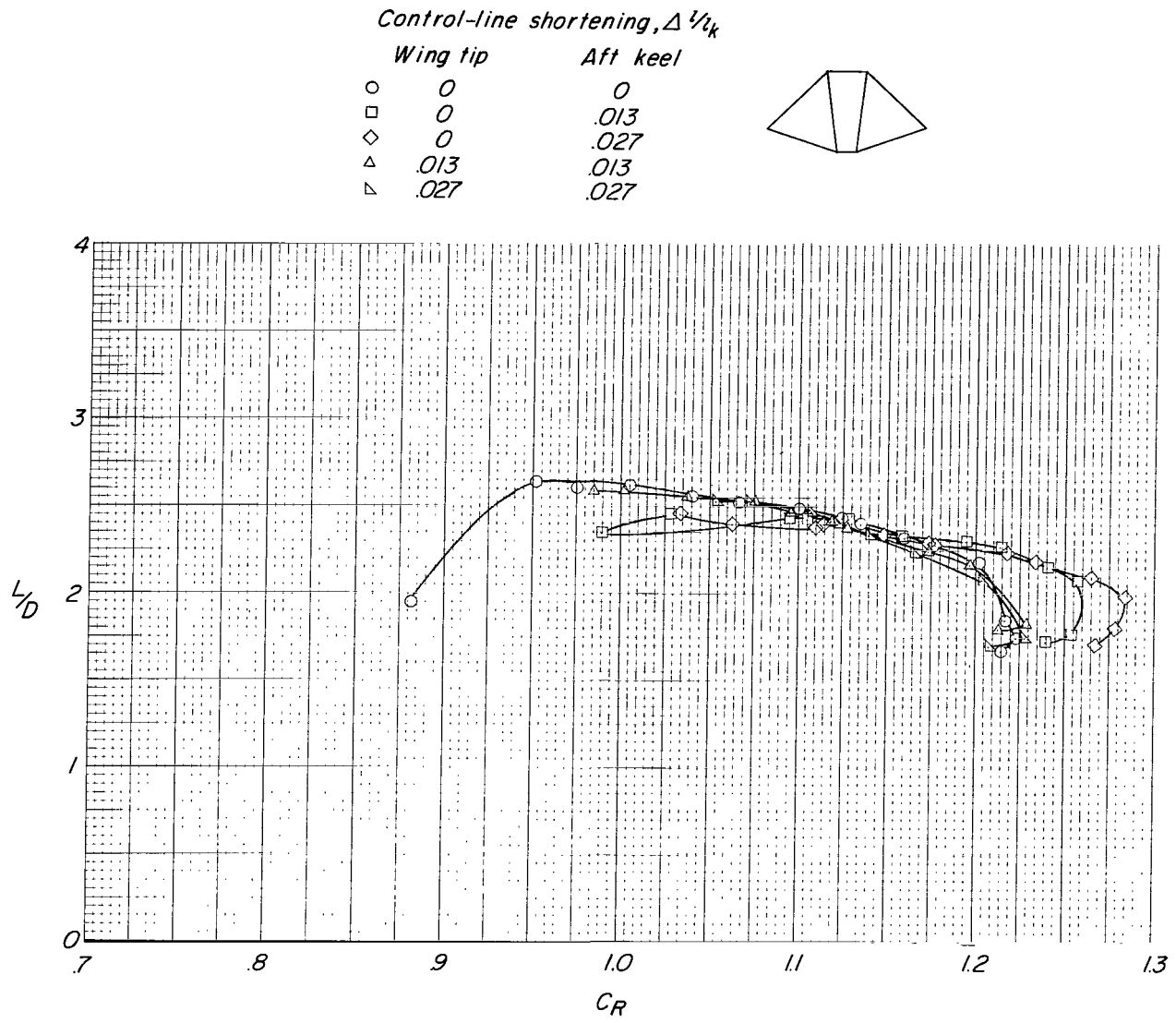
Wing tip      Aft keel

○	0	0
□	0	.013
◊	0	.027
△	.013	.013
▽	.027	.027



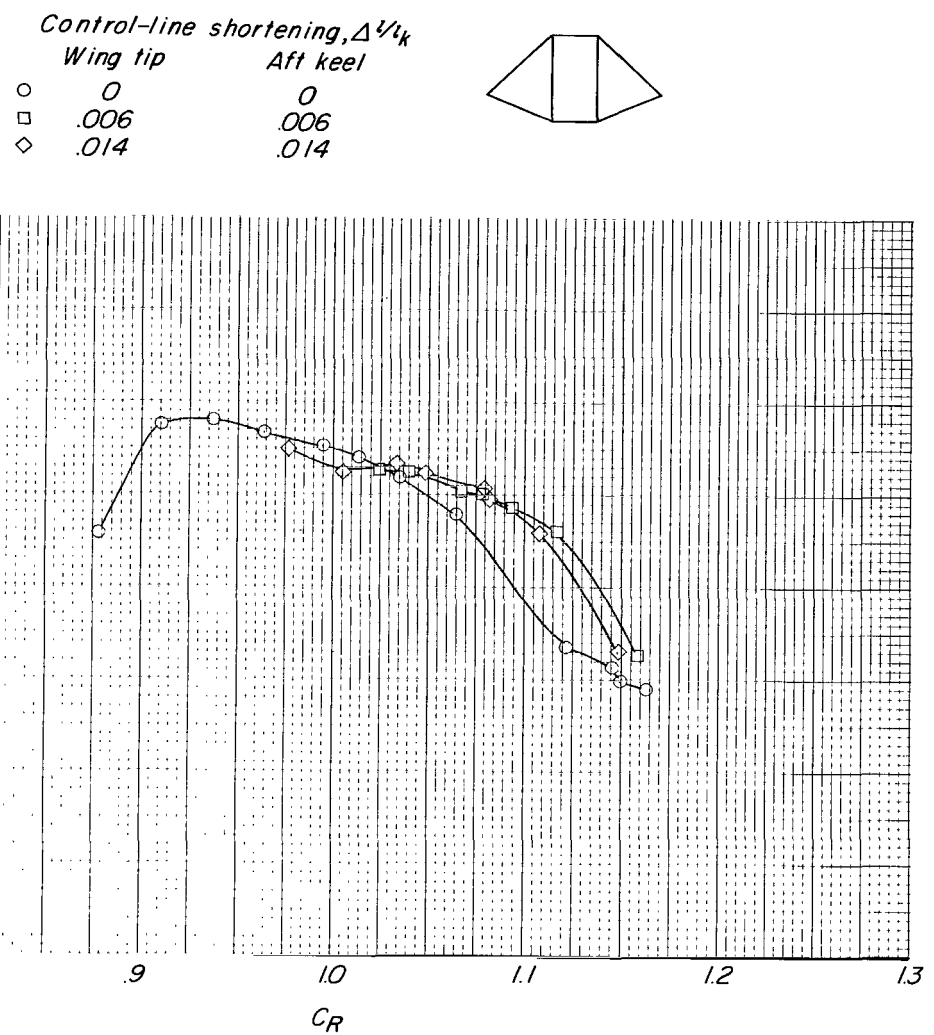
(b) Model 2.

Figure 47.- Continued.



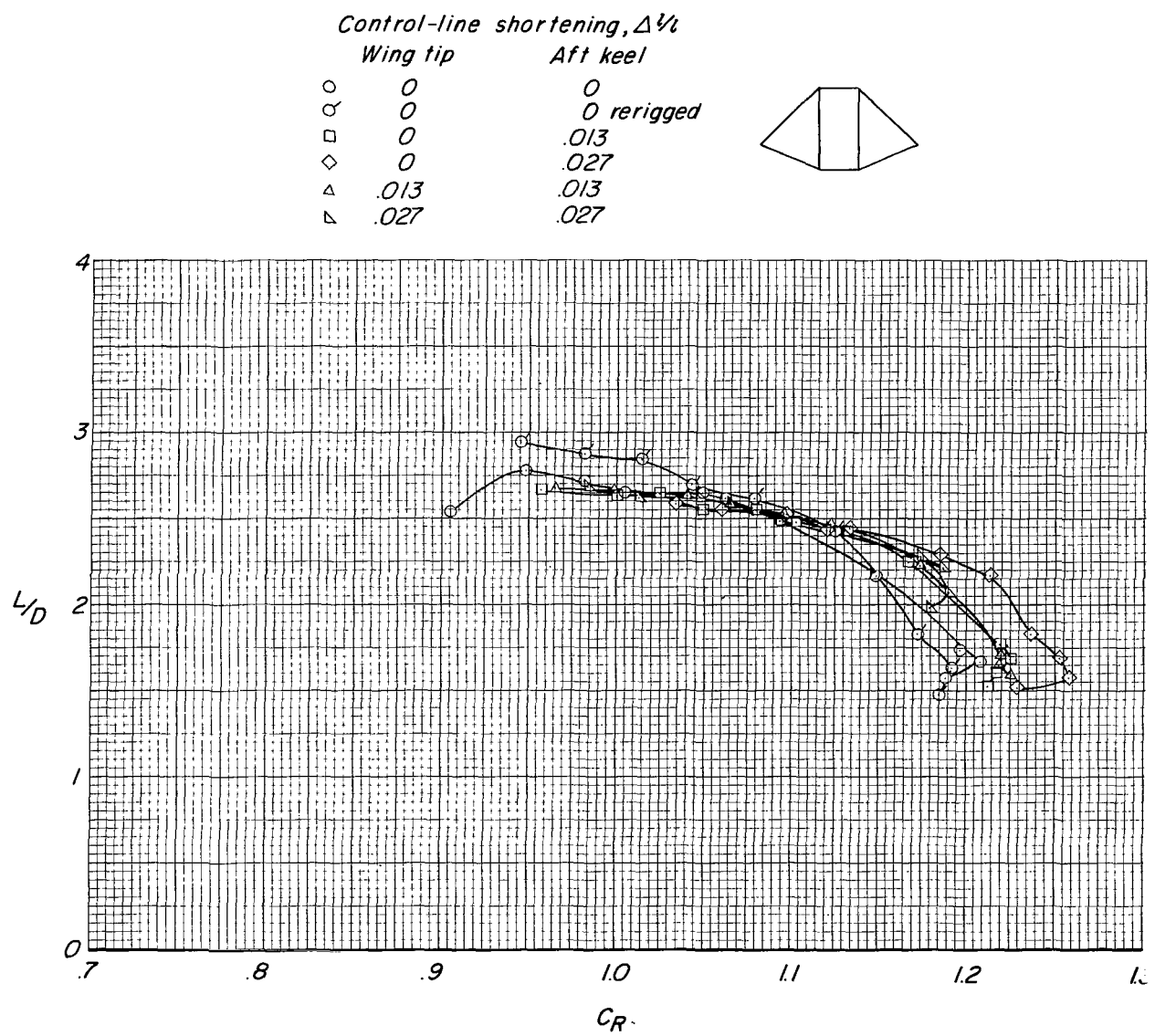
(c) Model 3.

Figure 47.- Continued.



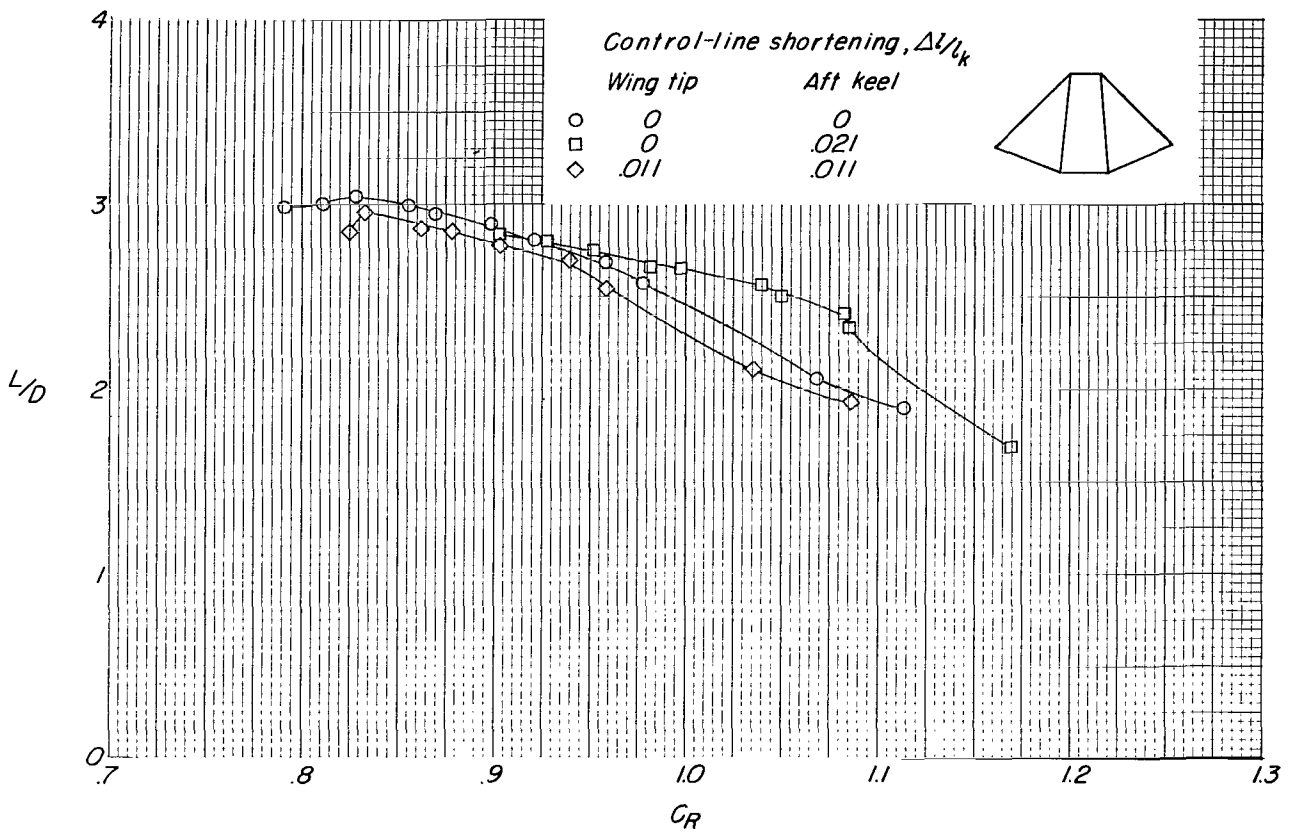
(d) Model 5.

Figure 47.- Continued.



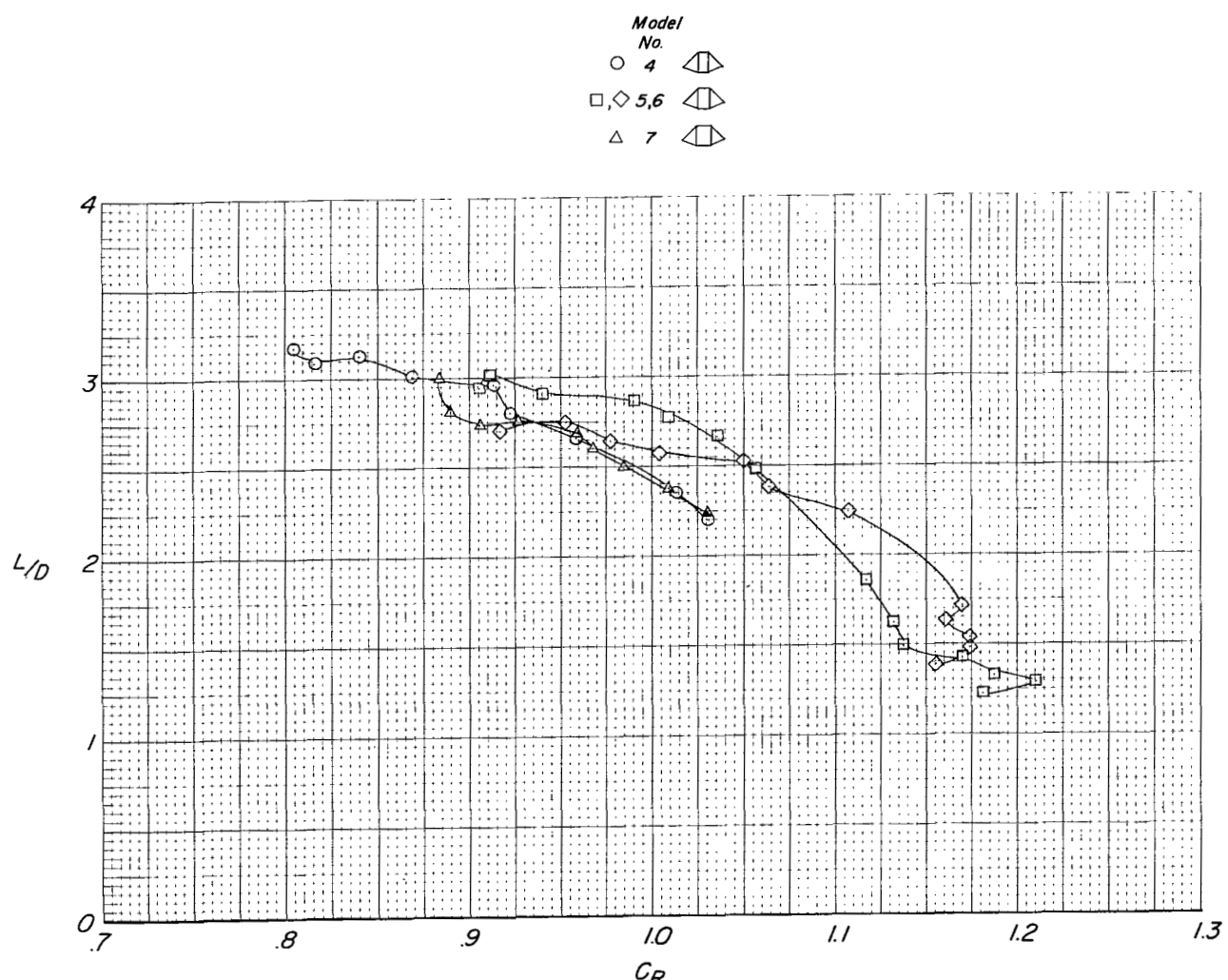
(e) Model 6.

Figure 47.- Continued.



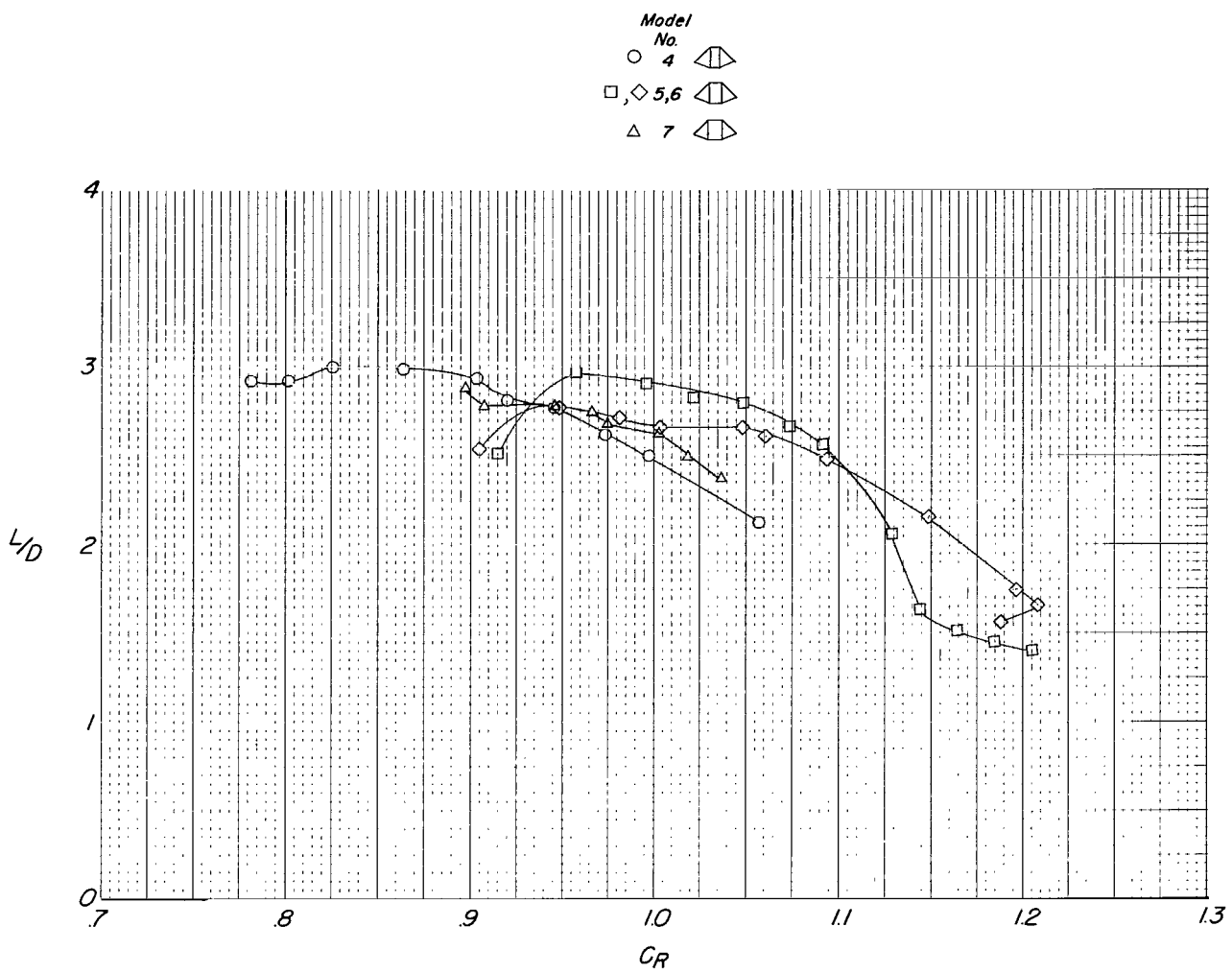
(f) Model 10.

Figure 47.- Concluded.



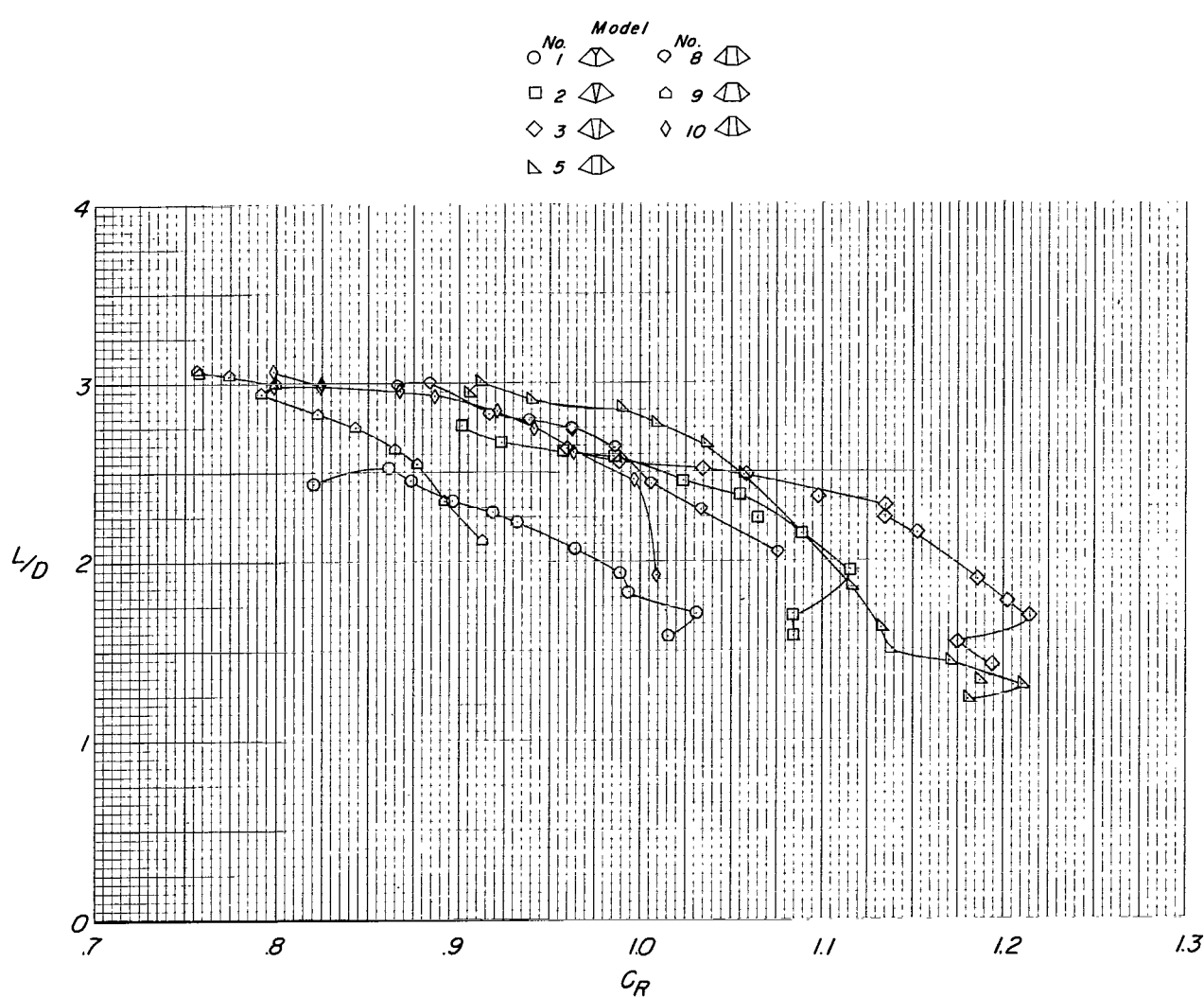
(a)  $q = 1.0 \text{ lb/ft}^2 (47.9 \text{ N/m}^2)$ .

Figure 48.- Effect of center-panel width on the variation of lift-drag ratio with resultant-force coefficient.



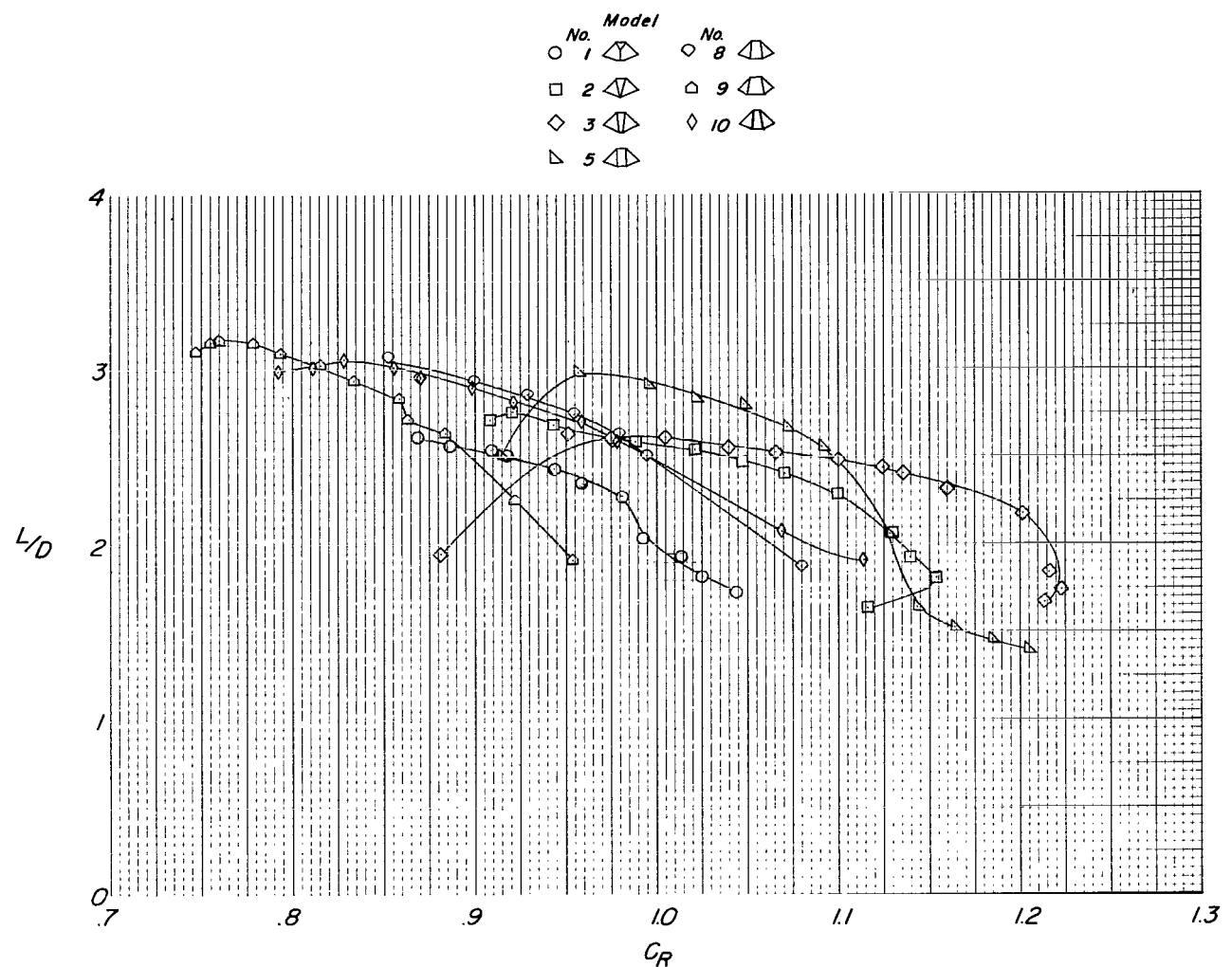
(b)  $q = 2.0 \text{ lb/ft}^2 (95.8 \text{ N/m}^2)$ .

Figure 48.- Concluded.



(a)  $q = 1.0 \text{ lb/ft}^2 (47.9 \text{ N/m}^2)$ .

Figure 49.- Effect of keel-cant angle on the variation of lift-drag ratio with resultant-force coefficient.



(b)  $q = 2.0 \text{ lb/ft}^2 (95.8 \text{ N/m}^2)$ .

Figure 49.- Concluded.

$\circ$	<i>Keel</i>		
$\square$	<i>Leading edge</i>		
$- - -$	<i>Twin keel parawing 5</i>	$\alpha_w, \text{deg}$	$C_R$
$- - -$	<i>Single-keel parawing(ref.1)</i>	28.5	1.050

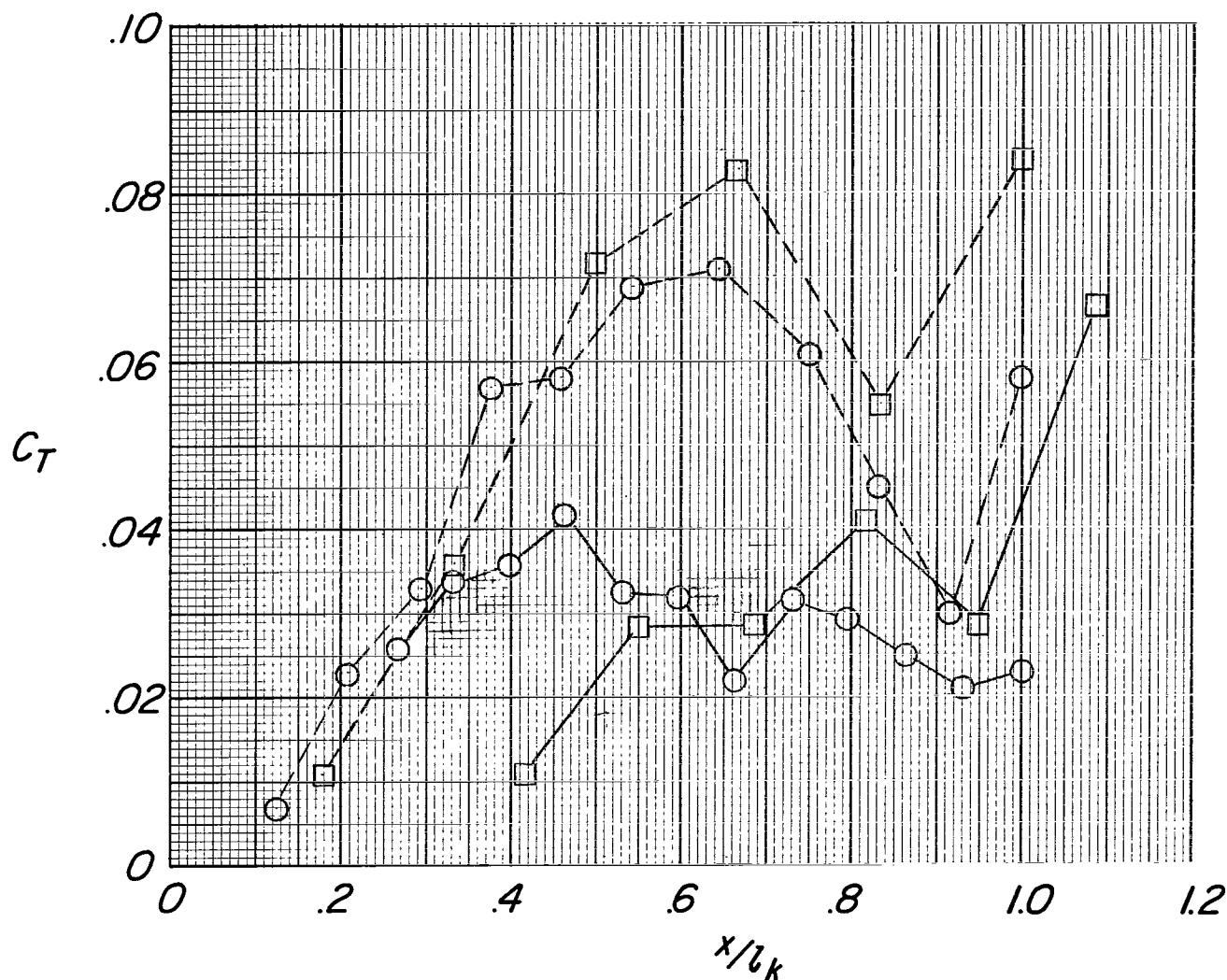


Figure 50.- Comparison of line-tension coefficients for a single-keel parawing (ref. 1) and twin-keel parawing model 5.  
 $q = 2.0 \text{ lb/ft}^2 (95.8 \text{ N/m}^2)$ .